UNIVERSITAT DE BARCELONA

Escola de Camins
Escola Tècnica Superior d'Enginyeria de Camins, Canals i Ports
UPC BARCELONATECH

TREBALL FI DE CARRERA

Títol

Seismic characterization of shallow subsoil with passive seismic prospecting at Rapolano Terme (Northern Apennines, Italy)

Autor/a

Pierre DEL COS DUTHOIT

Tutor/a

Lluís RIVERO (Universitat de Barcelona)
Dario ALBARELLO (Università di Siena)

Departament

Departament de Geodinàmica I Geofísica (Universitat de Barcelona)
Dipartimento di Geofisica (Università di Siena)

Data

26 de gener 2016

ABSTRACT

Passive seismic surveys have become popular in the last decades. Especially because it shows a high capacity for seismic subsoil characterization for a cheap cost. In particular, it is largely used for identification of seismic amplification site effects. The results have the capacity to define areas with the same seismic behaviour, more precisely whether the ground motion generated by a possible earthquake will be amplified or not.

To furnish the results, a large area was covered by the HVSR (*Horizontal to Vertical Spectral Ratio*) single station survey. In addition, few *array* multi-sensor configurations have been set. The correlation of all results aim to obtain the shear wave velocity - depth profiles and the identification of areas susceptible of seismic motion amplification. As well, another goal of this work is to clarify the presence of the Rapolano Fault (an important geological structure that delimits the East margin of the Siena basin). Finally, this study aspires to confirm the capability of the passive seismic prospecting techniques.

Kew words

HVSR, array survey, passive seismic prospecting, seismic subsoil characterization, shear wave velocity – depth profile, Rapolano Terme, Northern Apennines, Italy, Siena Basin, Rapolano Fault.

INDEX

List of figures

List of tables

INTRODUCTION

Because of its particular geodynamic situation, Italy exhibits high earthquake hazard comparing to other European countries. Since 1000 A.D., more than 30 000 seismic events, of medium and high intensity have stroke the country. Observations allowed to point out that for a single area, the earthquakes' damages can vary in very short distances, for buildings and infrastructures with similar characteristics. The phenomenon responsible of these outcomes, called seismic site effects, depend on local geologic features.

To prevent earthquake risk it is necessary to localize the areas subject to seismic amplification, a phenomena that occurs when seismic waves cross a discontinuity represented by the interface between two geological materials with different mechanic behaviour. Thus, it is essential to have a good knowledge of the subsoil structure, particularly regarding its mechanic characteristics.

In the las decades, passive seismic methods have shown capability for subsoil mechanic characterization for a cheap cost. Thus, these techniques allow to understand the subsoil structure up to high depths and to define areas with the same seismic behaviour and to identify the zones where the ground motion generated by a possible earthquake will be amplified or not.

This thesis is structured in two main parts. In the first section, an introduction to passive seismic methods is given. In addition to a short description of ambient vibrations, the single station method and the array one are presented with details on the sensors, the acquisition techniques and the data processing. The second part deals with the field study realized at Rapolano Terme area. Firstly, the local geological setting is introduced. Then the single station and multi-station ambient vibrations measurement campaigns are described. In the last section, the results are shown beside a geological interpretation.

PART 1: PASSIVE SEISMIC METHODS

I. AMBIENT VIBRATIONS

In absence of earthquakes, small vibrations are constantly present on the Earth surface. These are called *seismic noise*, *microtremors* or *ambient vibrations*. The amplitude of the movement is included in the range 10^{-4} – 10^{-2} mm, that's why it can't be felt by humans.

Since the 1950s, technical progress facilitated the recording and analysis of the seismic noise. It has been shown that this one contains useful information on the soil characteristics. This allowed the development of techniques that use the noise for improving the subsoil knowledge. With the actual technology and computing capacity these techniques have been improved. Nevertheless, there are still many open questions about the nature of the seismic noise (Figure 1).

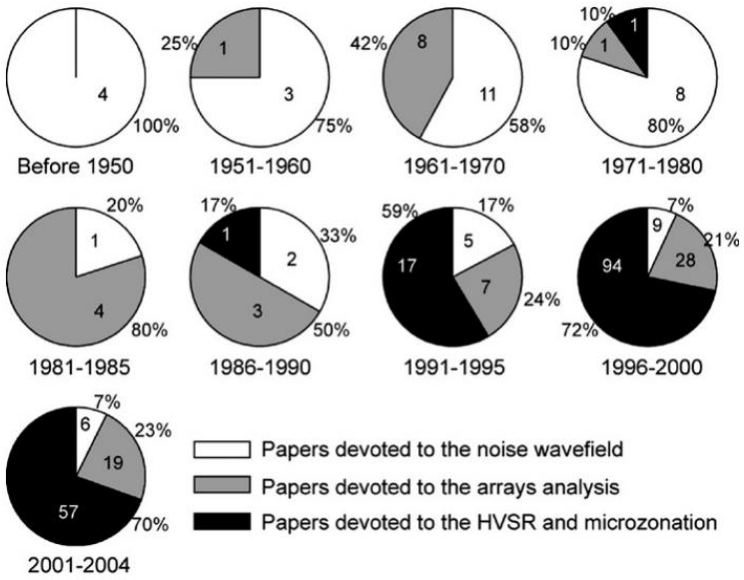

Figure 1. Growth in the number of papers in papers (in terms of percentage and number), from 1911 to 2004 devoted to the nature of noise wavefield analysis and to noise-based methods (Bonnefoy-Claudet et al., 2006).

1. Origin of ambient vibrations

The ambient vibration wavefield is originated by many different kind of sources such as tide, water waves striking the coast, turbulent wind, effects of wind on trees or buildings, industrial machinery, cars, trains, human footsteps, etc. The sources can be classified in two types: natural sources or *microseisms* with low frequency content and cultural ones or *microtremors* with higher frequency content. The frequency ranges are only indicative as they may change with the source and geological setting of any particular area (Asten and Henstridge, 1984; Gutenberg, 1958; SESAME, 2004). Nevertheless we can conclude that:

- At frequencies below 0,5 Hz, the sources are natural (ocean, large scale meteorological conditions). These ambient vibrations are called ***microseisms***.

- Between 0,5 and 1 Hz, sources are both natural (local meteorological conditions) and anthropic.
- For frequencies higher than 1 Hz, sources are essentially anthropic. This noise are called ***microtremors***.

In general all authors agree that 1 Hz is the approximate boundary between microseisms and microtremors, but is not a universal limit.

The spatial and temporal characteristics of the ambient noise field is closely related to its natural or cultural origin. Anthropic microtremors show clearly daily and weekly variations (Figure 2), related to cultural activities (Bonnefoy-Claudet, 2004). Other studies show the relationship between microseisms (low frequency content) and atmospheric conditions (Seo, 1997).

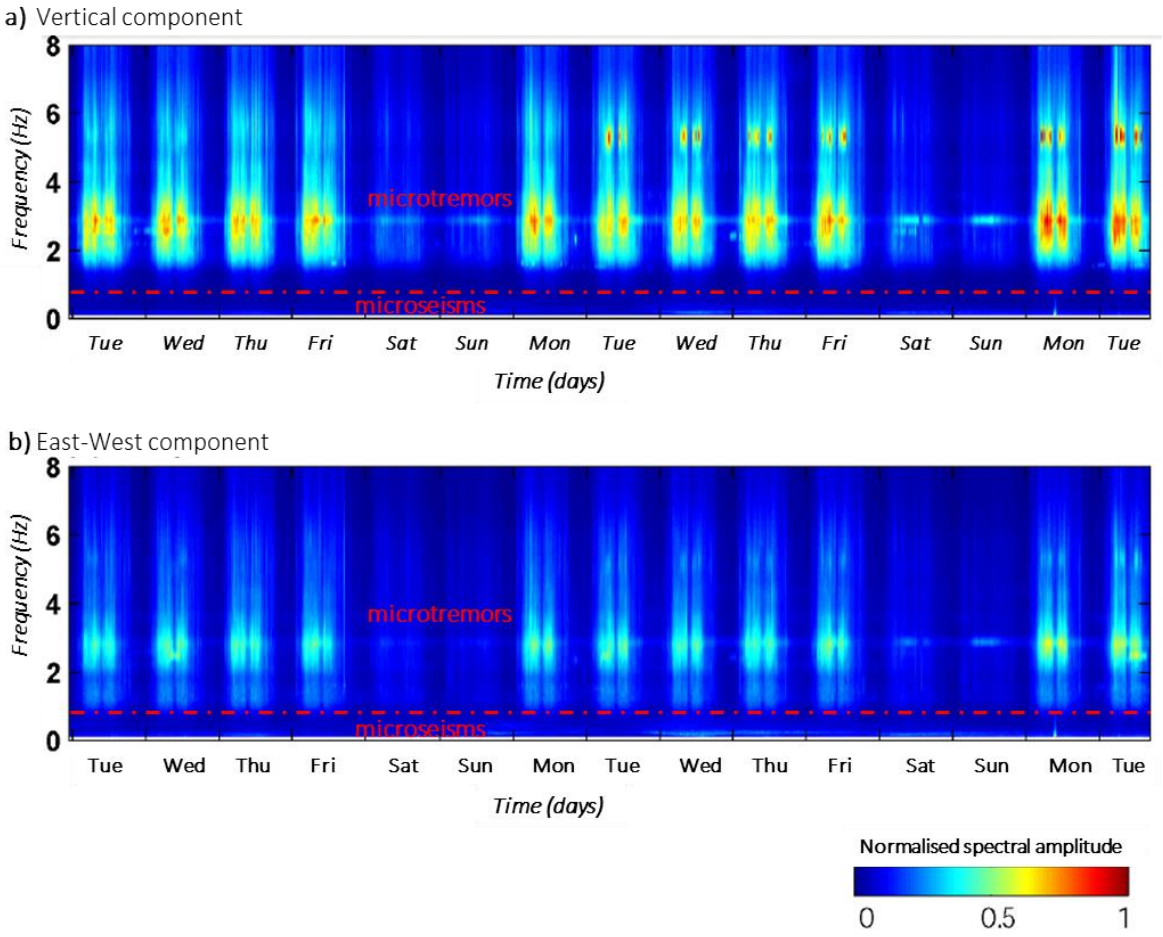

Figure 2. Normalized spectral amplitude vertical (a) and East-West (b) components of ambient vibrations recorded in Grenoble during two consecutive weeks.

2. The ambient vibrations as a stochastic process

The ambient vibrations can be seen as a stochastic process, whose study requires statistical approaches. Even if this kind of approach seems to determine a series of theoretical difficulties, the use of statistic operators allows to reduce the complexity of the analysis. In fact, when the amplitude of the ambient vibrations is considered a stochastic variable, a probability can be attributed to amplitude values (Okada, 2003).

Further, when record lengths exceed 4 minutes, the distribution of amplitude is well approximated by the normal distribution, and that average, variance and autocorrelation

function of the amplitude of seismic noise are constant regardless of the time of sampling. It has been shown that the frequency distribution of the amplitude of the ambient vibrations approaches a normal distribution as the number of sample increases (Nogoshi and Igarashi, 1971).

This demonstrates that the average signal structure is independent from the nature and the position of the sources. Furthermore, as the ambient vibrations are formed by waves that have travelled through a significant portion of the subsoil, the surface ground motion recordings allow to obtain information of the crossed medium.

3. Passive seismic techniques

From surface ambient vibrations recordings, passive seismic techniques are worth to acquire subsoil information. They are more effective in areas where the active methods are not applicable because of high noise levels, like in urban areas characterized by intense traffic. In addition, passive methods can be deployed in small areas, not forgetting that they are cheap and fast.

As the seismic noise covers a large band on the frequency domain, as well as the seismic phenomenon, passive seismic techniques are useful for seismic zonation studies, namely site effects studies (Albarello et al., 2011; Bonnefoy-Claudet et al., 2006; Mucciarelli and Gallipoli, 2001). Particularly, it is possible to identify the areas and the geological or lithological formations potentially more dangerous, because subjected to seismic amplifications. Actually, it is possible to obtain the resonance frequency and the S-wave velocity profile up to few tens of meters.

There are two main experimental configurations to study the ambient vibrations described hereafter: the single station method, in which the recordings are made by a single sensor, and the multi-station methods, also called array methods, in which a group of few sensors are necessary.

II. SINGLE STATION METHOD (HVSR: Horizontal to Vertical Spectral Ratio)

1. Introduction

The single station passive method also known as Horizontal to Vertical Spectral Ratio (HVSR), or H/V method, was used for the first time in 1971 by (Nogoshi and Igarashi, 1971). (Nakamura, 1989) triggered its popularization in 1989. The basic goal of single-station measurements is the identification of the resonance phenomena of soft sediments laying on the bedrock and the fundamental resonance frequency f_0 (Figure 3). Actually, the method allows to determine the presence of a possible impedance contrast (product of density and shear wave velocity).

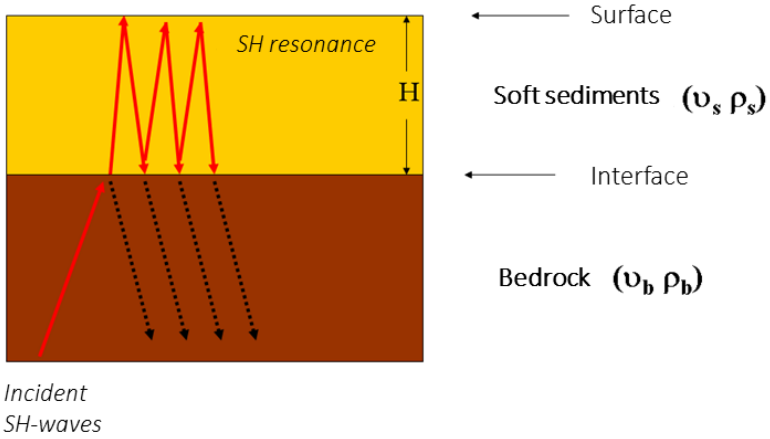

Figure 3. Resonance phenomena induced by a sharp impedance contrast in a horizontal layering setting (Albarello, 2014).

The method consists in computing the average ratio (H/V) of horizontal (H) to vertical (V) spectral components of ambient vibrations in function of the frequency ω. This result is presented in the H/V curve, namely horizontal to vertical spectral ratio curve, hereafter HVSR curve.

If the stratigraphic configuration is made of soft sediments based on a seismic bedrock, the HVSR curve shows a peak in correspondence with the resonance frequency. The peak's shape gives qualitative information about the resonance (Figure 4). When the recordings are made upon the seismic bedrock, characterized by S-wave velocities higher than 800 m/s, there is no amplification phenomena, so the HVSR curve is flat (Figure 5).

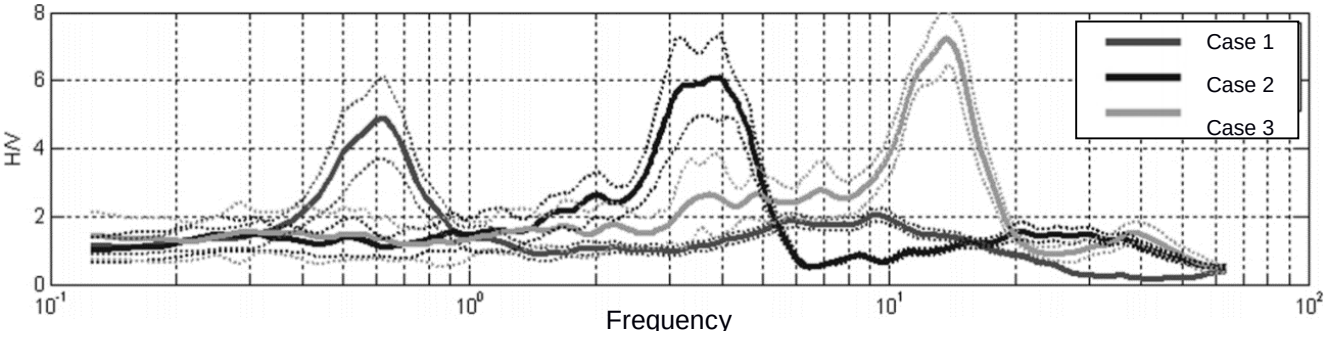

Figure 4. HVSR curve showing three different stratigraphic configurations. Case 1: the bedrock is at a depth of 300m (f_0=0.6 Hz). Case 2: the bedrock is at a depth of 20m (f_0=3.5 Hz). Case 3: the bedrock is at a depth of 4m (f_0=14 Hz) (from Albarello and Castellaro, 2011).

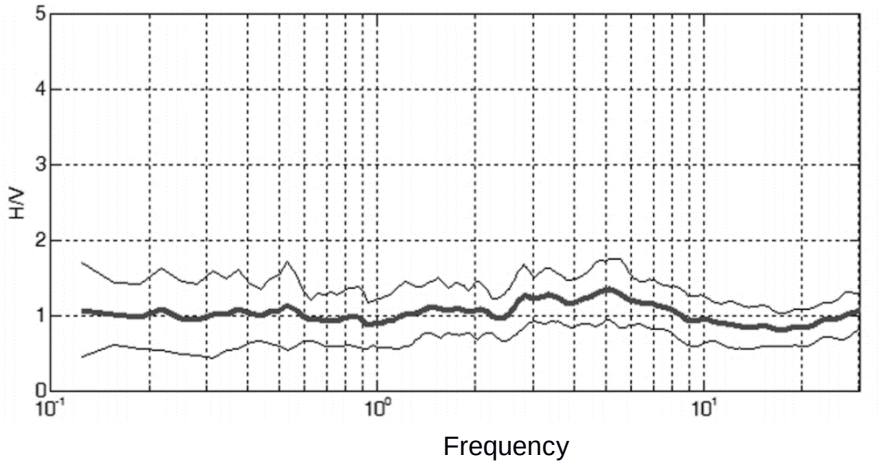

Figure 5. HVSR curve measured on a non-fractured and flat bedrock. There is no amplification phenomena in the whole frequency domain (from Albarello and Castellaro, 2011).

The fundamental mode resonance frequency (f_0), the average S-wave velocity (V_s) and the total thickness of the sedimentary cover (*H*) are linked by an approximate relationship:

$$f_0 = \frac{V_s}{4 \cdot H}$$

Thus, if the average S-wave velocity is known from other experimental data it is possible to obtain the thickness of the sedimentary cover. Therefore (Ibs-von Seht and Wohlenberg, 1999) obtained the bedrock depth in the Rhine basin in Germany from HVSR measurements. Otherwise, if the sedimentary cover thickness is known, the average S-wave velocity can be retrieved.

As well, with just few little spaced HVSR recordings it is possible to establish if the geological setting is simply horizontally layered (1D problem) or if there are lateral variations (2D/3D problem). In the first case, the HVSR curves and the peak frequency will be similar.

It is important to know that seismic wave amplification can also occur because of “topographic effects”. This happens in areas with irregular topography such as hills or ridges. Waves are reflected by the surface and focused in one point, this fact may amplify the ground motion (Figure 6).

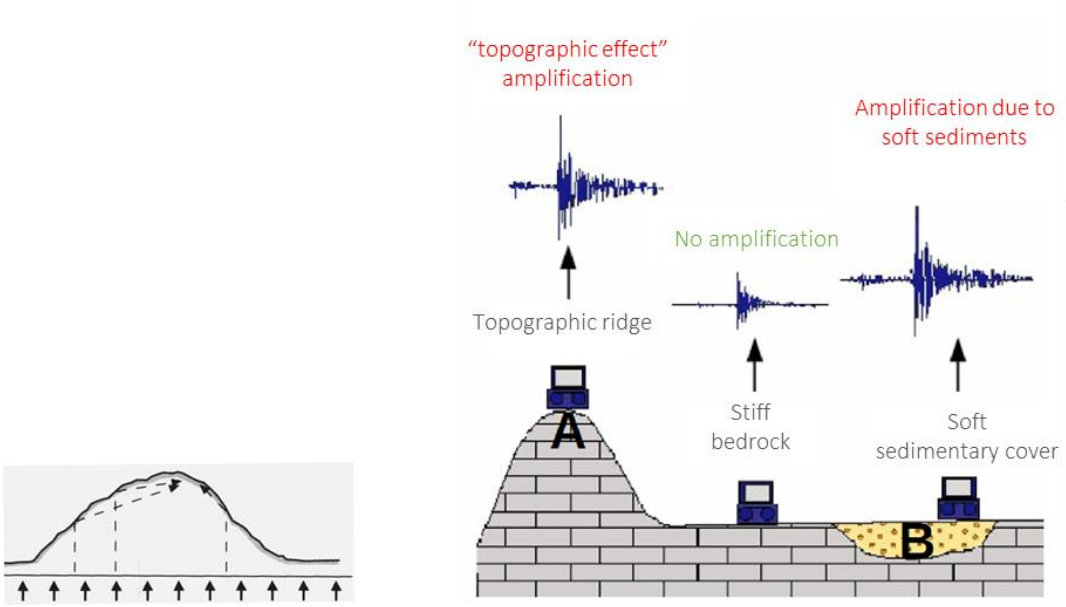

Figure 6. Topographic amplification (left). Summary of seismic amplification phenomenon (right).

2. Physical fundamentals of H/V method

The ambient vibrations wavefield is composed by volume waves (P and S) and superficial waves (Love and Rayleigh). The energy ratio associated to each kind of wave is variable and depends on the frequency window considered. Nevertheless, if we consider a time of enough minutes, the average properties of the seismic wavefield generated by many randomly distributed are conditioned by the medium and are independent from the source characteristics.

The physical interpretation of the H/V ratios as a function of frequency is to some extent controversial (Fäh et al., 2001; Lunedei and Albarello, 2010; Nakamura, 1989). A key element of the different H/V curves interpretation is to define which seismic phases are responsible of the peaks observed. Three different hypothesis have been analyzed (Castellaro and Albarello, 2011):

a. Body waves resonance:

If the wavefield recorded is constituted mainly by stationary vertically incident volume waves, the H/V peaks frequencies would correspond to the resonance frequency of S-waves in the soft sedimentary strata.

b. Ellipticity of the Rayleigh waves:

If the ambient vibration wavefield is dominated by surface waves, the Rayleigh-waves ellipticity (the horizontal to vertical ratio of the Rayleigh-waves movement) and the Love-waves amplitudes condition the HVSR curves. In this case, the underlying theory argumentations establish that in presence of soft sediment strata lying on a hard bedrock, the vertical component of the Rayleigh-waves motion vanishes at the frequencies corresponding with the S-waves resonance ones.

c. Importance of the Airy phase of Love-waves:

Also the Airy phase shows a maximum amplitude related to the S-wave frequency. It is a consequence of the fact that in their horizontal motion, superficial waves (Love and Rayleigh waves) are generated by the interferences of volume waves (signally the SH

components) with the soil surface. Then, surface waves would show resonance phenomenon linked with S-wave.

Even if these three interpretations of the H/V ratios are different, they have the same conclusions: On the one hand, the frequency corresponding to the maximum value of the HVSR curve have a strict correspondence with the local resonance frequency of the sedimentary cover. On the other hand, in absence of HVSR peak, there is no amplification phenomena, in correspondence with bedrock recordings (Bonnefoy-Claudet, 2004).

The outcome that needs to be cautiously analysed is given by the shape of the peaks. It is true that as the impedance contrasts between the hard and the soft layer increases, the HVSR peak is bigger. Nevertheless, this amplitude depends also on other factors as the contribution of each seismic phase to ambient vibrations, attenuation, the soft materials Poisson coefficient and the sources distribution (Lunedei and Albarello, 2010). That's why the peak's shape interpretation should be done cautiously.

3. Measurements

a. Sensor

The single station measurements are performed with a tri-directional sensor which measures the soil motion in three directions. In this work TROMINO sensors have been used (Figure 7).

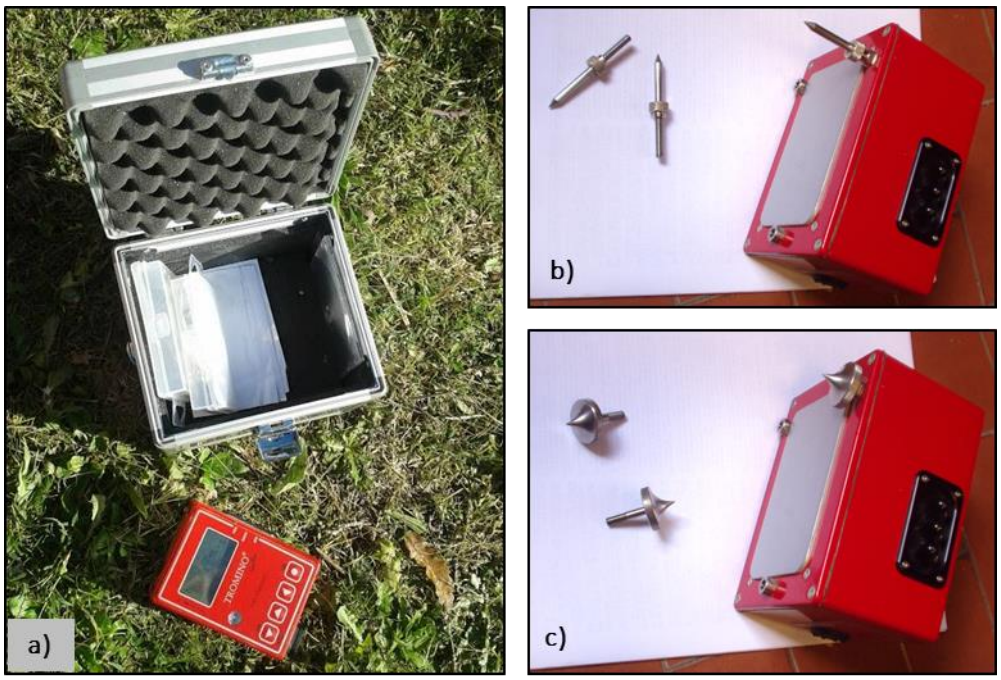

Figure 7. a) TROMINO sensor and its suitcase. b)Ground-sensor coupling devices for soft materials (5cm long sharp peaks). c) Ground-sensor coupling devices for hard materials (small adjustable feet).

b. Experimental conditions and recommendations

Soil-sensor coupling

The purpose of the survey is to measure the ambient vibrations. The motion to measure is so small that it has to be done carefully, especially regarding to the soil-sensor coupling and the reduction of nearby sources disturbance. To have better results

it is better to avoid measurements directly on artificial terrain and to reduce the possible disturbances nearby the sensor.

Recording duration and sampling frequency

Another important aspect is the recording duration. Because the aim of the passive measurements is to obtain the average ground motion, the acquired data must be statistically representative. The recording duration is bound to the investigation frequency band (for engineering purposes the interval is 0.1-20 Hz). Then, if the averages are made with 30 windows of 30 sec. the entire recording duration must be higher than 15 min *(30 windows * 30 sec. = 900 sec. = 15 min.)*. In addition, the frequency sampling must not be inferior to 50Hz so as to assure a spectral construction of at least 20Hz.

Sensor orientation

Eventually, to analyse disturbances due to “directional effects”, it is relevant to note the sensor orientation. Usually it is orientated toward geographic Nord, but in presence of topographic and morphologic elements, it is suggested to align the instrumentation with those ones. Nevertheless the “directional effects” must be examined prudently because they may be originated by the source characteristics (heterogeneous wavefield, directional sources), by topographic alignments or by geologic setting (stratigraphy and structure).

Other recommendations

A resume of the main recommendations to obtain the most reliable results is given in Table 1.

Type of parameter	Main recommendations	
Recording duration	Minimum expected f_0 [Hz]	Minimum recording duration [min]
	0.2	30'
	0.5	20'
	1	10'
	2	5'
	5	3'
	10	2'
Measurement spacing	→ Microzonation: start with a large spacing (for example a 500 m grid) and, in case of lateral variation of the results, densify the grid point spacing, down to 250 m, for example. → Single site response: never use a single measurement point to derive an f_0 value, make at least three measurement points.	
Recording parameters	→ Level the sensor as recommended by the manufacturer. → Fix the gain level at the maximum possible without signal saturation.	
In situ soil-sensor coupling	→ Set the sensor down directly on the ground, whenever possible. → Avoid setting the sensor on "soft grounds" (mud, ploughed soil, tall grass, etc.), or soil saturated after rain.	
Artificial soil-sensor coupling	→ Avoid plates from "soft" materials such as foam rubber, cardboard, etc. → On steep slopes that do not allow correct sensor levelling, install the sensor in a sand pile or in a container filled with sand. → On snow or ice, install a metallic or wooden plate or a container filled with sand to avoid sensor tilting due to local melting.	
Nearby structures	→ Avoid recording near structures such as buildings, trees, etc. in case of wind blowing (faster than approx. 5 m/s). It may strongly influence H/V results by introducing some low frequencies in the curves → Avoid measuring above underground structures such as car parks, pipes, sewer lids, etc.	
Weather conditions	→ Wind: Protect the sensor from the wind (faster than approx. 5 m/s). This only helps if there are no nearby structures. → Rain: avoid measurements under heavy rain. Slight rain has no noticeable influence. → Temperature: check sensor and recorder manufacturer's instructions. → Meteorological perturbations: indicate on the field sheet whether the measurements are performed during a low-pressure meteorological event.	
Disturbances	→ Monochromatic sources: avoid measurements near construction machines, industrial machines, pumps, generators, etc. → Transients: In case of transients (steps, cars,...), increase the recording duration to allow for enough windows for the analysis, after transient removal.	

Table 1. Basic recommendations for good ambient vibration recordings (SESAME, 2004).

In order to write down all the information related to the experimental conditions, field sheet provided by the SESAME Project (2004) was filled out for each recording (Figure 8). This contains information concerning the date, ground type, type of sensor-terrain coupling, sensor orientation, building density, nearby structures, transients (cars, pedestrians, trucks…), weather conditions (wind and rain) and other relevant data. As

well, the measurements have been geolocalized and a photographed. These reports are presented in Annex I.

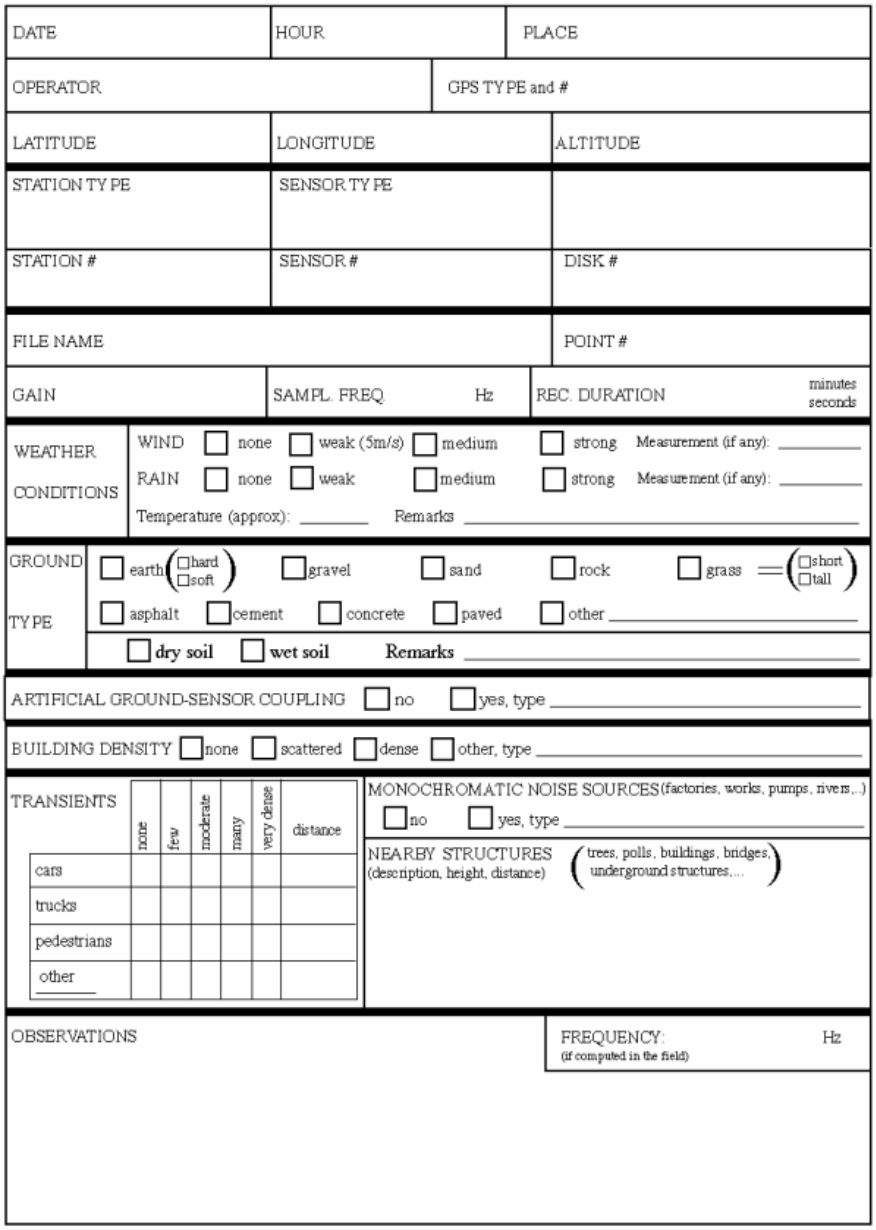

Figure 8. Measurement sheet (SESAME, 2004).

4. Data processing

The ground motion measurements are useful to compute the HVSE curves. This operation has been done with *Grilla* software. In this section, the steps to obtain reliable H/V curves from ambient vibrations recordings are presented.

a. HVSR curves computation

The temporal series of ground motion recorded can be analysed by different procedures in order to obtain de H/V spectral ratio curve and its confidence interval. The following procedure (D'Amico et al., 2004; Picozzi et al., 2005; SESAME, 2004) has been used to compute de HVSR curves.

The 20 minutes recording is split in 60 windows of 20 seconds. So the procedure is realized on every window and at the end the average is done (Figure 9). The length of the window is long enough to guarantee a good frequency definition and the number of windows is sufficient to assure statistically stable results.

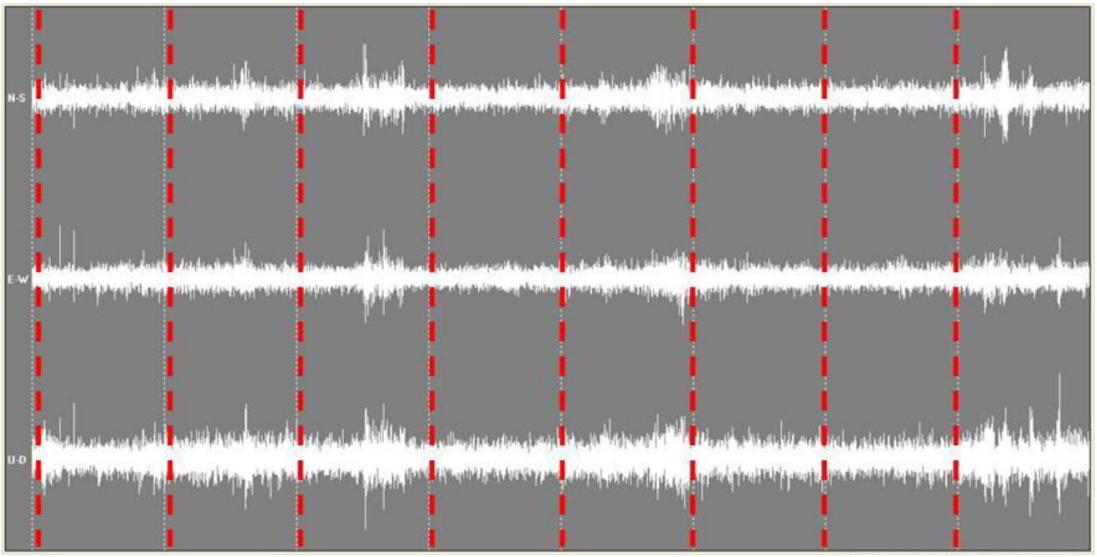

Figure 9. Splitting of the three ambient vibrations components in 20 seconds windows: (top) North-South, (middle) East-West and (bottom) Up-Down.

- Every window is pre-treated with linear detrend to guarantee the stationarity assumption validity. Also tapering (with the Hann cosines function) operation is realized for avoiding leakage. Then the spectral amplitudes are calculated with the Fast Fourier Transform algorithm. After that, the spectrum is smoothed with a triangular window up to 5% of the central frequency to avoid the presence of spurious peaks due to seismic, instrumental or numerical noise.
- For every frequency, the geometric mean of the horizontal components is computed. Afterwards, the horizontal to vertical ratio is determined for each window

$$H_{average} = \sqrt{H_{North-South} \cdot H_{East-West}}$$

- Eventually, the average of all H/V curves is calculated as well as the 95% confidence interval.

b. "Cleaning" the HVSR curves

To be statistically accurate, The HVSR curve should be characterized a low amplitude and frequency deviation. When this trait is not present, it is possible to "clean" the curve by taking off the H/V windows in which the signal is altered. This occurs typically in presence of impulsive signals generally with white spectrum. An example of signal "cleaning" in the frequency domain is shown in Figures 10 and 11.

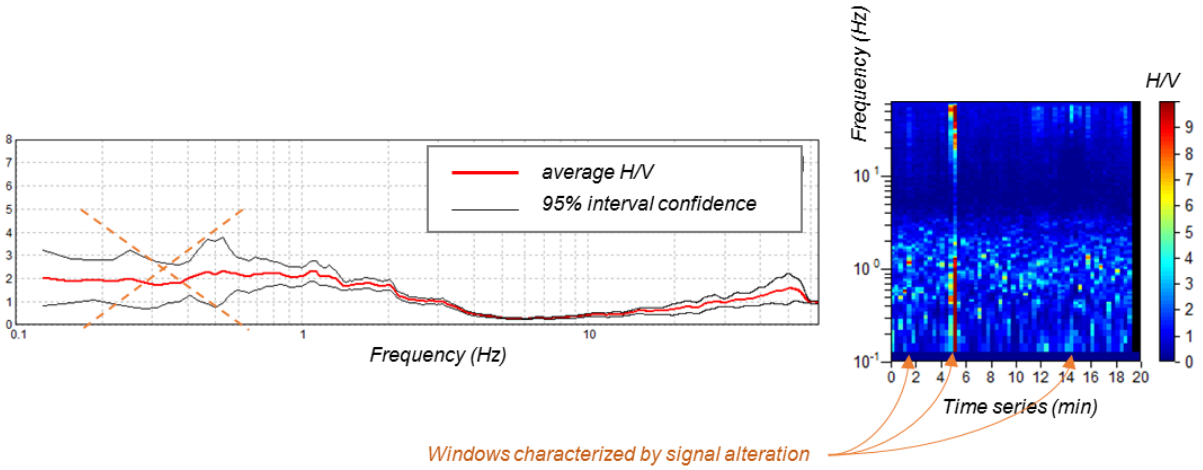

Figure 10. Non-cleaned HVSR curve (left) and H/V temporal series for every 20sec. window (recording M29).

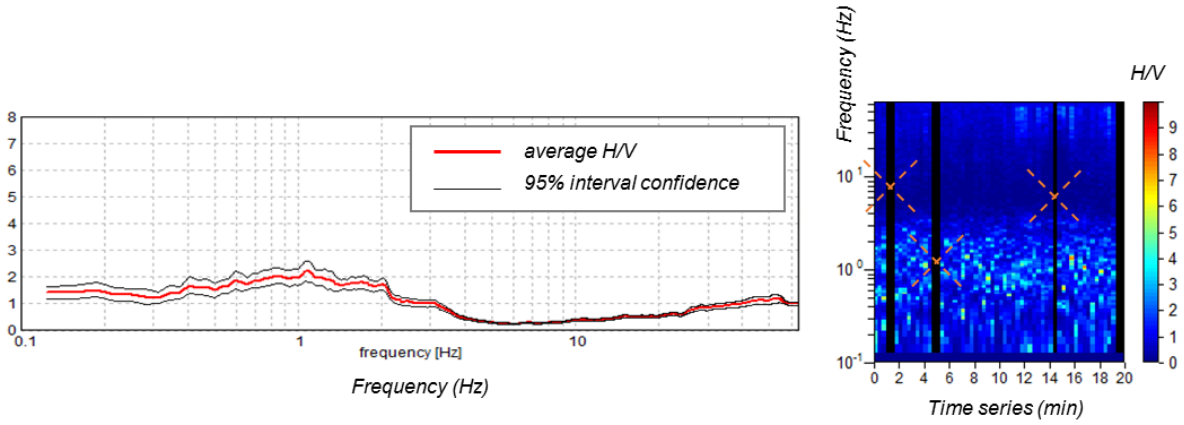

Figure 11. Cleaned HVSR curve (left) and H/V temporal series for every 20sec. window (measuring point M29).

c. Discriminating natural and anthropic H/V peaks

The H/V interpretation is done with both the result HVSR curve and the horizontal and vertical ground motion directional amplitude spectrums. This permits to distinguish the stratigraphic "real" peaks from the ones generated by anthropic disturbances (for instance those originated by electrical motors). The stratigraphic peak shows a relative minimum of the vertical motion component whereas the one generated by sources disturbances present narrow peaks in the vertical and horizontal directions. An example of this situation is exhibited in Figure 12.

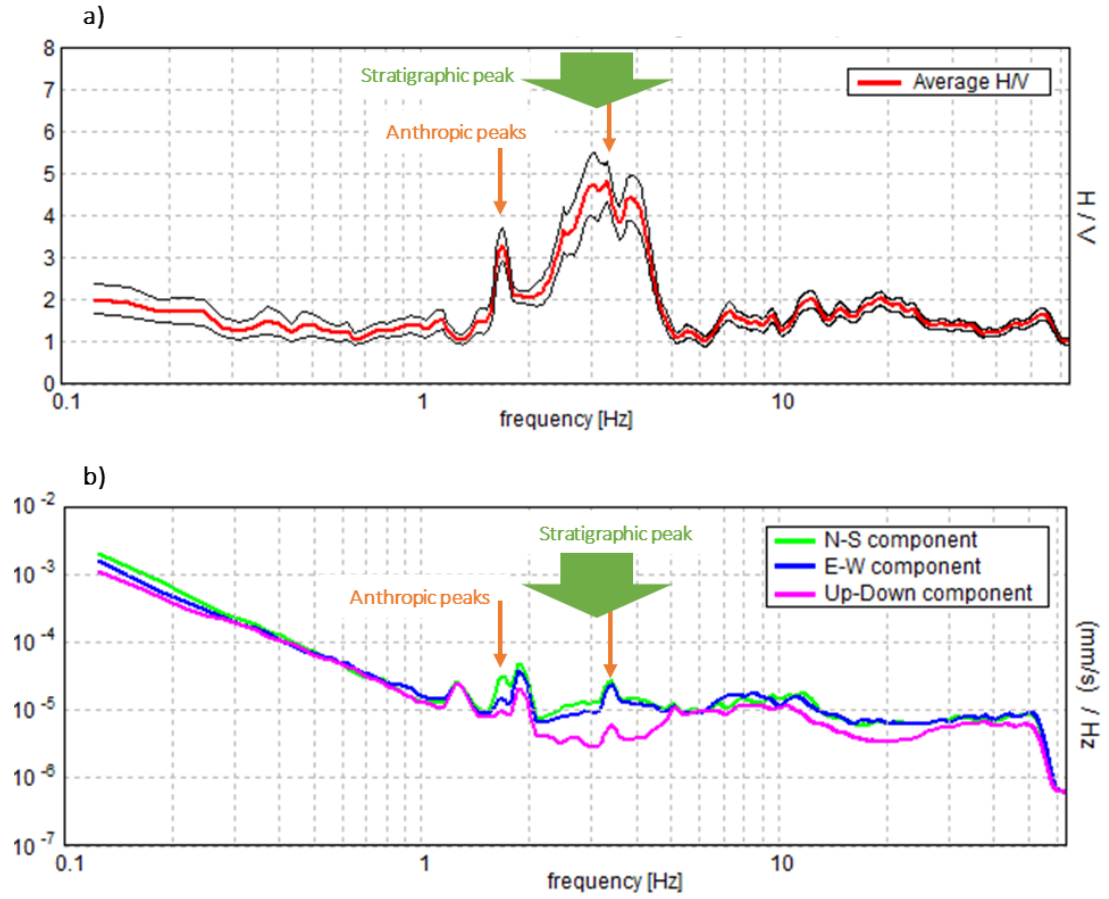

Figure 12. Example of HVSR stratigraphic peak (2-5 Hz) overlaid with two disturbance peaks of anthropic origin (1.8 and 3.3 Hz). HVSR curve (a) and single ground components spectrums (b) of the measuring point M17.

d. Examine directional effects

To see if there are directional effects (in the horizontal directions), it is worth to compute the H/V – azimuth diagram (Figure 13). Nevertheless the "directional effects" must be examined prudently because they may be originated by the source characteristics (heterogeneous wavefield, directional sources), by topographic alignments or by geologic setting (stratigraphy and structure).

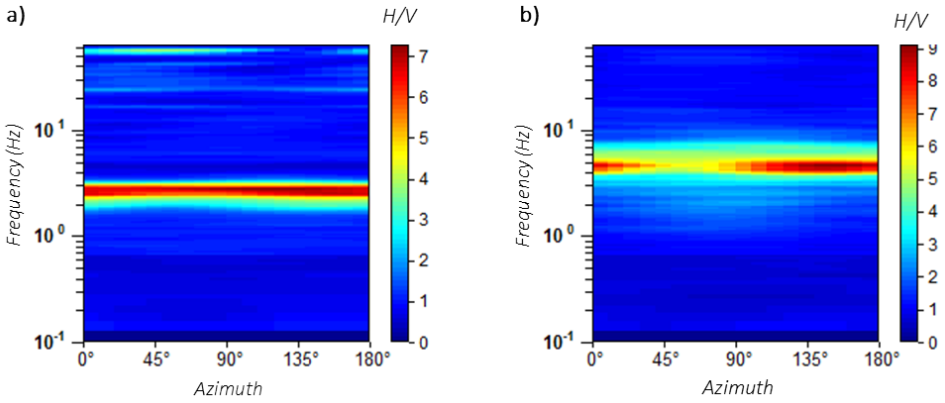

Figure 13. The figures show the H/V in function of the frequency and the azimuth. a) The H/V is constant for all directions, namely no directional effect is present (measuring point M32). b) The H/V varies in function of the azimuth. There is a directional effect, the horizontal ground motion is stronger in North-South direction (N150º) than in East-West direction (Measuring point M19.2).

e. Criteria for assessing the quality of measurements

The SESAME European Project (2004) provides criteria for the reliability of the curves and gives suggestions for the interpretation of the most common situations (Figure 14). These criteria are based on statistical analysis of the measured data and its goal is to reveal unclear measurements. In that case it would be recommendable to realize further investigations (repeat the recordings, change the coupling conditions between the sensor and the ground, etc.). The first part is dedicated to the evaluation of the reliability of the HVSR curve. The second one analyses the morphology of the HVSR peak. This second analysis has to be done carefully, because in case of lithological gradual transition the HVSR peak is not sharp and the amplification affects a large frequency band. In this case it is possible that the recordings don't satisfy the reliability criteria.

Criteria for a reliable H/V curve

i) $f_0 > 10 / l_w$

and

ii) $n_c(f_0) > 200$

and

iii) $\sigma_A(f) < 2$ for $0.5f_0 < f < 2f_0$ if $f0 > 0.5Hz$

or $\sigma_A(f) < 3$ for $0.5f_0 < f < 2f_0$ if $f0 < 0.5Hz$

Criteria for a clear H/V peak

(at least 5 out of 6 criteria fulfilled)

i) $\exists\, f^- \in [f_0/4, f_0] \mid A_{H/V}(f^-) < A_0/2$

ii) $\exists\, f^+ \in [f_0, 4f_0] \mid A_{H/V}(f^+) < A_0/2$

iii) $A_0 > 2$

iv) $f_{peak}[A_{H/V}(f) \pm \sigma_A(f)] = f_0 \pm 5\%$

v) $\sigma_f < \varepsilon(f_0)$

vi) $\sigma_A(f_0) < \theta(f_0)$

- l_w = window length
- n_w = number of windows selected for the average H/V curve
- $n_c = l_w \cdot n_w$. f_0 = number of significant cycles
- f = current frequency
- f_{sensor} = sensor cut-off frequency
- f_0 = H/V peak frequency
- σ_f = standard deviation of H/V peak frequency ($f_0 \pm \sigma_f$)
- $\varepsilon(f_0)$ = threshold value for the stability condition $\sigma_f < \varepsilon(f_0)$
- A_0 = H/V peak amplitude at frequency f_0
- $A_{H/V}(f)$ = H/V curve amplitude at frequency f
- f^- = frequency between $f_0/4$ and f_0 for which $A_{H/V}(f^-) < A_0/2$
- f^+ = frequency between f_0 and $4f_0$ for which $A_{H/V}(f^+) < A_0/2$
- $\sigma_A(f)$ = "standard deviation" of $A_{H/V}(f)$, $\sigma_A(f)$ is the factor by which the mean $A_{H/V}(f)$ curve should be multiplied or divided
- $\sigma_{logH/V}(f)$ = standard deviation of the $\log A_{H/V}(f)$ curve, $\sigma_{logH/V}(f)$ is an absolute value which should be added to or subtracted from the mean $\log A_{H/V}(f)$ curve
- $\theta(f_0)$ = threshold value for the stability condition $\sigma_A(f) < \theta(f_0)$
- $V_{s,av}$ = average S-wave velocity of the total deposits
- $V_{s,surf}$ = S-wave velocity of the surface layer
- h = depth to bedrock
- h_{min} = lower-bound estimate of h

Threshold Values for σ_f and $\sigma_A(f_0)$

Frequency range [Hz]	< 0.2	0.2 – 0.5	0.5 – 1.0	1.0 – 2.0	> 2.0
$\varepsilon(f_0)$ [Hz]	0.25 f_0	0.20 f_0	0.15 f_0	0.10 f_0	0.05 f_0
$\theta(f_0)$ for $\sigma_A(f_0)$	3.0	2.5	2.0	1.78	1.58
$\log \theta(f_0)$ for $\sigma_{logH/V}(f_0)$	0.48	0.40	0.30	0.25	0.20

Figure 14. Statistical criteria for reliability of results (SESAME, 2004).

The SESAME Project (2004) doesn't consider relevant the peaks with an H/V ratio inferior to 2. Nevertheless, those can be attributed to low impedance contrasts. To get round this limitation, (Castellaro and Albarello, 2011) proposed another criteria classification of HVSR results that integrates the *SESAME* propositions with the same goal, namely give some advice for the curves interpretation. It has been largely developed on the seismic microzonation studies executed after the Aquila earthquake occurred on the 9th April 2009.

All measurements made in this work have been classified with this last criteria which is based on three HVSR reliability classes:

- **Class A**: Trustworthy and interpretable HVSR curve, which represents a reference measurement that can be considered representative of the dynamical behavior of the subsoil at the site of concern by itself.
- **Class B**: Suspicious HVSR curve, which should be used with caution and only if it is coherent with other measurements performed nearby.
- **Class C**: bad HVSR curve (it is hardly interpretable), to be discarded.

Criteria used to classify a single measurement as of class A are:

i. Stationarity: HVSR curve included in the frequency range of interest shows a persistent shape for at least the 30% of the measurement windows;

ii. Isotropy: the azimuthal amplitude variations do not exceed 30% of the maximum;

iii. Absence of artefacts: there are not symptoms of electromagnetic noise or peaks of industrial origin into the frequency range of interest;

iv. Physical plausibility: HVSR maxima are characterized by a localized lowering of the vertical amplitude spectral component;

v. Statistical robustness: SESAME criteria for a reliable H/V curve are fulfilled;
vi. Representative sampling: the measurement took place for at least 15 minutes.

A measurement is in class B if one or more of the previous conditions are not fulfilled.

Measurements of class B become of class C if:
- A rising drift exists from low to high frequencies, it indicates a movement of the instrument during the acquisition,
- Or electromagnetic disturbances affect several frequencies in the frequency range of interest.

Actually, these criteria aimed at the "first-glance" identification of good and unreliable measurements (A and C classes respectively) and at identifying doubtful results (B class), that require careful inspections. These criteria do not concern the possibility to provide a physical interpretation of the curve in terms of "absence/presence" of resonance phenomena. For this purpose, the SESAME conditions for "peak clearness" were taken into account. On this basis, two sub-classes (type) were introduced:
-**Type 1*:*** the HVSR curve presents at least one "clear" peak in the frequency range of interest (possible resonance).
- Type 2: the HVSR curve does not present any "clear" peak in the frequency range of interest (absence of resonance).

5. Results interpretation

a. Exploratory usage of HVSR curves

Horizontal-to-Vertical Spectral Ratios deduced by single station measurements of ambient vibrations are an important tool for a cheap and fast seismic characterization of the shallow subsoil. This technique allows to identify the seismic resonance phenomena induced by the presence of a sharp seismic impedance contrast in the subsoil and the relevant resonance frequency.

Carrying out extensive single station measurements permits to identify the areas and the geological formations potentially more dangerous because subjected to seismic amplification. For this reason, the single station method is widely used in the frame of microzonation studies.

b. Stratigraphic usage of HVSR curves

By exploiting the well-known approximate relationships relating the resonance frequency (f_0) of the sedimentary cover with its thickness (h) and the average S-wave velocity (V_S) it is possible to obtain information on the shallow subsoil structure (see, e.g., Ibs-von Seht and Wohlenberg, 1999):

$$f_0 \approx \frac{V_s}{4h} = \frac{1}{4T_n}$$

In combination with other experimental data (boreholes, seismic surveys…), it is possible to obtain more information about the subsoil structure. If the strata thicknesses are well known, it is feasible to get the S-wave velocities. As well, if S-wave velocity data (V_S) is available, it is possible to obtain the sedimentary cover thickness (h). Nevertheless, in absence of the seismic velocity data, Albarello et al. (2011) proposed the use of a simple abacus where only the knowledge of the resonance frequency f_0 is required (Figure 15):

f_0 (Hz)	h (m)
< 1	> 100
$1 - 2$	$50 - 100$
$2 - 3$	$30 - 50$
$3 - 5$	$20 - 30$
$5 - 8$	$10 - 20$
$8 - 20$	$5 - 10$
> 20	< 5

Figure 15. Approximate summary relationship between HVSR peak frequency (f_0) and impedance contrast depth (h) (Albarello et al., 2011)

c. Joint-inversion

Finally, HVSR curves obtained from single station measurements are necessary data to compute S-wave velocity profiles using a joint-inversion procedure. To this purpose, dispersion curves acquired from multi-station measurements are also mandatory. This procedure is explained in section “Joint-inversion procedure” (p. 23).

6. Limits of the HVSR method

The HVSR theory makes the assumption of horizontal stratified strata, overlaid on the seismic bedrock. The presence of particular geological and geometrical settings may complicate the HVSR curves analysis (Belvaux et al., 2012). As well speed inversion in the stratigraphy, namely a profile presenting speed decrease with depth may hide the resonance phenomena as no peak is found. These effects can be apparent in presence of a stiff strata of thickness inferior to one meter. In addition, the absence of a high impedance contrast may reduce the peak of the HVSR or even mask it.

2D-3D structures

It is the case of settings with strong lateral speed variation in contradiction with 1D assumption. It has been shown that for 2D and 3D structures, the H/V curves exhibit clear peaks in the “flat” parts of the structures, and broad peaks or plateau-like shapes of low amplitude in parts with strong lateral sediment thickness variation (valley edges). For 2D models, the H/V peak frequencies agree within +/-20% the theoretical 1D resonance frequencies in the flat parts of the structure and overestimates by around 15% the resonance frequency at valley edge. For 3D models, the H/V peak frequencies are close to the theoretical 1D resonance frequency at sites with gentle slopes, while the frequency is strongly underestimated (up to 80%) for sites with steep underground slopes (Guillier et al., 2006).

Velocity inversions

Seismic velocity inversions may result in an H/V ratio below 1 for a wide range of frequencies, due to the decrease of the horizontal spectral components and to a possible rise of the vertical component. This is not the only cause for H/V < 1 which may have a different origin (e.g., Rayleigh wave ellipticity, strong transients on the vertical components, etc.) over a restricted frequency ranges (Castellaro and Mulargia, 2009).

III. ARRAY SURVEY METHODS

The multi-stations methods are based on ambient vibrations measurements by an array of some geophones distributed at the surface of the subsoil to be explored. As the sensors are located closely enough in space, the arriving seismic signal waveforms can be correlated between adjacent sensors. With the acquired data it is possible to retrieve the surface waves dispersion curve, namely the distribution of surface wave velocity, V_R, in function of the frequency. With this dispersion curve, it is possible to compute the S-wave velocity profile with an inversion procedure (Figure 16).

These passive seismic methods allows to characterize a site down to great depths (hundreds of meters) avoiding the need of large and heavy active sources, and with cheap exploring costs (Okada, 2003).

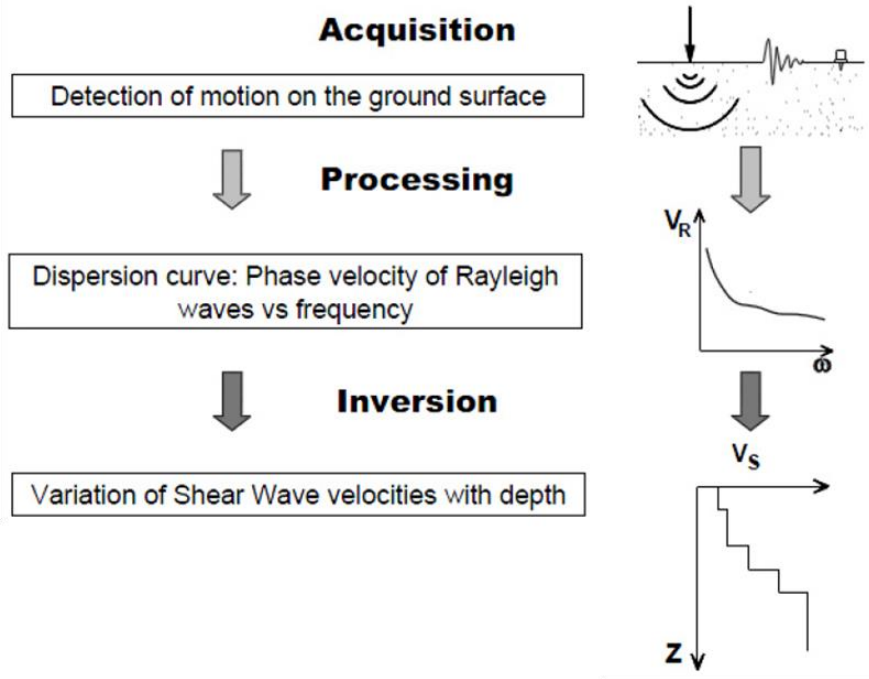

Figure 16. Flow chart of multi-stations surface wave tests (Pileggi, 2013).

1. Sensors and acquisition technique

a. Sensors

The ambient vibrations are recorded with an array of several geophones. Vertical geophones are more frequently used because they are useful for active seismic methods too (Figure 17). These allow to retrieve the dispersion curves of Rayleigh waves. As Love waves motion is only horizontal, to estimate the Love wave dispersion curve 3-component geophones are unavoidable.

Figure 17. Acquisition system (left) and geophones (right) used for multi-station recordings.

b. Array configuration

The array configuration refers to the geophones relative location (Figure 18). This point is relevant for sampling a large frequency band and to determine possible directional effects. There are some recommendations for a good geophones positioning:

- The longest extent between the geophones is the same order of magnitude as the depth to investigate
- The shortest distance between the geophones has to be larger than half of the minimum wavelength investigated.
  It is important to take account of the sampling frequency and the expected S-wave velocity ($\frac{\lambda}{2} = \frac{V_S}{2 \cdot f}$). For example, if the sampling frequency is 128Hz and the S-wave propagation velocity higher than 250m/s, the sensors have to be distant of at least 1m ($= 250/(2 \cdot 128)$).
- The number of sensors has to be sufficient to give a representative sampling of the distances between geophones included within the longest and smallest inter-geophone distance, to avoid spatial aliasing
- The orientation of all pairs of geophones has to sample the largest azimuthal directions

There isn't an ideal configuration since each one has advantages and drawbacks. With a circle array configuration, the directional coverage is very good but the distance between geophones is not so varied, so the sampled wavelength is rather narrow. For this study, a cross array configuration has been used, with irregular spacing between geophones. This one and allows to get the dispersion curves for a large wavelength range and to get a good directional coverage. Moreover, it is easy and quick to set.

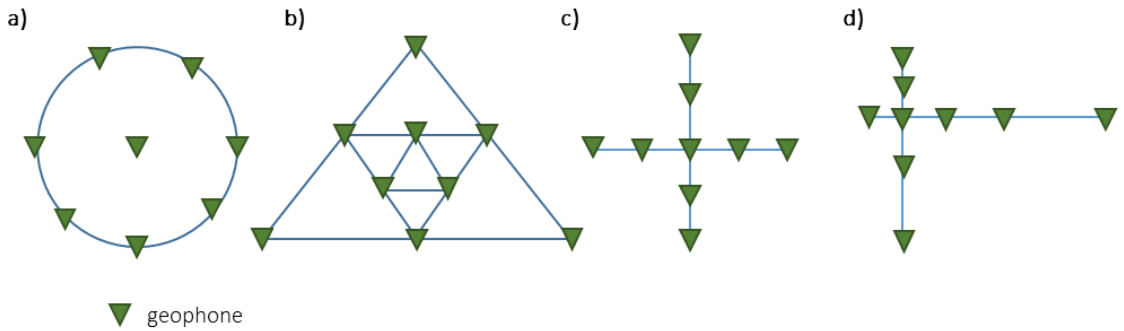

Figure 18. Few array configurations: a) circle, b) based on triangles, c) cross with regular spacing, d) cross with irregular spacing.

2. Data processing and dispersion curves

From the multi-station ambient vibration recordings, it is possible to obtain the surface waves dispersion curves with many procedures. In this work, the data has been treated with the two following methods:

Frequency-wavenumber spectral method (f-k)

Its principle is to detect a relatively strong wave from within the complex assemblage of microtremors (Okada, 2003). It is based on the wavefield analysis in the frequency-wavenumber domain (Capon, 1969; Lacoss et al., 1969; Schmidt, 1981). In this work this method has been applied through the *Geopsy* software.

Extended Spatial AutoCorrelation method (ESAC)

This method is based on the spatial autocorrelation of the seismic signal (Aki, 1957; Ohori et al., 2002). A code developed by the Geophysics department of University of Siena has been employed.

ESAC method gives reliable estimates of dispersion characteristics within a larger frequency band. Whereas the f-k method is limited on both sides. For low frequencies the limitation is either caused by the vanishing spectral energy contribution of the vertical Rayleigh waves component (accentuated around the frequency of H/V spectral peak) or by the array resolving capabilities (related to its length). For the high frequencies, the restriction is given by spatial and temporal aliasing (Ohrnberger et al., 2004).

Nevertheless, other effects as source characteristics and particular propagation effects may lead to misinterpretation. To limit this insufficiency it is recommended to use various combinations of analysis methods.

3. S-wave velocity profiles estimation from ambient vibrations recordings

a. Principle

Propagation velocity of Rayleigh waves is strongly determinate by S-waves velocity of the considered strata ($V_R \approx 0.9\, V_S$). Further, Rayleigh waves travel through deeper portions of subsoil with increasing the period (Figure 19). Then, from a dispersion curve, it is possible with inversion procedures to obtain an estimation of the S-wave velocity profile up to a depth given by the minimum frequency of the dispersion curve (Figure 20).

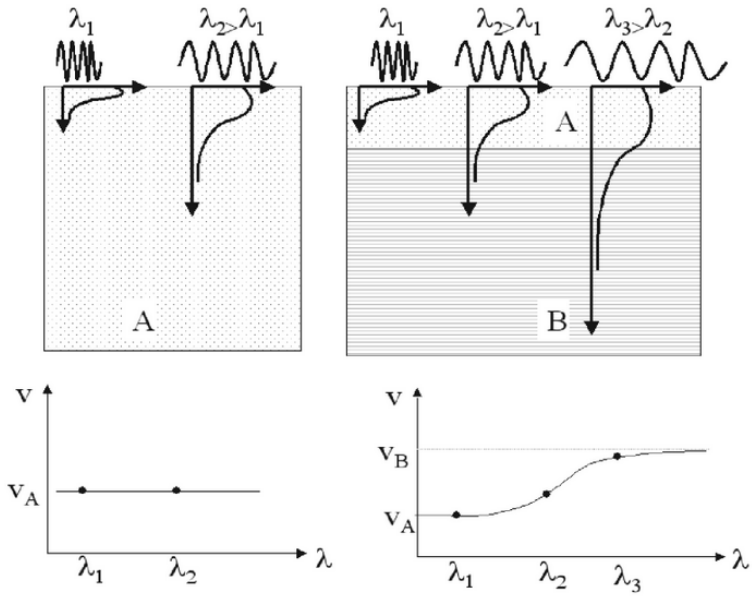

Figure 19. Surface wave dispersion. In a homogeneous half space (left) all the wave lengths sample the same material and phase velocity is constant. When the properties change with depth (right) the phase velocity depends on the wavelength, forming a dispersion curve (Okada, 2003)

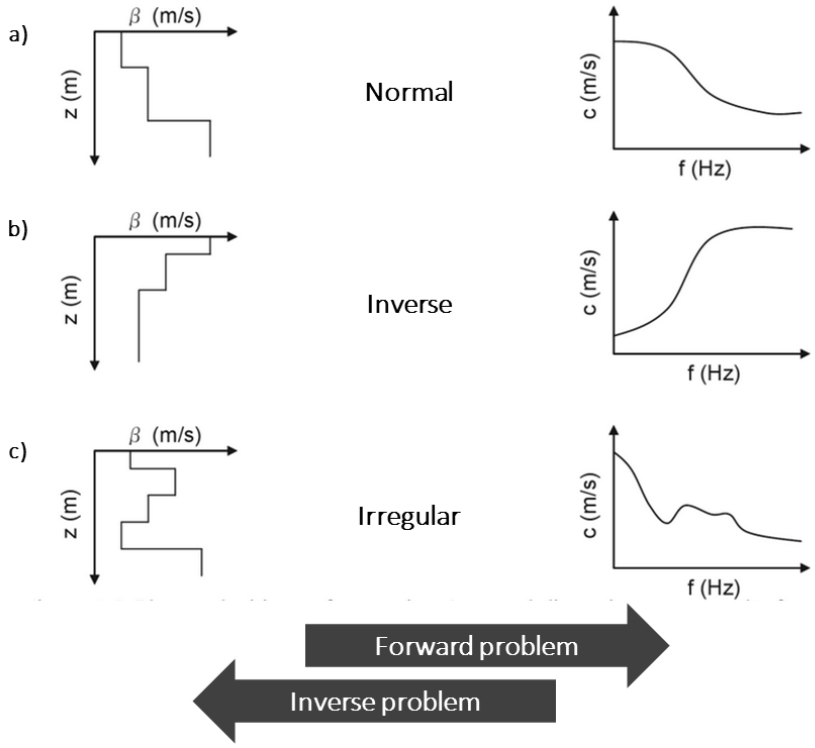

Figure 20. S-wave velocity profiles (left) and its dispersion curves (right). a) A normal dispersion curve results from a profile where S-wave velocity increases with depth. b) For a profile where S-wave velocity decreases with depth, a reverse dispersion curve will be observed over some rang of frequency. c) For an irregular S-wave velocity profile, phase velocities show a complex relation with frequencies (Okada, 2003).

Actually, the dispersion curve is not always as smoothed and “clean” as these theoretical examples. It can present pronounced variations due to interaction of higher modes. This is why the dispersion curve has to be interpreted along with the S-wave velocity profile obtained with an inversion procedure.

b. Exploration depth

Regarding the exploration depth capability, the array methods have some limitations due to experimental conditions and instrumental characteristics:

- On the one hand, an array which maximum inter-geophone distance is **L** can sample a maximum wavelengths **λ** ranging from about 2**L** to 5**L**. On the other, the portion of subsoil explored by a superficial wave is about ½ its wavelength **λ**. Thus, the maximum exploration depth is around **L** to 2.5**L**.
- Another constraint is given by the geophones frequency. For example, if 4.5Hw geophones are used, the minimum wave frequency sampling is around 2-3Hz, which corresponds to waves crossing depths of 100 to 300m. So the maximum exploratory depth is around 50 to 150m.
- Finally, the existence of sharp velocity contrast tends to confine the waves in the soft upper strata. This means that the dispersion curve will not give valuable information of wave-velocity going through the stiff bottom strata.

c. "Fast and dirty" inversion

Few procedures have been developed to obtain the S-wave velocity profiles from only the dispersion curves (Albarello et al 2010). These have been called by the authors "fast and dirty" because the results are very approximate and the inversion procedure is quick. That's why it's worth for field preliminary interpretation.

One limitation of this "dirty" technique is that the data provided by the surface wave dispersion curves is limited to the top strata. This fact is emphasised in geological configurations with sharp impedance contrast, namely when the energy associated to superficial waves remains in the upper part of the discontinuity separating top soft sediments lying on hard bedrock. Furthermore, the H/V curve is strongly conditioned by the characteristics (depth and impedance contrast) of the sediments-bedrock interface.

d. Joint-inversion procedure

Resuming, the HVSR ratio and the surface wave dispersion curve display different sensitivities to the S-wave velocity and thickness of the sedimentary layers. More precisely, the dispersion curve provides a constraint on the S-wave velocity of the top soft materials, generally made of sediments, while the fundamental frequency f_0 estimated from the HVSR ratio peak, represents a constraint for the total sedimentary-cover thickness.

This led few authors (Parolai et al., 2005; Picozzi et al., 2005; Scherbaum et al., 2003) to develop procedures which exploit both the HVSR and the dispersion curves in order to obtain better defined S-waves velocity profiles. This methods are called joint inversion procedures. In this work, an efficient procedure based on genetic algorithms has been used to perform the joint inversions.

e. Genetic algorithms

Genetic algorithms belong to the class of evolutionary algorithms that generate solutions for the optimization of non-linear inverse problems by the analysis of thousands of possible models and by the usage of techniques inspired by the natural evolution theory of Darwin (Goldberg, 1989). The genetic algorithm used in this work with an iterative procedure consists in (Albarello et al., 2011):

A population of individuals, namely candidate solutions evolve toward better solutions. Each individual has a set of chromosomes, namely its properties (thickness of each

strata, S and P wave velocity, density and damping factors) which can be muted and selected (Figure 21).

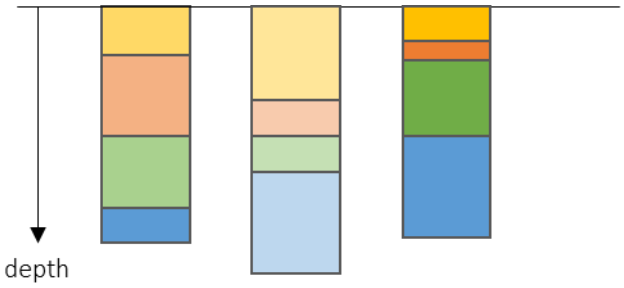

Figure 21. Schematic representation one generation of three different individuals. Each one consists in a combination of few strata, and each strata is characterized by its thickness, S-wave velocity, P-wave velocity, density and damping factors.

Forward simulation procedure

Theoretical HVSR and effective dispersion curves have been modeled as suggested in Lunedei and Albarello (2009). The authors speculate the subsoil as a flat stratified viscoelastic medium where surface waves (Rayleig and Love, with relevant higher modes) propagate only. From this model, both theoretical HVSR and effective dispersion curves can be computed from the following parameters: *thickness of each strata, S and P waves velocity, density and damping factors*.

Inversion procedure

- Initialization

First, a set of models is generated in the parameters domain by means of random criterion. It is the first generation.

- Iteration process

- Each model is scored according to its misfit value. It is a measure of the distance between the experimental curves (HVSR and dispersion curve) and the ones produced by the theoretical model via the forward simulation code.
- A new generation is created by applying the genetic operators: *cross-over*, *mutation* and *elite selection* operators.

Cross-over*:* This operator generates new profiles by crossing, via a random rule, the variables of two original profiles, chosen proportionally to their score.

Mutation*:* It changes some values of the new profile, according to a specific mutation probability.

Elite selection*:* It selects a number of best models, which directly transit in the new generation.

- Ending

If the maximum generation number is reached, the iteration process is stopped. Otherwise it keeps going on. The best individual of the last generation is the solution of the inversion problem.

For this study, for each joint-inversion 20 inversions have been computed and each iteration process contains 200 generations of 100 individuals (possible solutions). Thus, each inversion computed 400 000 S-waves velocity profiles.

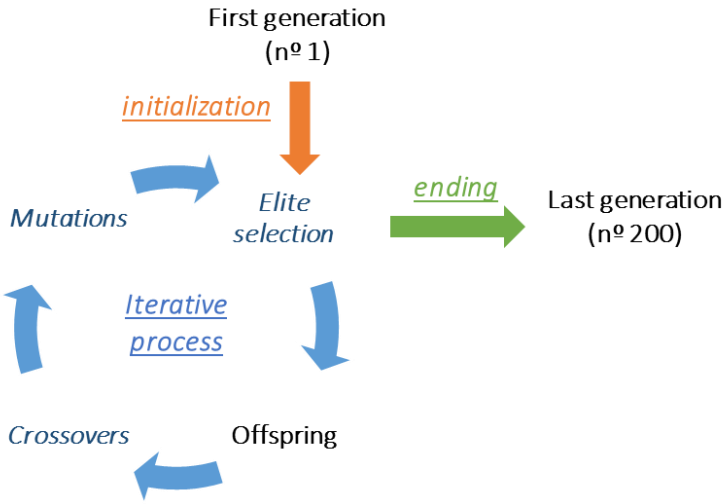

Figure 22. Schematic representation of the inversion procedure used in this work.

PART 2: RAPOLANO TERME FIELD STUDY

I. GEOLOGICAL SETTING

1. The Siena Basin

The Rapolano Terme area is located in the eastern side of the Siena Basin (Costantini et al., 1982; Martini and Sagri, 1993), a tectonic depression developed during the Neogene extensional collapse of the hinterland of the Northern Apennines (Bertini et al., 1991; Carmignani et al., 1994) (Figure 23). The Siena Basin represents the central part of a broad tectonic depression about 90 km long and NNW-SSE oriented (Figure 24), known as the Siena-Radicofani Basin (Bossio et al., 1993, with references therein).

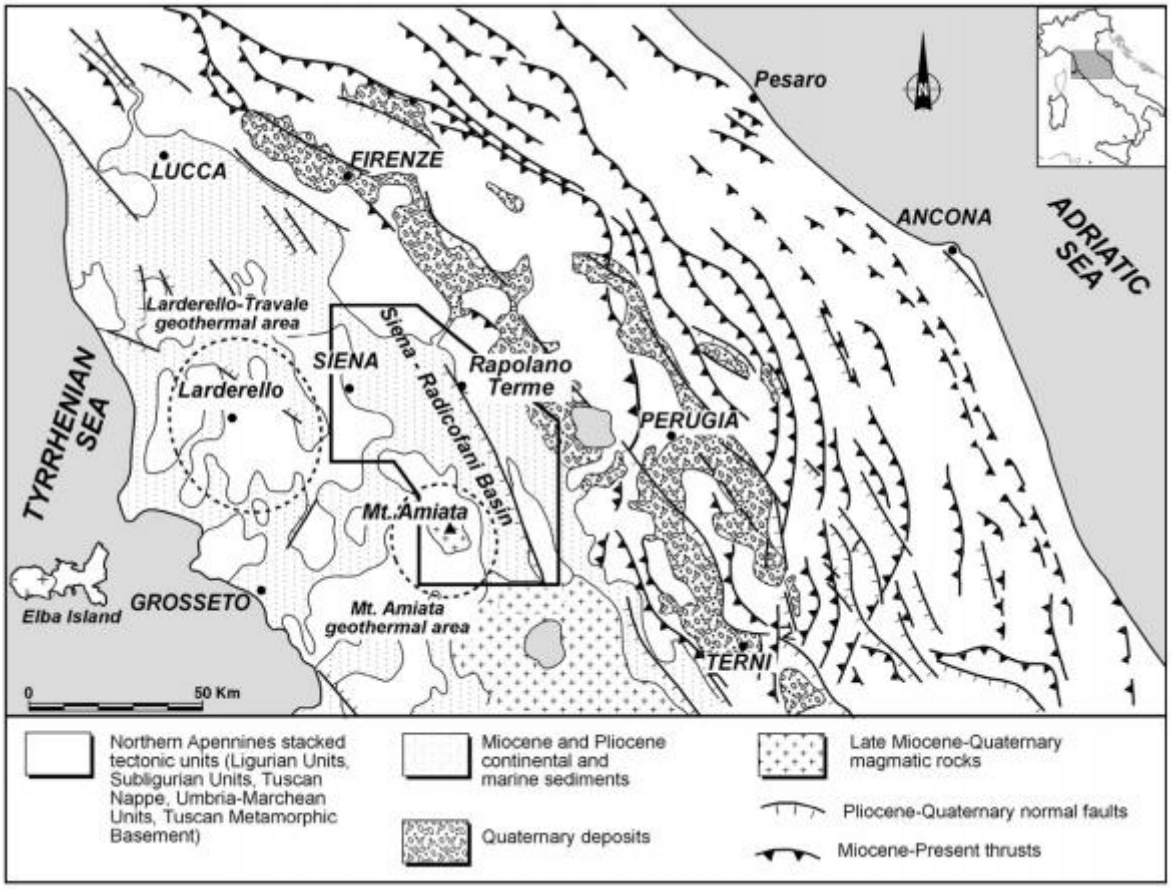

Figure 23. Geological sketch map of the Northern Apennines and its geological evolution (from Liotta et al., 1998, modified by Brogi, 2007). The location of the study area, enlarged in Figure 9, is also indicated.

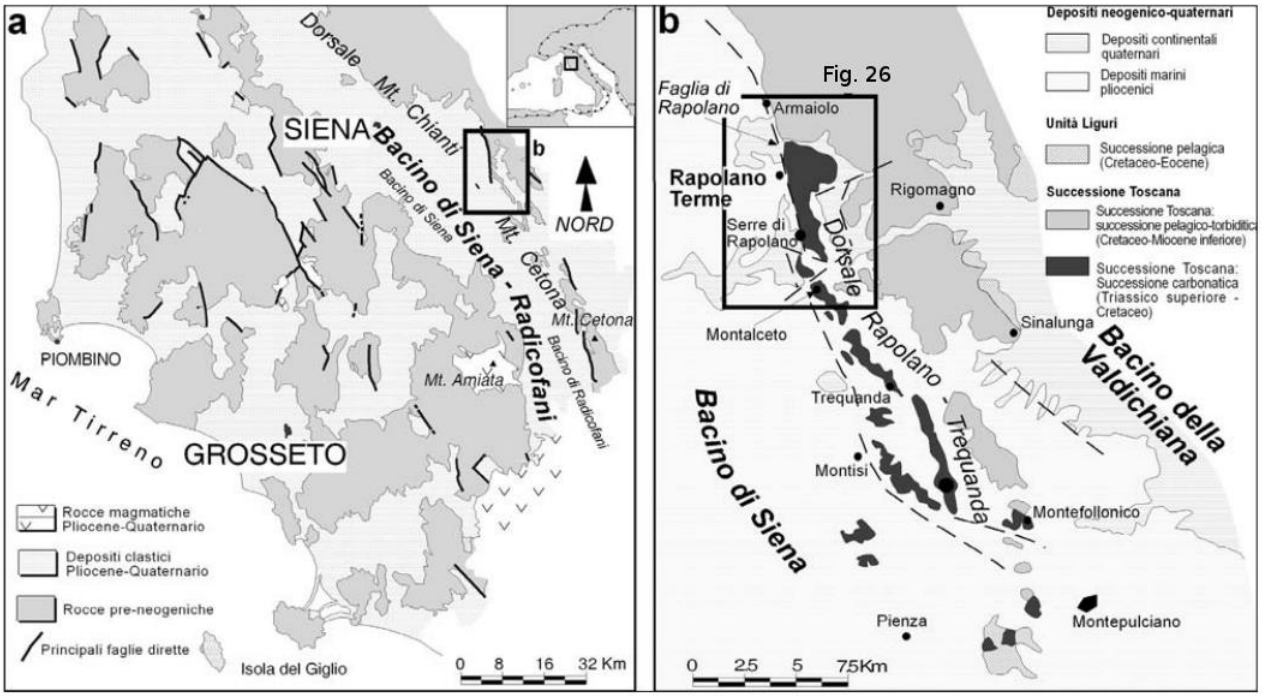

Figure 24. a) Geological sketch map of the Siena-Radicofani Basin. The black rectangle indicates the enlarged area in b. b) Geological sketch map of the Rapolano area and Rapolano-Trequanda ridge. The black rectangle indicates the study area.

The northern part of this tectonic depression, named the Casino Basin, was mainly filled by Late Miocene continental to brackish sediments (Lazzarotto and Sandrelli, 1977). The southern part (of the Radicofani Basin) consists of Early-Middle Pliocene marine sediments, whereas Middle-Late Miocene deposits were encountered at depth by boreholes (Bossio et al., 1993; Liotta, 1996, 1994; Liotta and Salvatorini, 1994). In the central part (of the Siena Basin), Early-Middle Pliocene and Quaternary deposits are broadly exposed (Costantini et al., 1982; Gandin, 1982; Gandin and Sandrelli, 1992).

Pliocene sediments mainly consist of marine clays, marly-clays, sands, gravels and conglomerates. The Quaternary sediments are composed of continental gravels, sands with interbedded clays, and travertines.

2. The Rapolano Fault

The eastern margin of the Siena Basin is bounded by a west-dipping, NNW-SSE striking normal fault known as the Rapolano Fault (Bertini et al., 1991; Bonini and Sani, 2002; Brogi, 2002; Costantini et al., 1982) (Figure 24). This fault corresponds to the northern prolongation of the fault system delimiting the eastern margin of the Radicofani Basin, described for the Mt. Cetona area (Liotta, 1996; Liotta and Salvatorini, 1994; Passerini, 1965).

The Rapolano Fault separates, in several places, Neogene sediments from pre-Neogene rocks exposed in the Rapolano-Trequanda Ridge (Figure 25), part of the Mts. Chianti and Mt. Cetona morphotectonic feature where pre-Neogene carbonate and turbiditic rocks of the non-metamorphic Tuscan Succession are broadly exposed (Figure 24). They consist of Late Triassic-Cretaceous carbonate-siliceous and Cretaceous-Early Miocene pelagic-turbiditic successions (Bernoulli et al., 1979; Decandia and Lazzarotto, 1972; Kalin et al., 1979; Lazzarotto, 1973; Losacco, 1952; Losacco and Del Giudice, 1958).

The Rapolano Fault dissected both the Pliocene sediments and the Tuscan Nappe carbonate and pelagic-turbiditic successions. Faulting began during the Upper Zanclean and ended in the lower

Piacenzian. These boundaries are in correspondence with the Pliocene sedimentation of the Siena basin (Brogi et al., 2005) and with paleontological studies. Because of that, the fault is buried under deposits that are more recent and make the mapping of the structure more difficult. Nevertheless, the fault has been mapped at the surface for about 10 km from Rapolano to Trequanda and the alignment of the thermal sources allows to sketch it (Figure 26).

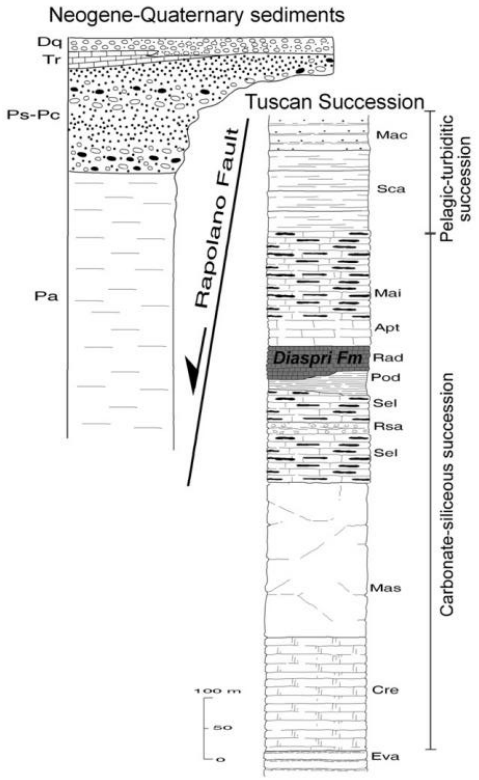

Figure 25. Tectonic and stratigraphic relationships amongst the Neogene-Quaternary sediments and pre-Neogene Tuscan succession exposed in the Rapolano Terme area (Brogi, 2007).

Key: Eva, Burano Fm (Late Trias) (only drilled); Cre, Calcari a Rhaetavicula contorta Fm (Late Trias); Mas, Calcare Massiccio Fm (Early Lias); Sel, Calcare Selcifero Fm (Middle-Late Lias); Rsa, Calcare Rosso ammonitico Fm (Late Lias); Pod, Marne a Posidonomya Fm (Dogger); Rad, Diaspri Fm (Malm); Apt, Calcari ad Aptici Fm (Early Cretaceous); Mai, Maiolica Fm (Early Cretaceous); Sca, Scaglia Toscana Fm (Early Cretaceous-Oligocene); Mac, Macigno Fm (Late Oligocene-Early Miocene); Pa, marine clays (Early-Middle Pliocene); Ps-Pc, marine sands (Ps) and conglomerates (Pc) (Early-Middle Pliocene); Tr, travertines (Pleistocene-Holocene); Dq, continental gravels, sands and clays (Pleistocene-Holocene).

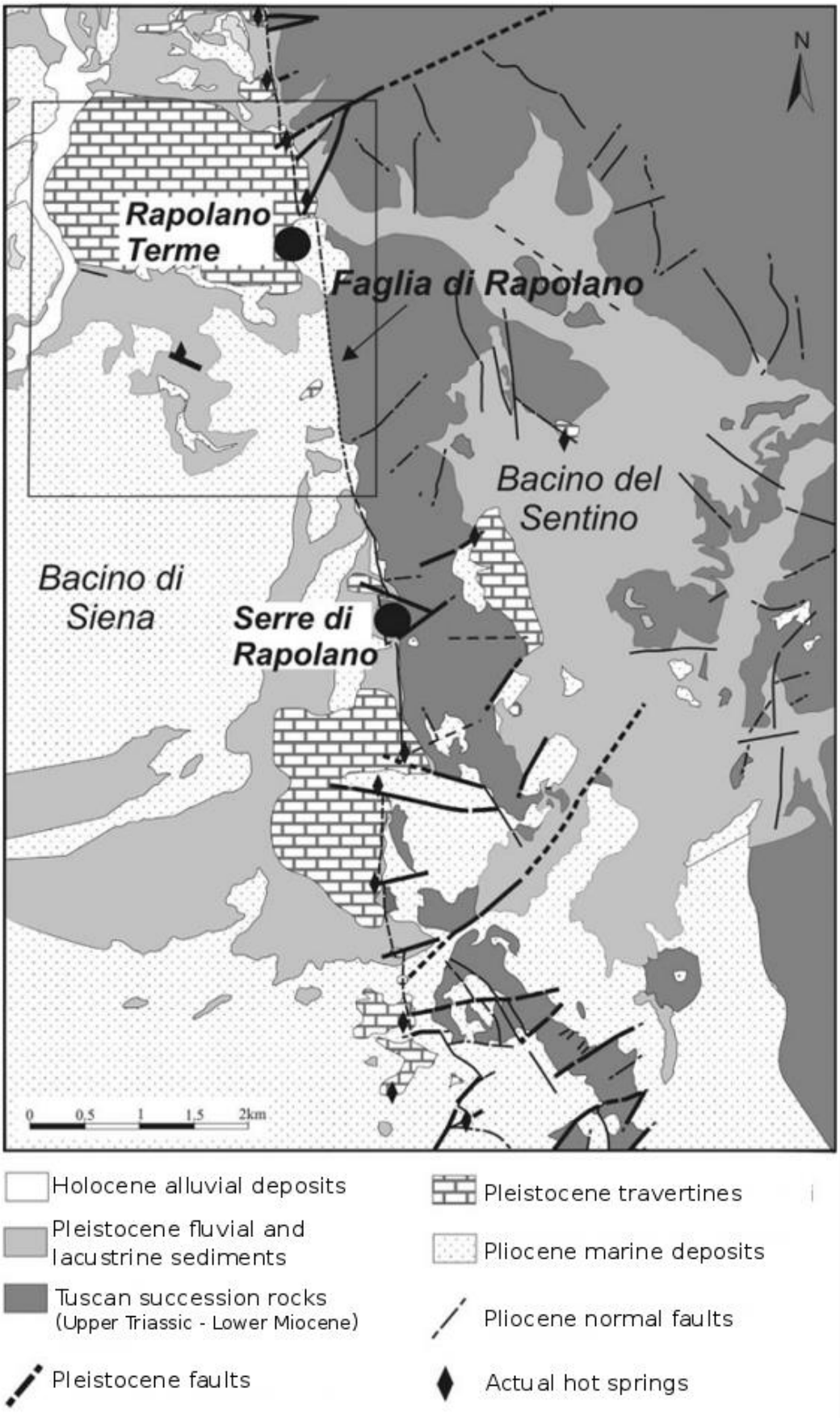

Figure 26. Geological sketch map of the Rapolano area. The travertine deposits and the present thermal springs are located along the Rapolano Fault where this latter has been dissected by Quaternary, near orthogonal faults [Brogi, 2004].

Rapolano Fault's maximum vertical displacement is greater than 500 m (Brogi, 2002), based on evidence from geological cross-sections and seismic reflection profiles (Figure 27).

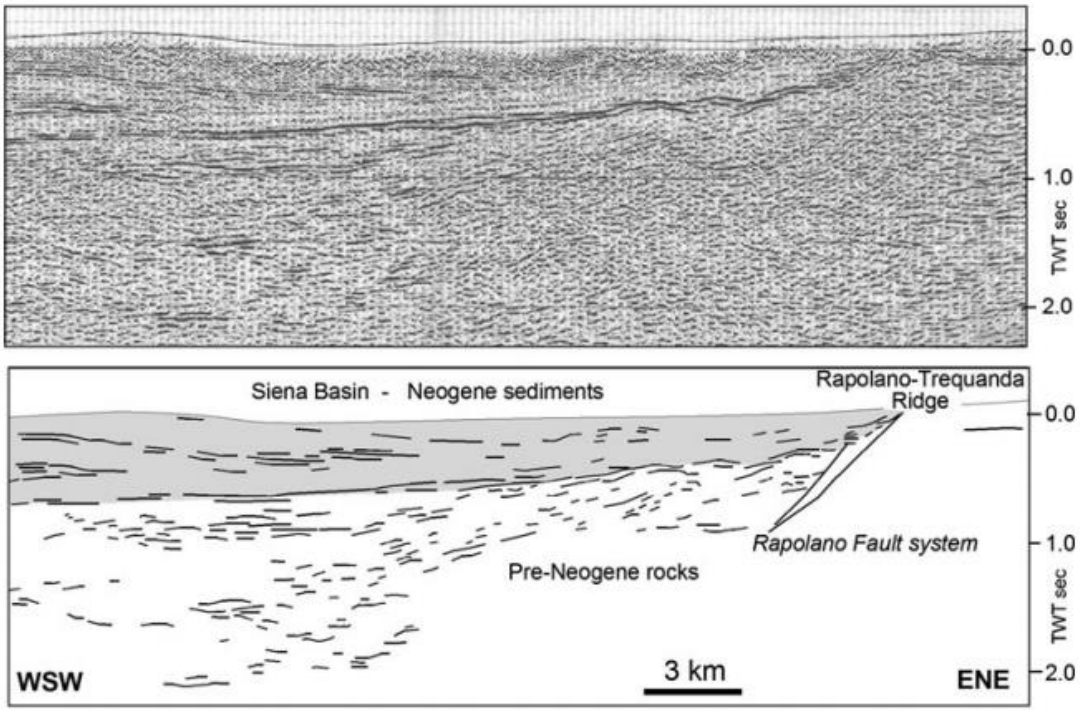

Figure 27. Reflection seismic profiles and interpretation. The trace crosses Rapolano Terme Village and its orientation is N073º. [Brogi et al., 2009].

3. Travertines, hydrothermal fluid circulation and seismic activity

Pleistocene-Holocene travertine masses and active thermal springs are aligned along the Rapolano Fault (Brogi, 2004), where these structures have been dissected by Quaternary normal faults (Figure 26). Hydrothermal fluid circulation began during the Pleistocene and is ongoing, with widespread upwelling of hydrothermal fluids (39 ºC) and CO2 leakage (Baldi et al., 1992; Brogi, 2007; Brogi and Capezzuoli, 2009; Minissale et al., 2002).

Travertines cover about 14km^2 and are up to 50m thick, they deposited by hot fluids issuing from thermal springs and flowing into adjacent morphological depressions. They are deposited in palustrine and fluvio-lacustrine envirenments, and in thin water layers running off slopes. Varying depositional geometries characterize these carbonate rocks: tabular and fan-slope bodies, fissure ridges, terraced mounds, cones and waterfall deposits (Brogi and Capezzuoli, 2009; Guo et al., 1996; Guo and Riding, 1999, 1998, 1994, 1992). Presently, they are intensely quarried for ornamental stone.

The seismic activity of the area and the travertine deposition are strongly related (Sibson, 1992). The fault-valve conceptual model suggests that the cycle of seismic stress produces cycling reopening of fractures and the reactivation of permeability linked to earthquake occurrence on faults. Thus, the travertine dating indicates a tectonic activity at least ascribed to the Middle-Late Pleistocene (Figure 28) (Brogi et al., 2009).

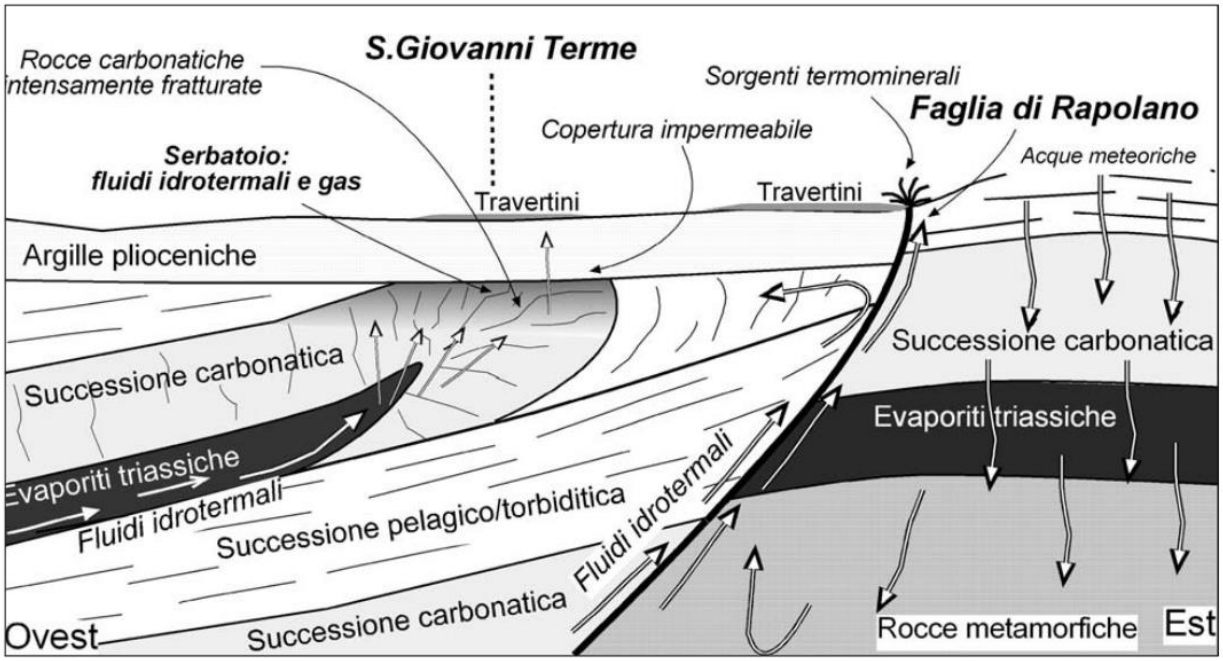

Figure 28. Schematic, not to scale, geological cross-section, W-E oriented, showing the relationships between the tectonic setting of the Terme S.Giovanni area and the hydrothermal fluid circulation. The fluids arising along the damaged zone of the Rapolano Fault follow a shallow pathway: in contrast, the hydrothermal fluids flowing from the Terme S,Giovanni thermal springs circulate at deepest levels. They are stocked within the nucleus of the Mt. Cetona anticline (dissected by the Rapolano Fault in this zone) which gives rise to a reservoir due to the highly fractured carbonate rocks. The fluids can escape toward the surface through vertical fractures related to the damaged zone of a fault system to which the normal fault giving rise to the travertine fissure-ridge belongs. All these faults are about parallel to the geological section and thus they cannot be reported (Brogi et al., 2007).

4. Geological map

The geological map presented at Figure 29 covers the whole study area. The legend that is used in this map and in the following ones is given at Figure 30.

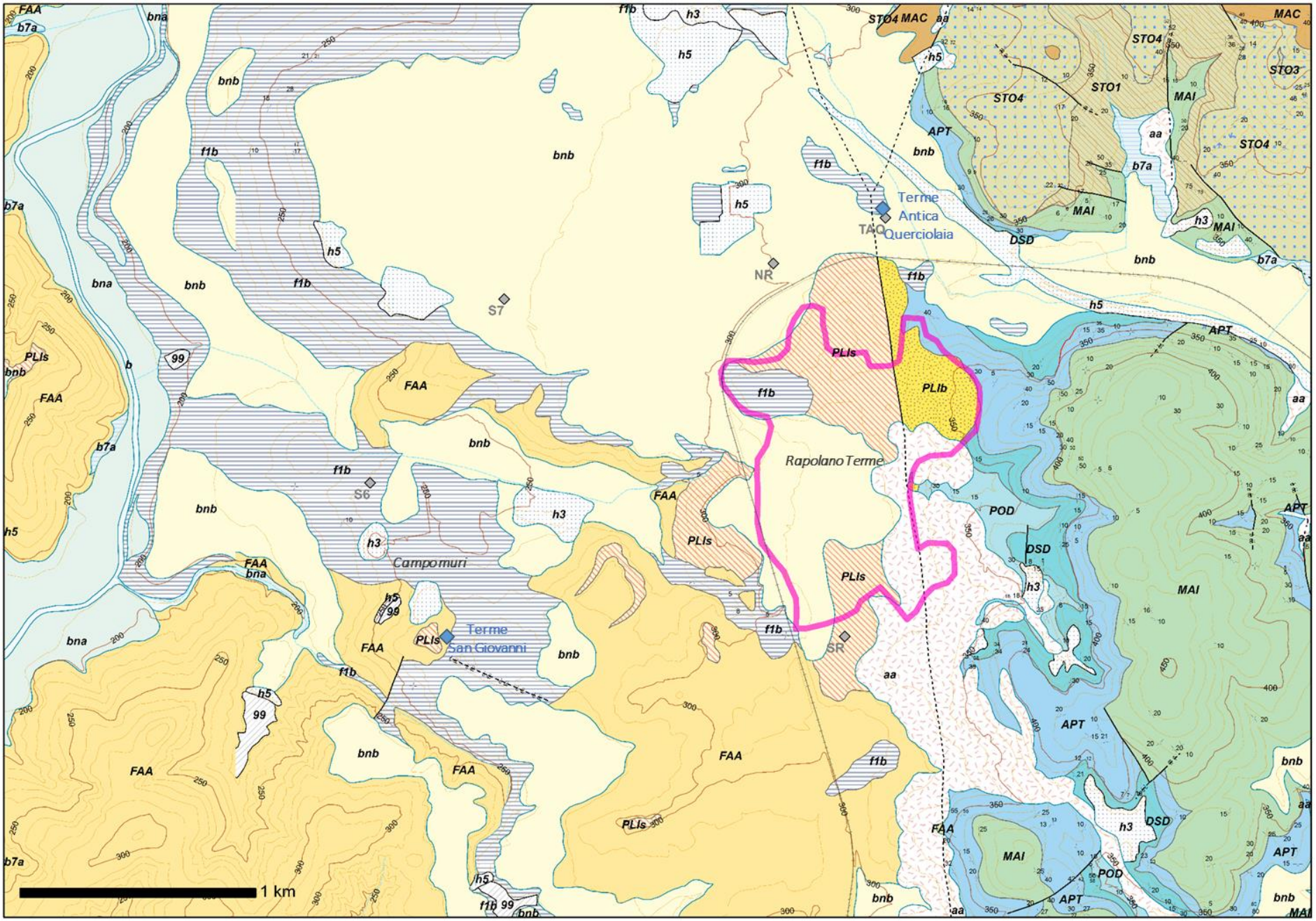

Figure 29. Geological map of Rapolano Terme Area (Lazzarotto et al., 2008). The legend is presented at Figure 30.

Figure 30. Legend of the geological map.

II. MEASUREMENT CAMPAIGNS AND DATA ANALYSIS

Altogether, 86 single station measurements have been realized in order to cover the study area with a dense grid of points and to characterize the different geological formations. Few recordings were made in the same emplacement in order to check the repeatability of the measures. In addition, 4 array measurements have been deployed on different geological materials. The whole campaign took place between the 26th June and the 3rd August 2014.

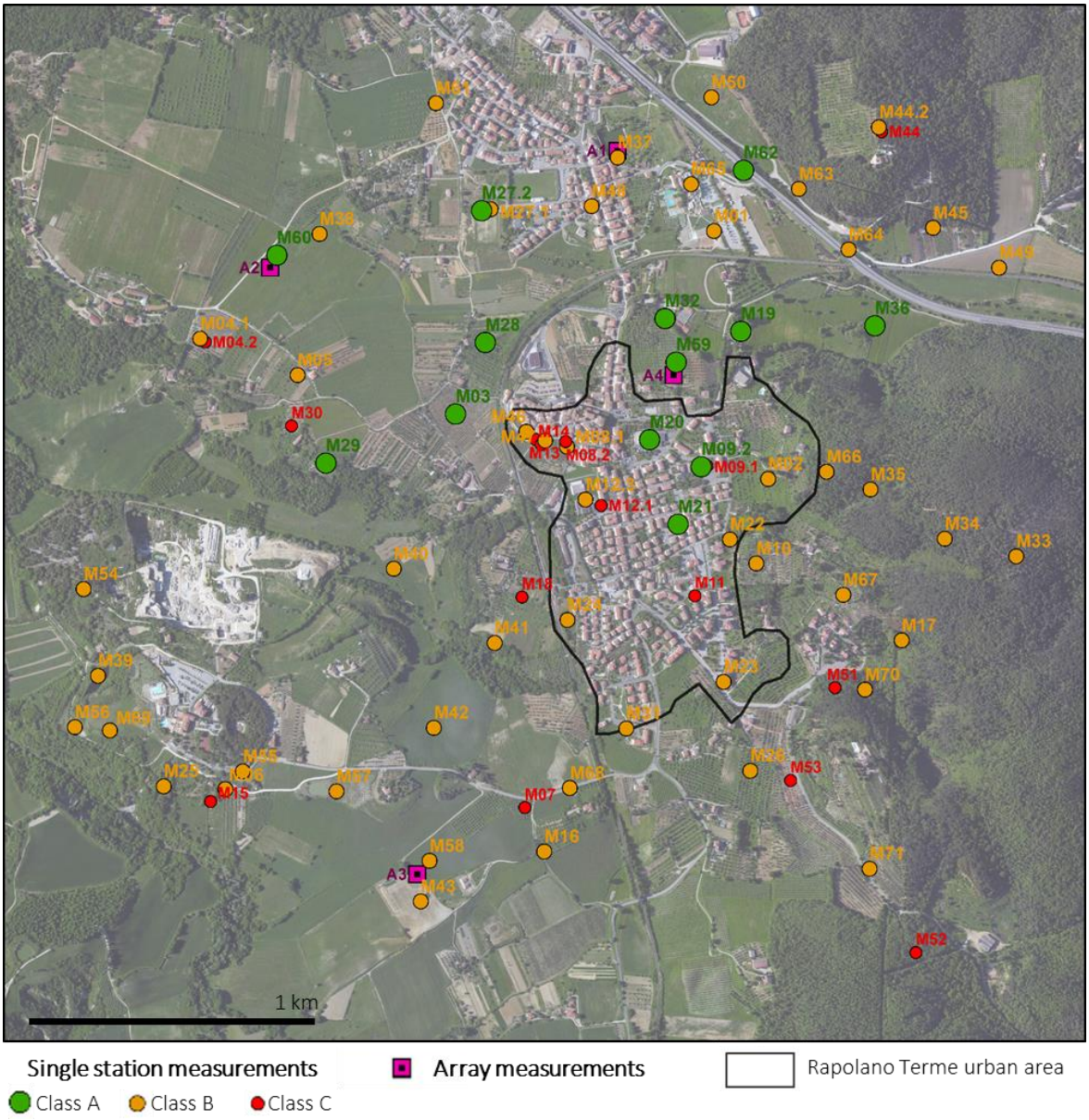

Figure 31. Ambient vibrations measurements location. Single station measurements are represented classified in quality classes: trustworthy and interpretable (class A), suspicious and to be used if it is coherent with other measurements performed nearby (class B) and to be discarded (class C).

1. Single station campaign

For the single station recordings, TROMINO sensors have been used (Figure 7). Almost all recordings last 20 minutes and the sampling frequency is 128 Hz.

a. Data management

Every measurement has been georeferenced on a GIS system (ArcGIS) and a report has been done for each one. This last contains information about the experimental conditions (soil-sensor

coupling, weather conditions…) and pictures of the measurement. As well, the analysed data is represented by the HVSR curve plot, a plot showing the HVSR curve in each time series window, another one with the HVSR curve in function of the azimuthal direction and a last one with the three ground motion spectral components. The peak frequency and its amplitude are also presented. Finally, the statistical reliability criteria (from SEAME, 2005) is computed. These reports are presented on annex I.

b. Nearby anthropic disturbances

After each campaign, the measurements have been quickly analyzed in order to check their quality. The first HVSR curves ,obtained on working days, showed narrow peaks in the three directions (N, E, up). These recordings, strongly distorted have been classified in class C, namely not reliable (Table 2).

These peaks are originated by monochromatic disturb sources as factories, works, pumps, etc. A possible hypothesis is that the travertine industry, important at Rapolano Terme, may be the cause of these disturbances, especially the activity related to cutting the rock.

In order to found out if this is linked to industrial activity, other measurements were made on the same location through different days of the week. On week-end recordings, particularly on Sundays, the disturbances are still present but amplitude is smaller and the HVSR curves look interpretable (Figure 32 and Figure 33). For this reason, the following measurements were done on Sundays.

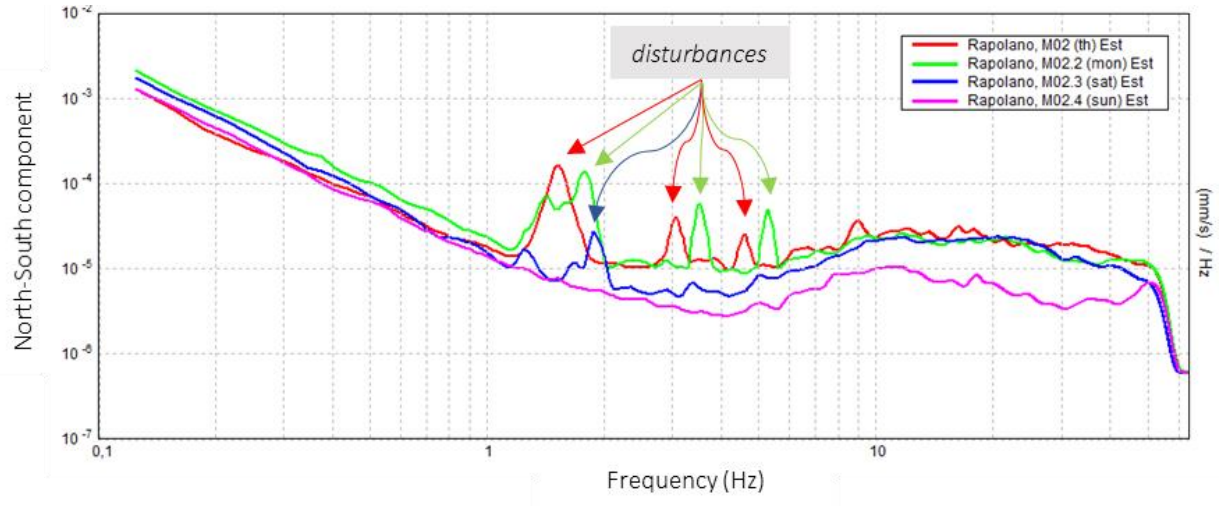

Figure 32. East-West spectral ground motion component realized on Thursday (red), Monday (green), Saturday (blue) and Sunday (purple) on site M02.

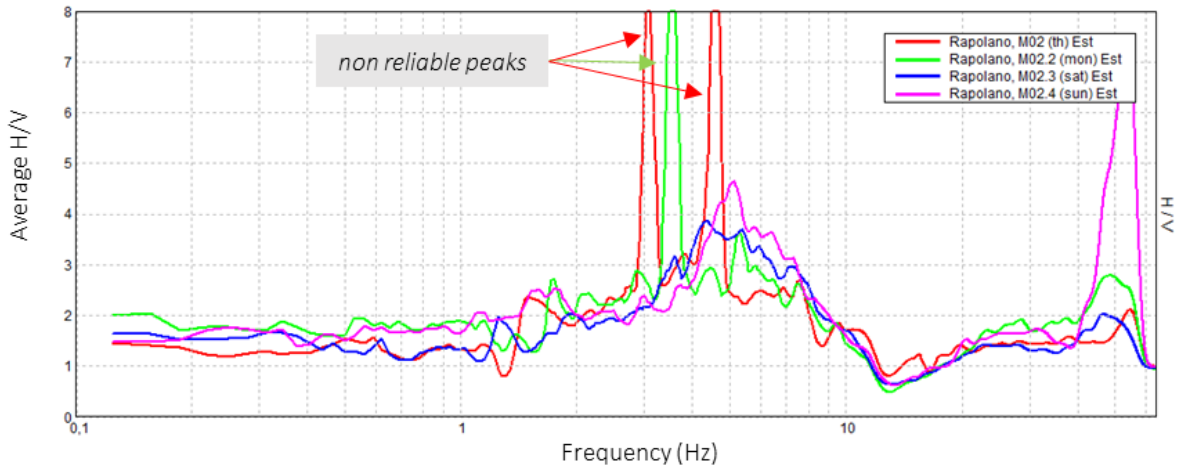

Figure 33. Industry disturbances on HVSR curves.

c. Data quality

Once the HVSR curves were obtained, the reliability of each one was evaluated using the criteria presented in “Criteria for assessing the quality of measurements” (p. 15). Eventually, 13 measurements were classified as trustworthy and interpretable (class A), 49 as suspicious, namely to be used with caution if they are coherent with other measurements performed nearby (class B) and 24 recordings are not interpretable and have to be discarded (class C). This moderate quality is explained in consequence of the presence of artefacts from anthropic origin and because the isotropy criteria was generally not fulfilled, respectively affecting 65% and 57% of class B HVSR curves (Table 2).

Regarding the “peak clearness”, the SESAME (2004) conditions were not attained for the majority of the recordings, only 8 measurements show a “statistically clear peak”. This is due to the disturbances, or because the peak cover a more or less large frequency band (Figure 31 and 34).

point ID	day of the week	reliability criteria						class	type
		stationarity	isotropy	no disturb	physical plausibility	statistical robustness	duration		
M01.1	thu	-	-	NO	-	-	-	C	-
M01.2	mon	-	-	NO	-	-	-	C	-
M01.3	sat	-	-	NO	-	-	-	C	-
M01.4	sun	OK	OK	NO	OK	OK	OK	B	
M02.1	thu	-	-	NO	-	-	-	C	-
M02.2	mon	-	-	NO	-	-	-	C	-
M02.3	sat	-	-	NO	-	-	-	C	-
M02.4	sun	OK	OK	NO	OK	OK	OK	B	2
M03	sun	OK	OK	OK	OK	OK	OK	A	2
M04.1	sun	NO	OK	OK	OK	OK	OK	B	2
M04.2	sun	-	-	NO	-	-	-	C	2
M05	sun	NO	OK	OK	OK	OK	OK	B	2
M06	sun	NO	NO	NO	OK	OK	NO	B	2
M07	sun	OK	NO	NO	OK	OK	OK	C	2
M08.1	sun	OK	NO	NO	OK	OK	OK	B	2
M08.2	sat	-	-	NO	-	-	-	C	2
M09.1	sun	NO	OK	NO	OK	OK	NO	C	2
M09.2	sun	OK	OK	OK	OK	OK	OK	A	2
M10	sun	OK	NO	NO	OK	OK	OK	B	2
M11	mon	-	-	NO	-	-	-	C	2
M12.1	mon	-	-	NO	-	-	-	C	2
M12.2	sat	-	-	NO	-	-	-	C	2
M12.3	sun	OK	OK	NO	OK	OK	OK	B	2
M13	mon	-	-	NO	-	-	-	C	2
M14	mon	-	-	NO	-	-	-	C	2
M15	sat	-	-	NO	-	-	-	C	2
M16.1	sat	-	-	NO	-	-	-	C	2
M16.2	sun	OK	NO	NO	OK	OK	OK	B	2
M17	sat	OK	NO	NO	OK	OK	OK	B	2
M18	sat	-	-	-	-	-	-	C	2
M19.1	sat	-	-	NO	-	-	-	C	2
M19.2	sun	OK	OK	OK	OK	OK	OK	A	2
M20	sun	OK	OK	OK	OK	OK	OK	A	2
M21	sun	OK	OK	OK	OK	OK	OK	A	2
M22	sun	OK	OK	NO	OK	OK	OK	B	2
M23	sun	OK	OK	NO	OK	OK	OK	B	2
M24	sun	OK	NO	NO	OK	OK	OK	B	2
M25	sun	OK	OK	NO	OK	OK	OK	B	1
M26	sun	OK	NO	OK	OK	OK	OK	B	2
M27.1	sun	OK	OK	OK	OK	OK	NO	B	1
M27.2	sun	OK	OK	OK	OK	OK	OK	A	1
M28	sun	OK	OK	OK	OK	OK	OK	A	1
M29	sun	OK	OK	OK	OK	OK	OK	A	1
M30	sun	NO	OK	NO	OK	OK	NO	C	2
M31	sun	OK	NO	OK	OK	OK	OK	B	2
M32	sun	OK	OK	OK	OK	OK	OK	A	2
M33	sun	OK	NO	NO	OK	OK	OK	B	1
M34	sun	OK	NO	NO	OK	OK	OK	B	1
M35	sun	OK	NO	NO	OK	OK	OK	B	2
M36	sun	OK	OK	OK	OK	OK	OK	A	2
M37	sun	OK	NO	OK	OK	OK	OK	B	2
M38	sun	OK	OK	NO	OK	OK	OK	B	2
M39	sun	NO	OK	NO	OK	OK	OK	B	2
M40	sun	OK	NO	NO	OK	OK	OK	B	2
M41	sun	OK	OK	OK	OK	OK	OK	B	2
M42	sun	OK	NO	OK	OK	OK	OK	B	2
M43	sun	OK	NO	OK	OK	OK	OK	B	2
M44.1	sun	OK	NO	NO	OK	OK	OK	C	2
M44.2	sun	OK	OK	NO	OK	OK	OK	B	2
M45	sun	OK	NO	OK	OK	OK	OK	B	1
M46	sun	OK	NO	NO	OK	OK	OK	B	2
M47	sun	OK	NO	NO	OK	OK	OK	B	2
M48	sun	OK	OK	OK	OK	OK	OK	B	2
M49	sun	OK	NO	NO	OK	OK	OK	B	2
M50	sun	OK	NO	OK	OK	OK	OK	B	2
M51	sun	OK	NO	NO	OK	OK	OK	C	2
M52	sun	OK	NO	NO	OK	OK	OK	C	2
M53	sun	OK	NO	NO	OK	OK	OK	C	2
M54	sun	OK	OK	NO	OK	OK	OK	B	2
M55	sun	OK	OK	NO	OK	OK	OK	B	2
M56	sun	OK	OK	NO	OK	OK	OK	B	2
M57	sun	OK	NO	NO	OK	OK	OK	B	2
M58	sun	OK	OK	NO	NO	OK	OK	B	2
M59	sun	OK	OK	OK	OK	OK	OK	A	2
M60	sun	OK	OK	OK	OK	OK	OK	A	2
M61	sun	NO	OK	OK	OK	OK	OK	B	2
M62	sun	OK	OK	OK	OK	OK	OK	A	2
M63	sun	OK	NO	OK	OK	OK	OK	B	2
M64	sun	OK	NO	OK	OK	OK	NO	B	2
M65	sun	NO	NO	OK	OK	OK	NO	B	2
M66	sun	OK	NO	NO	OK	OK	OK	B	2
M67	sun	Ok	OK	NO	OK	OK	OK	B	2
M68	sun	OK	NO	NO	OK	OK	OK	B	2
M69	sun	OK	OK	NO	OK	OK	OK	B	2
M70	sun	NO	NO	NO	OK	OK	OK	B	2
M71	sun	NO	NO	OK	OK	OK	OK	B	2

Table 2. Reliability of single station measurements.

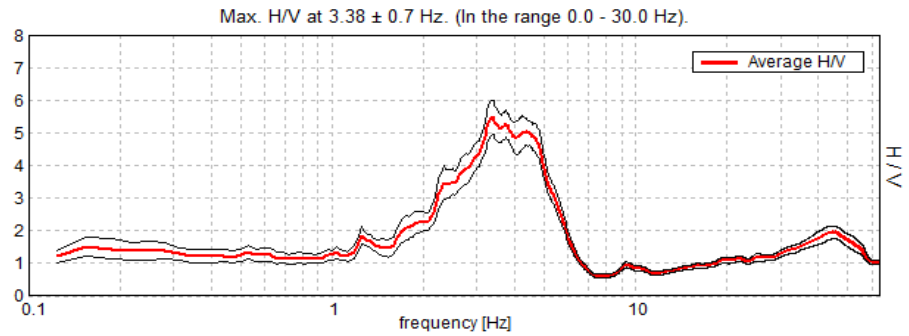

Figure 34. HVSR peak classified as type 2. Even if its shape is not sharp and symmetric, the peak looks interpretable (measurement M21, class A).

2. Multi-station campaign

a. Measurements

In order to obtain the dispersion curves (Rayleigh waves velocity,V_R, vs frequency), 4 array measurements in 2D configuration were carried out on Tuesday 29th of July. For these recordings, 16 vertical geophones with a 4.5 Hz resonance frequency and a digital acquisition system BrainSpy produced by Micromed have been used (Figure 17). The geophones were displayed in a cross array configuration with irregular spacing (Figures 31 abd 35). The recordings last 20 minutes and the sampling frequency is 128 Hz.

The location of these array measurements have been selected in order to sample different geological materials and configurations (Figure 37).

- The array A1 has been carried out on quaternary travertine deposits (*f1b*)
- The array A2 has been realized on quaternary alluvial terrace deposits, probably lying on travertines (*bnb*)
- The array A3 has been effected on marine Pliocene Azure clays formation (*FAA*)
- The array A4 has been executed on marine Pliocene sands and sandstones deposits (*PLIb*).

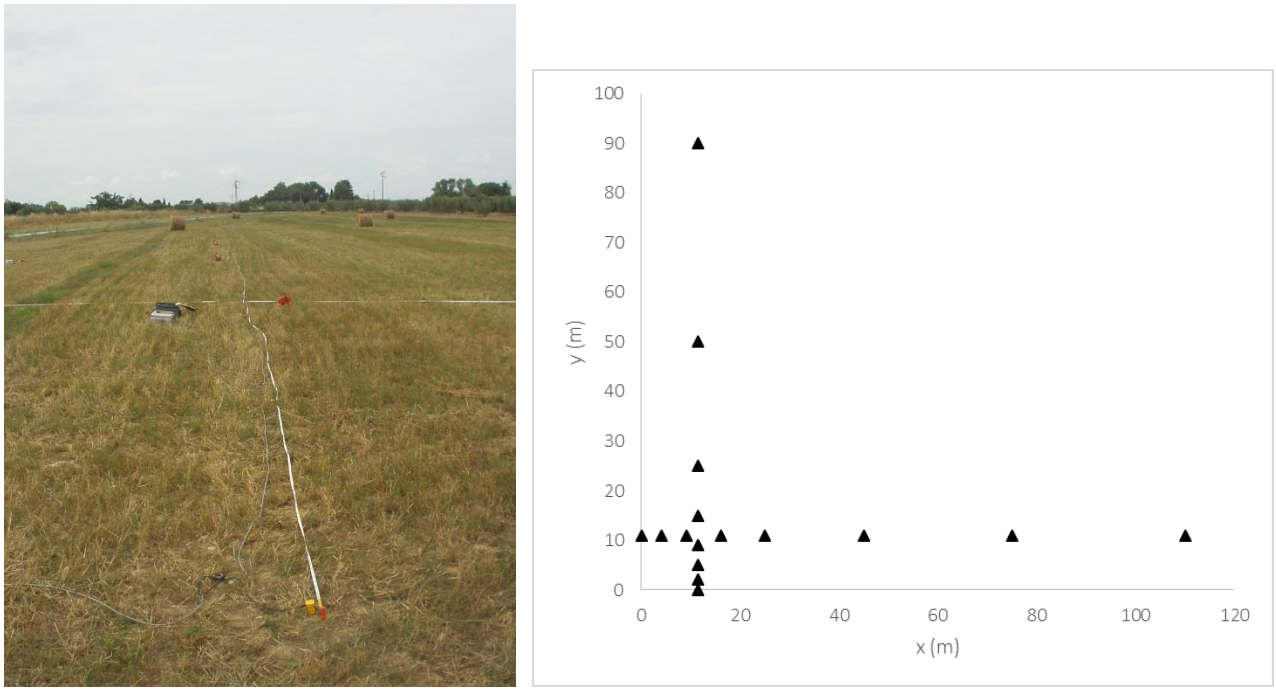

Figure 35. A2 array configuration: cross with irregular spacing (each triangle represents a geophone).

The shortest and longest inter-geophone distance are relevant to define the reliable frequency band of the dispersion curves, as well as to determine the exploration depths. These values are shown in Table 3.

array	A1	A2	A3	A4
shortest inter-geophone distance (m)	1	2	2	2,7
longest inter-geophone distance (m)	115	126	127	107

Table 3. Shortest and longest inter-geophone distance of each array measurement.

b. Dispersion curves

The dispersion curves have been computed with the ESAC and f-k procedures (Figure 36). These curves are discussed further, in section “Results interpretation” (p. 39).

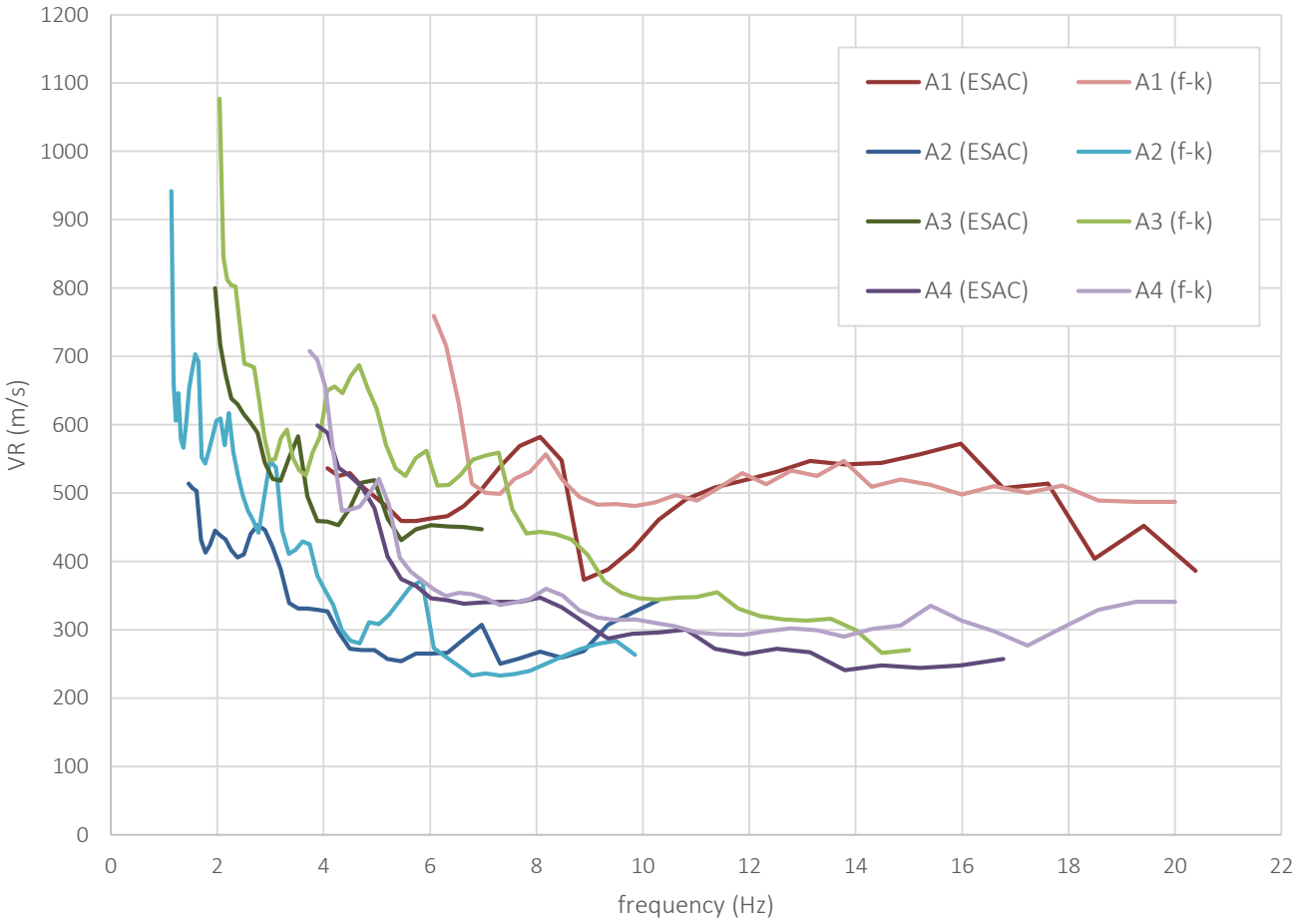

Figure 36. Dispersion curves obtained from array recordings with the ESAC end f-k procedures.

III. RESULTS INTERPRETATION

In this section, the results obtained from both the single station and array measurement campaigns are presented and a geological interpretation is given.

1. Frequencies map

The frequencies map (Figure 37) sums up the HVSR curves obtained with the single station measurements. Each dot represents one measuring point. If the dot is white, the HVSR curve is flat, otherwise its colour indicates the HVSR peak frequency. The size of each coloured dot reflects the HVSR peak amplitude. Finally, the quality class of the recording point is marked with *A* for trustworthy curves and with *B* for curves which should be used with caution and only if it is coherent with other measurements performed nearby.

Along the Rapolano Fault, the HVSR curves present peaks with high amplitude and frequency comparing to the other areas. Westwards the frequency and the amplitude of HVSR peaks decrease progressively. Eastwards, there is not a general trend, nevertheless the amplitudes and frequencies are lower than the ones close to the fault. This quick analysis allows to confirm that resonance phenomenon are expected at the study area. These may be stronger along the Rapolano Fault, namely where HVSR peak amplitudes are higher. There, the resonance frequencies are comprised between 2.6 and 6Hz.

To have a better comprehension, the study are has been divided in five zones which show rather similar characteristics. For each ones, results obtained from both single station and multi-station ambient vibrations measurements are presented. Then an interpretation is given in concordance with the local geological setting and with information from other surveys carried out in the study area (Annex II).

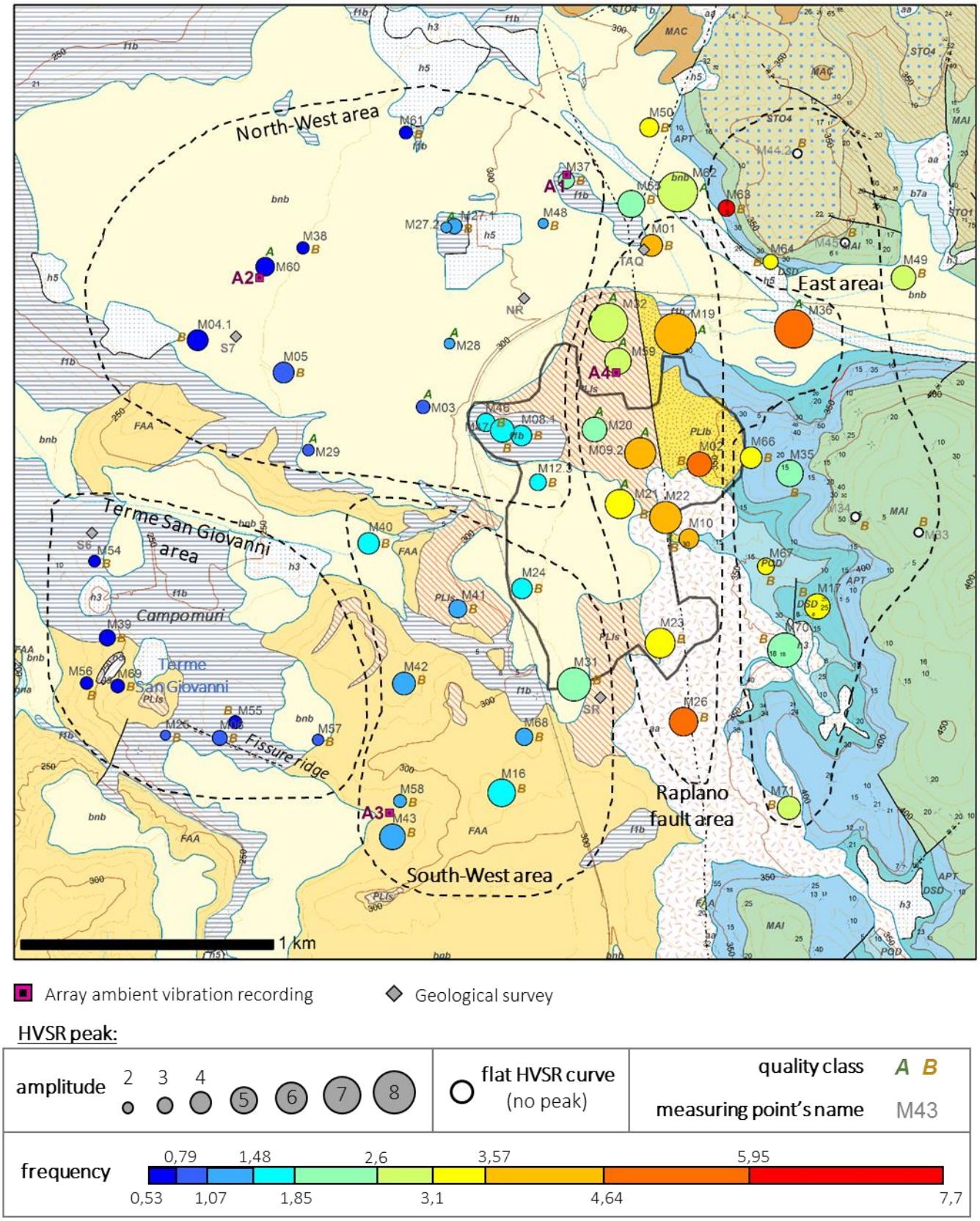

Figure 37. Frequencies map and sub-areas division.

2. North-West area

The North-West zone is a flat area, gently leaning westward. The surface is covered by alluvial terrace sediments (bnb) lying on travertines masses (f1b) also softly dipping toward West, both dated from the Middle-Late Pleistoce. Near to the Rapolano Fault, there is an active hot spring that is being operated by a wellness centre named Terme Anitca Querciolaia, and it is associated to actual travertines deposition.

Close to “NR” geological survey (Annex II) the travertines are locally called “gallazzone”, which refers to the fact that carbonate deposition from hydrothermal contribution was contemporaneous to continental sands and silts deposition. For this reason, the carbonate deposits are thinly layered, non-mature and impure. At the East side of the area, close to the Rapolano Fault, layered travertines outcrop and in the first 6.5 meters of subsoil at Terme Antica Querciolaia (“TAQ”) borehole (Annex II), and between 1 and 5 m deep at “NR” borehole. .However, at the West side of the area a more compact and brighter type of travertines outcrop, with thicknesses up to 60-80 meters. At the borehole S7 (Annex II), no travertines have been found in the first 15 meters below the surface. These continental Quaternary materials made of the terraced sediments (bnb) and travertines (f1b) deposited on marine Pliocene sediments, constituted by the yellow sands and sandstone formation (PLIs), the azure clays formation (FAA).

In this area, 16 single measurements have been carried out on the terrace alluvial sediments (bnb) and on travertines masses (f1b). Among these ones, 5 are classified as class A (good quality) and 11 as class B (middle quality). As well, two array recordings named A1 and A2 have been realized on eastward travertines deposits (A1) and on westward terrace alluvial sediments (A2) respectively.

Single station measurements and HVSR curves

The HVSR curves present broad peaks (class 2), at low frequencies increasing eastward from 0.25 to 2.1 Hz (Figure 38). The peaks’ amplitude is comprised in between 1.9 and 4.0. These peaks are associated to an impedance contrast, probably this corresponds to the contact between the Pliocene marine sediments (FAA) and the bedrock, formed by pre-Neogene rocks. The frequencies increase eastward indicates that this contact may be deeper towards West, so it is probably lightly dipping westward.

At high frequencies, the H/V spectral ratio is below zero for frequencies in between 2-5Hz and 30-50Hz. This trend shows a probable velocity inversion, namely the existence of a stiffer strata (high Vs) lying on a softer one (lower Vs). It can be hypothesised that a more compact travertine layer is present within the Neogene sediments.

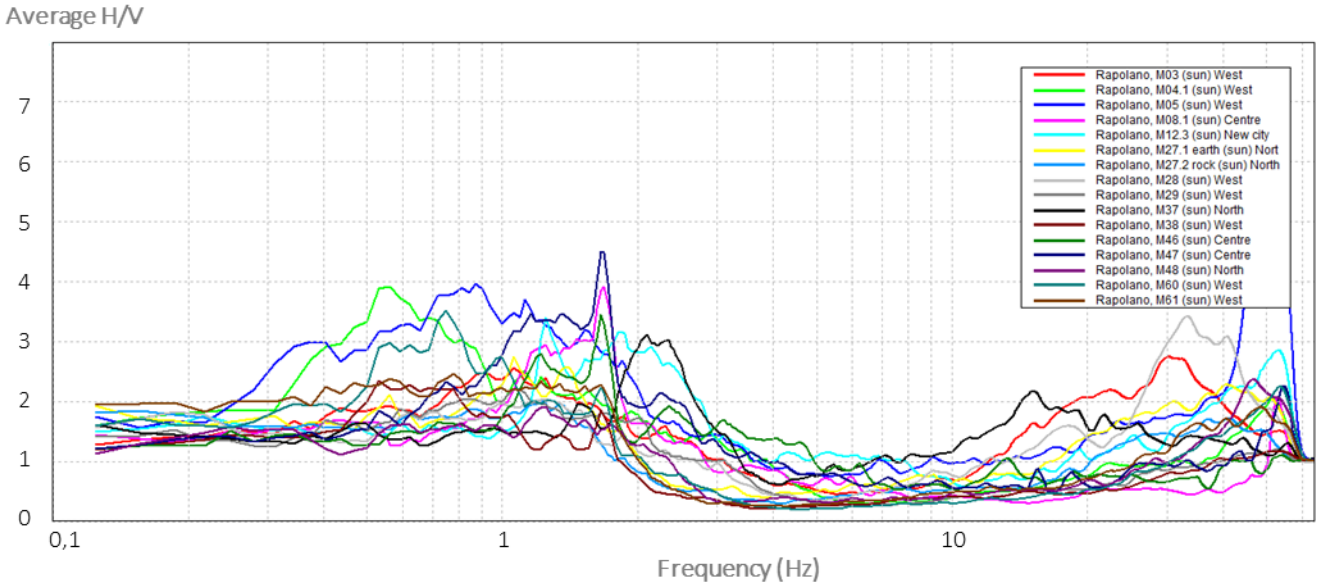

Figure 38. HVSR curves from North-West Rapolano measuring points: M03, M04.1, M05, M08.1, M12.3, M27.1, M27.2, M28, M29, M37, M38, M46, M47, M48, M60, M61.

Array measurement A1 and dispersion curves

The first array measurement, A1, was realized on layered travertine deposits (f1b) at Parco delle Acque, close to Terme Antica Querciolaia. The geophones have been placed following an irregular spacing cross configuration scheme. The first axis is 110m long and with an azimuth of 155º (toward SSE), and the second axis is 66m long, perpendicular to the first one. The shortest inter-geophone distance is 1m and the longest one is 115m (Figure 39).

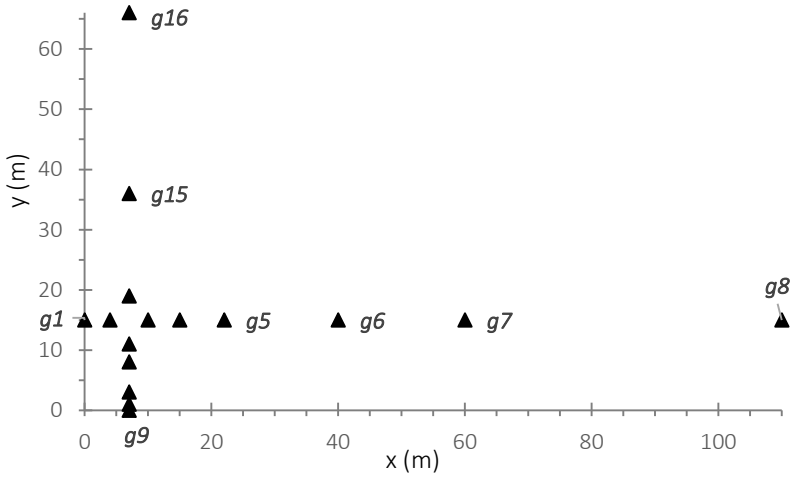

Figure 39. Array A1 configuration (the triangles represent the 16 geophones distribution).

The dispersion curves have been computed with the ESAC and f-k procedures (Figure 40). The two results have a similar trend between 7 and 9 Hz, and between 11 and 18 Hz. In these frequency domains, the surface wave velocities (V_R) are comprised between 500 and 550 m/s. The ESAC velocities show a non-classic trend. First, at low frequencies (corresponding to deeper profundities), the velocities are pretty low, not higher than 580 m/s, whereas the f-k results give velocities up to 760m/s. Also, at 9 Hz the ESAC surface wave velocities show a gap below 400m/s. The f-k curve shows a more classical trend, so it has been chosen to perform the joint inversion.

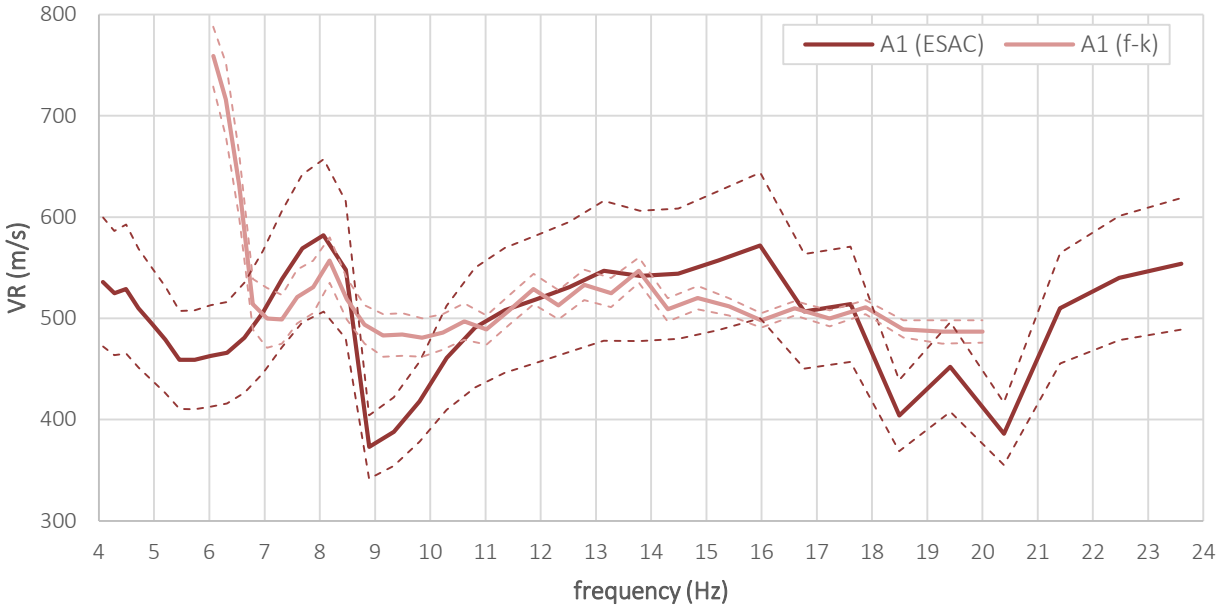

Figure 40. Array A1 dispersion curves (and 95% confidence intervals) computed with ESAC and f-k procedures.

Joint inversion A1

Combining the dispersion curve from array A1 and the HVSR curve from single station measurement M37, the S-wave velocities profile has been computed through a joint inversion (Figure 41). The modelled dispersion curve succeed in fitting the experimental one from 8 Hz onwards.

At 60 m deep, the S-wave velocities jump from 520 m/s to 1270 m/s (Figure 42). The materials above this contrast have an average velocity of 490 m/s. This abrupt velocity increase is probably referred to the contact between the Neogene sediments and the bedrock constituted by pre-Neogene rocks.

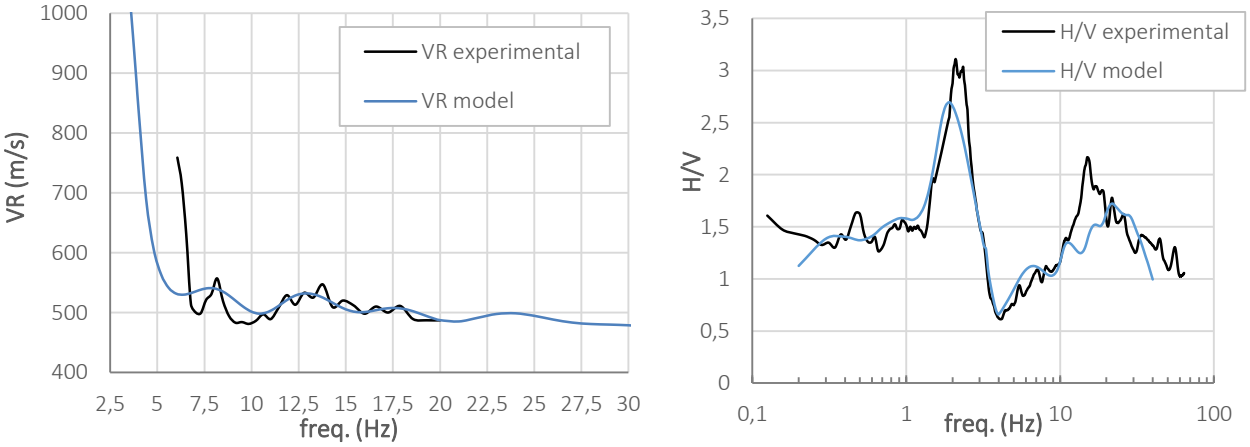

Figure 41. Inversion A1 experimental and model curves: dispersion curves (left) and HVSR curves (right).

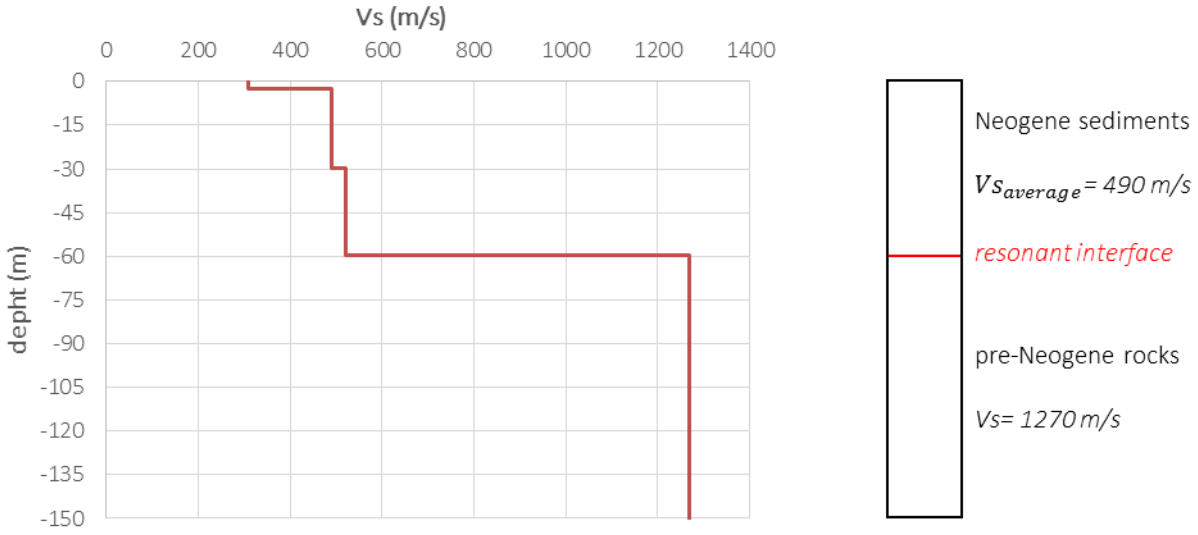

Figure 42. Inversion A1 S-wave velocity profile (left) and geological interpretation (right).

Array measurement A2 and dispersion curves

The second array measurement, A2, was carried out on terraced sediments (bnb) probably lying on travertine deposits because of its bright colour. The first axis of the cross array configuration is 110 m long and directed to South-West, and the second one is 90 m long, oriented to North-West. The shortest inter-geophone distance is 2 m and the longest one is 126 m (Figure 43).

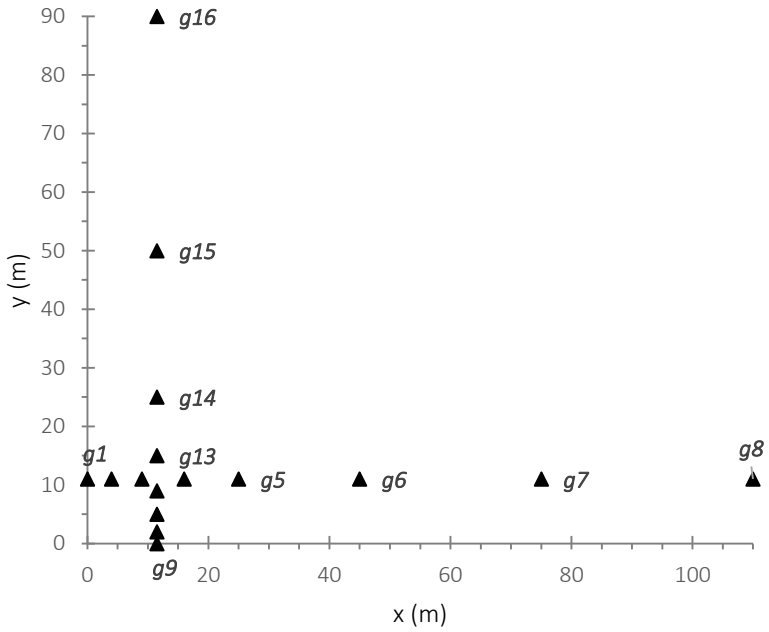

Figure 43. Array A2 configuration (the triangles represent the 16 geophones distribution).

The dispersion curves computed with the ESAC and f-k procedures (Figure 44) are similar from 1.5 Hz and 10 Hz. For higher frequencies, the waves' energy was not enough to give reliable results (the curves show different and strange trends). Between 6 and 9 Hz, surface wave velocities (V_R) are comprised between 200 and 300 m/s. At lower frequencies, the velocity increases until more than 800 m/s (f-k), and at lower frequencies, the velocity calculated with both procedures increases lightly.

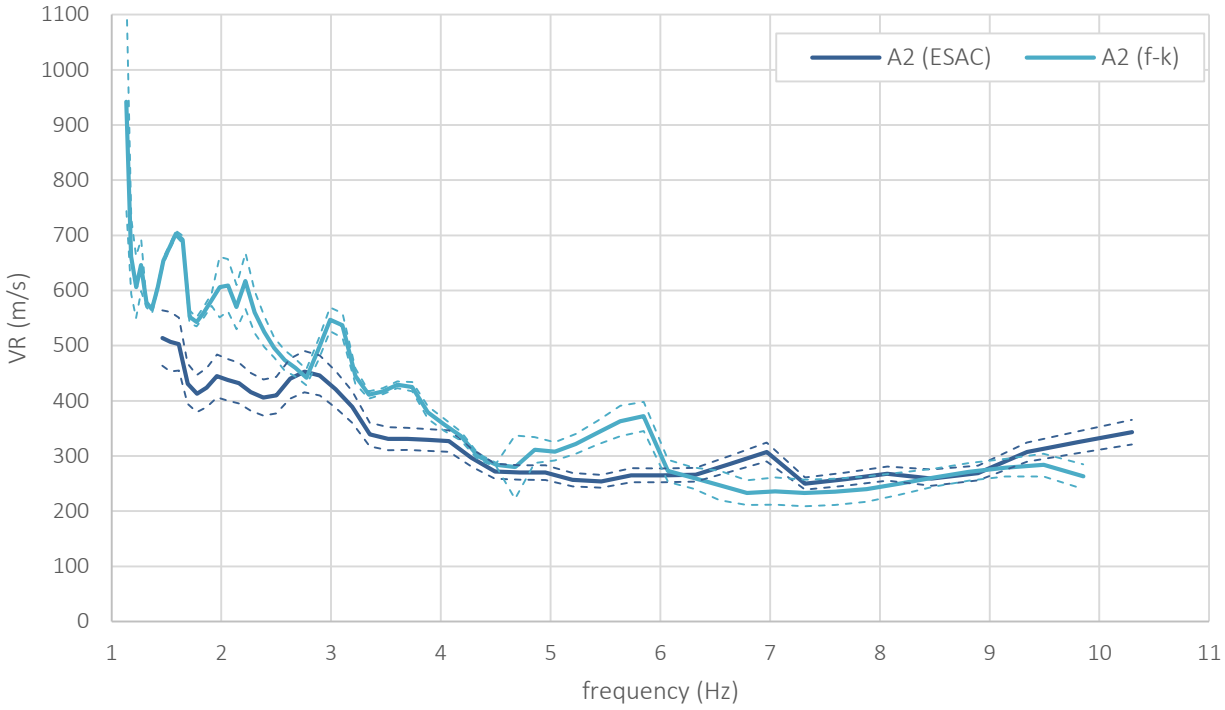

Figure 44. Array A2 dispersion curves (and 95% confidence intervals) computed with ESAC and f-k procedures.

Joint inversion A2

To perform the joint inversion, the dispersion curve obtained at the array A2 with the ESAC procedure was combined with the HVSR curve of measuring point M60. This last one is strongly affected by disturbances, so to reduce this phenomena, is has been smoothed with a seven point triangle window (Figure 45). It is possible to observe that the modelled dispersion curve has surface waves (V_R) values close to the ESAC or the f-k experimental dispersion curves depending on the frequency range.

The H/V peak at 0.75 Hz corresponds to a velocity contrast located at 102 m deep, in which velocities increase abruptly from 212 m/s to 1022 m/s (Figure 46). This is probably the same contrast found at the joint inversion A1, separating Neogene sediments from pre-Neogene rocks. The average Vs of the Neogene sediments is 315 m/s. It is notable that within these sediments, Vs increases to 470 m/s from 32 to 82 m deep. This fact may be attributable to the presence of more compacted sediments, probably stiffer travertines masses. This observation is in concordance with the fact that H/V curves exhibit values below 1 over a large frequency-band (Figure 38).

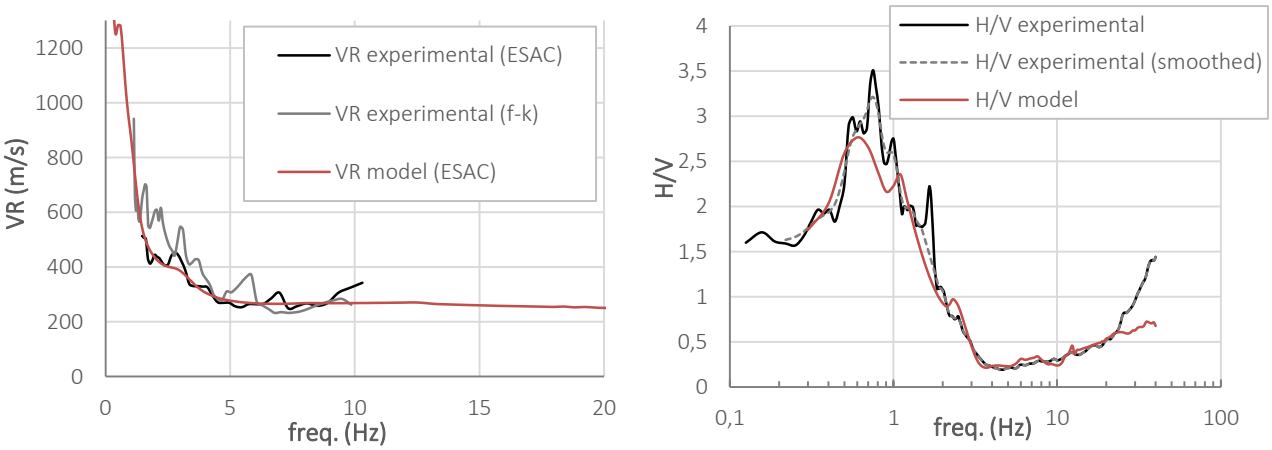

Figure 45. Inversion A2 experimental and model curves: dispersion curves (left) and HVSR curves (right).

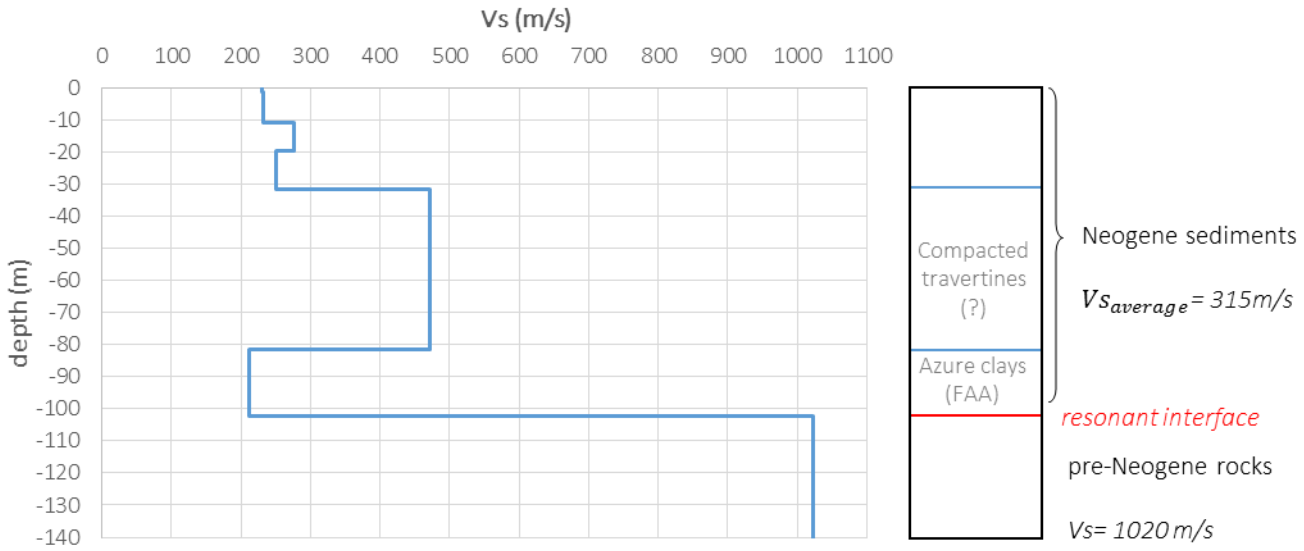

Figure 46. Inversion A2 S-wave velocity profile (left) and geological interpretation (right).

3. South-West area

The South-West area is covered by marine Pliocene sediments, formed by the Azure clays formation (FAA) and by the Yellow sands and sandstones formation (PLIs), stratigraphically lying on the clays. At the middle of the area there are some travertines (f1b) outcrops.

In this zone, 9 single station measurements have been carried: five recording points are located on the Azure clays formation (FAA), one on the Yellow sands and sandstones formations (PLIs), and the 3 others on terraced alluvial sediments overlaying the Pliocene sediments (Figure 37). As well, an array measurement (A3) was realized on the Azure clays.

Single station measurements and HVSR curves

The reliability class of the associated HVSR (Figure 47) curves is B. These show a peak which frequency ranges between 1.3 on the West side, and 2.1 Hz on the East side, and which amplitude varies from 2.5 to 6.3. These peaks indicate the presence of an impedance contrast, probably the same as mentioned before that separates the sediment cover, namely the Neogene materials and the bedrock formed by pre-Neogene rocks.

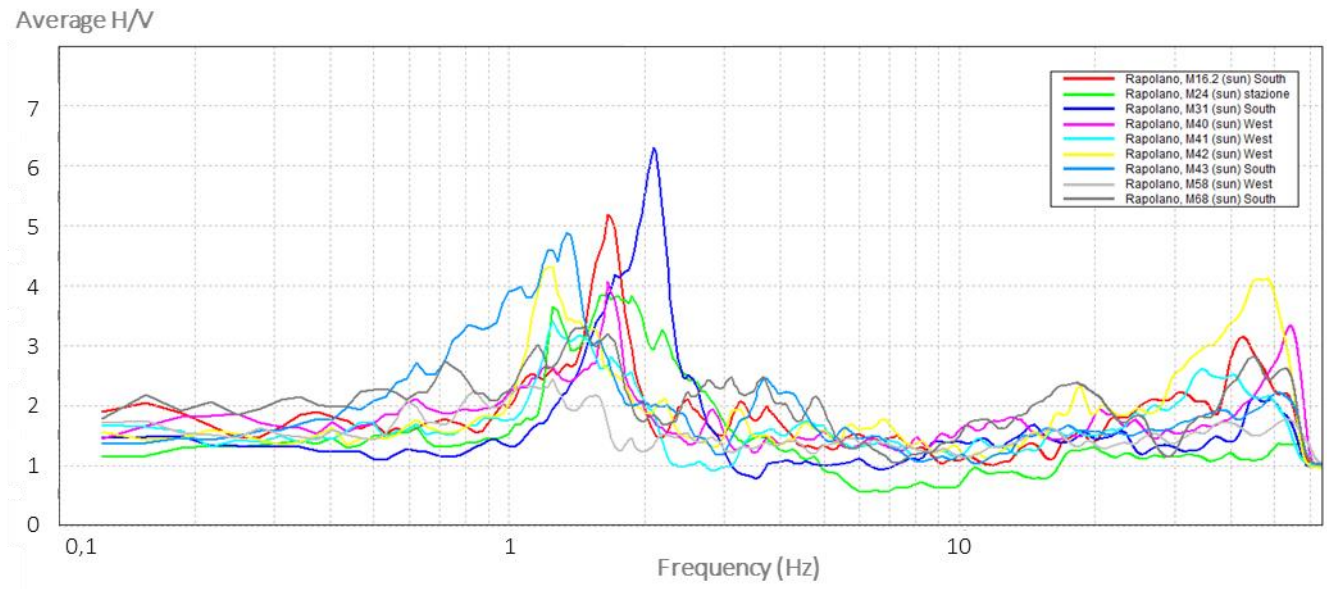

Figure 47. HVSR curves from South-West Rapolano measuring points: M16, M24, M31, M40, M41, M42 , M43, M58, M68.

Array measurement A3 and dispersion curves

The multi-station measurement carried on the Azure clays formation has an irregular spacing cross configuration. The first axis is 110 m long and it is directed to North-East, the second one is 90 m long and is orientated to North-West, perpendicularly to the first one. The shortest geophone inter-distance is 2m and the longest is 127m (Figure 48).

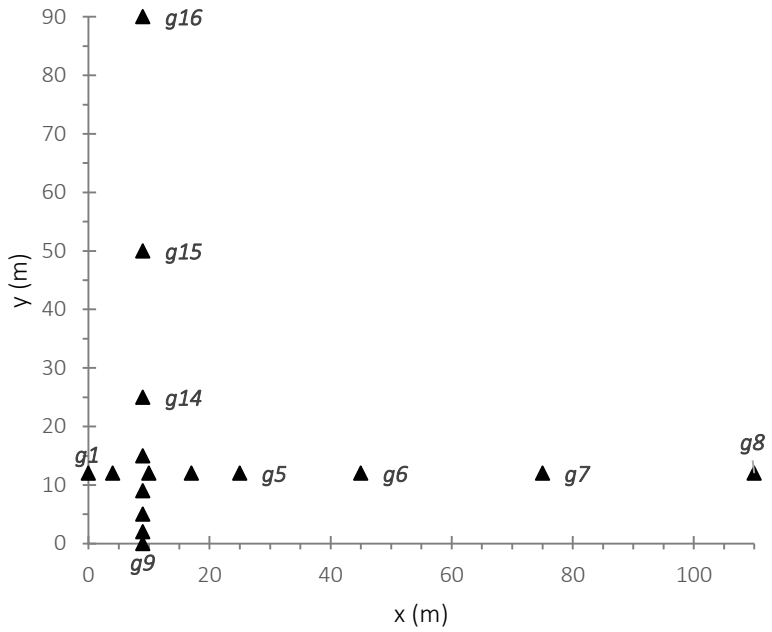

Figure 48. Array A3 configuration (the triangles represent the 16 geophones distribution).

The dispersion curves have been computed with the ESAC and the f-k procedures (Figure 49). Both curves show the same trend, with an irregular augmentation of surface wave velocities (V_R) from high frequencies ($V_R \approx 300\, m/s$ at 14 Hz) to low frequencies ($V_R \approx 900\, m/s$ at 2 Hz). It is noticeable that surface wave velocities (V_R) obtained with the f-k method shows higher velocities than the one obtained with the ESAC procedure.

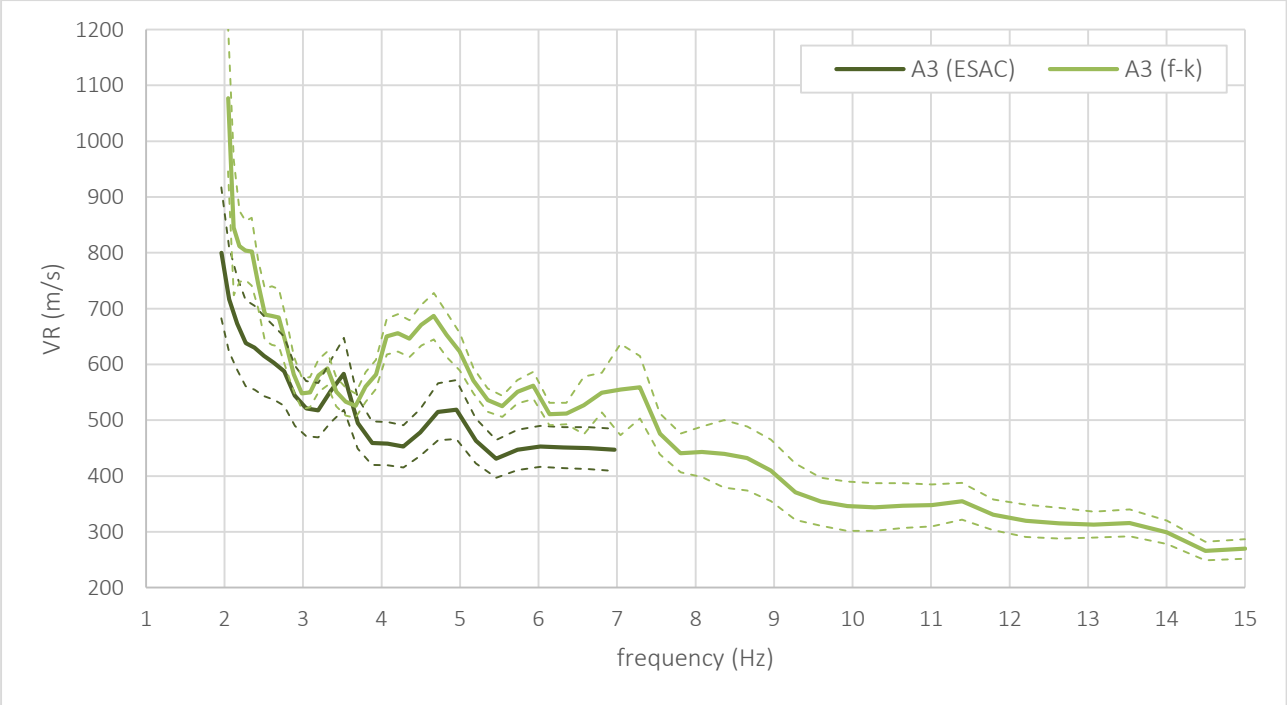

Figure 49. Array A3 dispersion curves (and 95% confidence intervals) computed with ESAC and f-k procedures.

Joint-inversion A3

The joint-inversion was computed combining the HVSR curve obtained from the measurement M43 and the two dispersions curves (ESAC and f-k) calculated from the array recording A3 (Figure 50). Two models have been calculated because the general trend of both dispersion curves (ESAC and f-k) is quite similar.

On the one hand, the model obtained with the ESAC dispersion curve presents the impedance contrast related to the H/V peak at 1.3 Hz at a depth of 73m (Figure 51). The S-waves velocities (Vs) change from 490m/s to 750m/s. The average S-wave velocity is 415 m/s for the top layers, and 825 m/s for the bottom layers up to 200 m deep. On the other hand, the S-wave velocities computed with the f-k dispersion curve display a contrast at 91m deep. It is characterized by a velocity increase from 555m/s to 720m/s, associated to the main H/V peak at 1.3Hz 91m deep. In this model, the top layers average Vs is 460m/s and the bottom ones up to 200 m deep is 910 m/s.

This velocity contrast may be the same as found in the other array measurements, so the contrast between Neogene sediments, in this point represented by the Azure clays formation (FAA), and pre-Neogene rocks may be at a depth comprised between 73 and 91 m. This information is compatible with SR borehole (Annex II) which indicates the presence of soft materials on the 15 first meters of the subsoil.

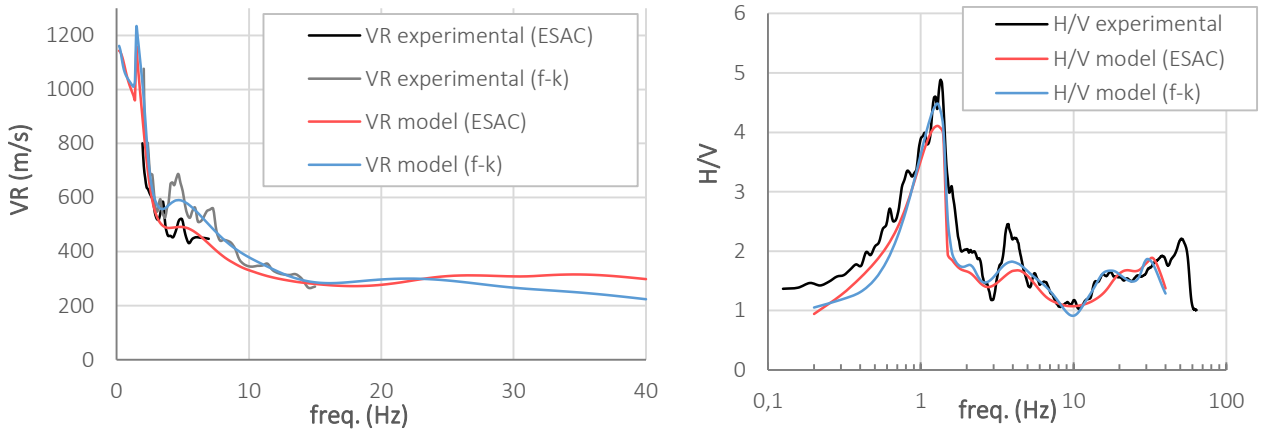

Figure 50. . Inversion A3 experimental and model curves: dispersion curves (left) and HVSR curves (right).

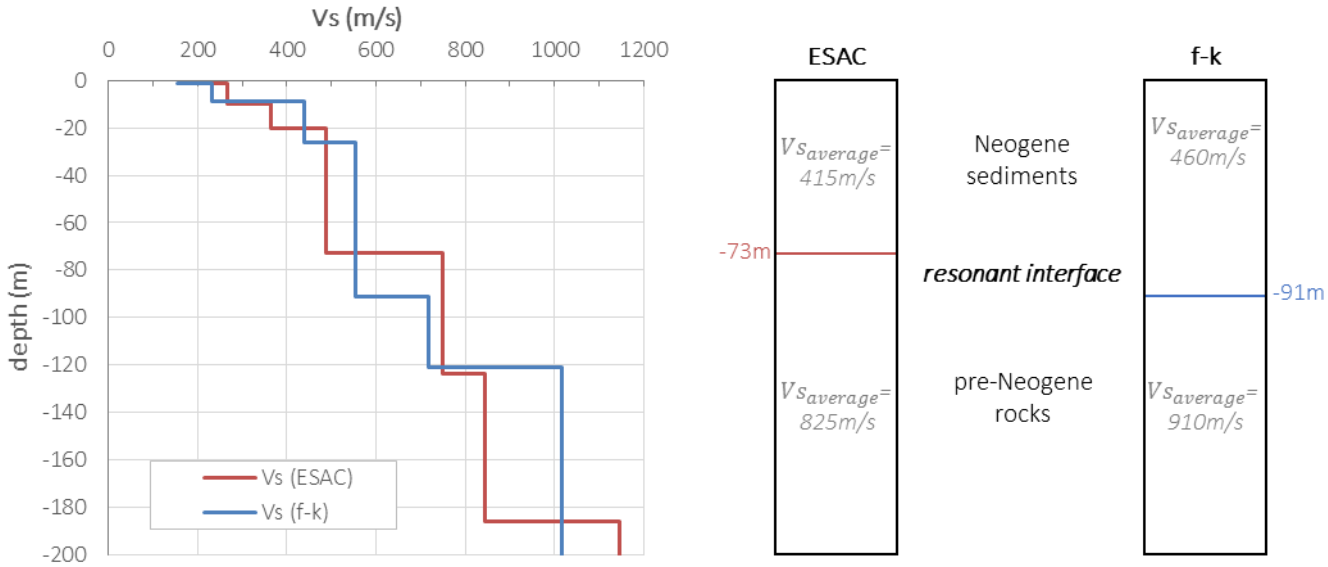

Figure 51. Inversion A3 S-wave velocity profiles (left) and geological interpretation (right).

4. Terme San Giovanni area

The Terme San Giovanni area measurements are situated on Quaternary travertines masses (f1b) and the Pliocene Azure clays formation (FAA). The area is distinctive because of the thermal activity. Indeed, a well-being centre called Terme San Giovanni takes advantage of an active hot thermal springs. This hot fluid circulation is also related to the deposition of layered travertines that are being extracted for ornamental stone at Campo Muri quarry located 200 meters northward called Campo Muri (Figure 37). As well, an archaeological site called Campo Muri was discovered by means of the quarry activity. It is an Etruscan-Roman (III c. B.C. – IV c. A.C.) settlement that developed around the thermal springs (Brogi et al., 2007).

In this area, the travertines are present in two distinctive morphologies related to different depositional characteristics. The first one is present in the major part of the area. The travertine deposits are layered with thicknesses up to 25 meters (Brogi et al., 2007). As well, these have been found at the 40 meters at borehole S6 (Annex II) at depths below 23 m, so the travertines are at least 17 meters thick at this point. The hydrothermal fluids that originated these travertines masses come from a spring located on a mofette which is set on a fluvial terrace of the Ombrone River.

The second morphologic structure is located 20 meters South of Terme San Giovanni centre. It a 250 meters long travertine fissure-ridge in WNW-ESE orientation (Figure 52). The fluids that created this ridge came along a fissure created by a 10 m slip normal fault.

Figure 52. Travertine fissure-ridge near Terme San Giovanni.

Single station measurements and HVSR curves

An amount of 8 single station measurements have been carried out in this zone (Figure 37). All of them have a B reliability class. The HVSR curves show low amplitude (1.9 to 3.1) and broad peaks at low frequencies comprise between 0.6 and 1.0 Hz (Figure 53).These H/V peaks are probably related to the impedance contrast separating the soft sediment cover materials, namely Quaternary travertines (f1b) and Pliocene Azure clays (FAA), and the Pre-Neogene Tuscan succession.

Measurement points M25 and M39 have H/V amplitudes below 1 for a frequency band ranging from 2 to 30 Hz. The recording M56 shows the same trend between 5 and 15 Hz. This trend is the same as seen in the North-West Rapolano area. It is probably linked to the existence of a velocity inversion, namely to the presence of more compact travertines (with higher S-wave velocities) within the Neogene sediments.

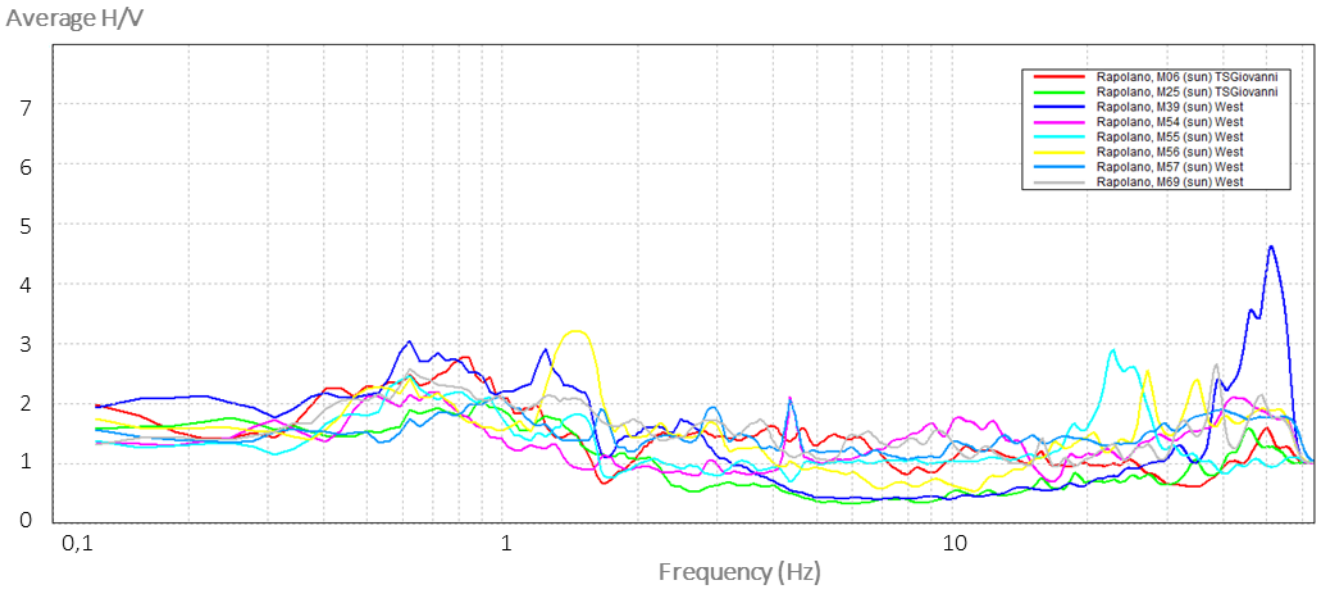

Figure 53. HVSR curves from Terme San Giovanni area measuring points: M06, M25, M39, M54, M55, M56, M57, M69.

5. Rapolano Fault area

The eastern side of the Siena Basin is bounded by the Rapolano-Fault, a west-dipping, NNW-SSE striking normal fault that crosses the eastern side of Rapolano Terme municipality. It dissected both the Pliocene sediments and the pre-Neogene rocks. Moreover, the faulting activity and the Pliocene sedimentation are contemporaneous. The Pliocene sediments are represented by the Azure clays (FAA) and the Yellow sands and sandstones formations (PLIs) outcropping on West side of the fault, as well as the Marine polymictic conglomerate formation (PLIb) on East side of it. The pre-Neogene rocks from the non-metamorphic succession outcrop eastwards, in the Rapolano-Treaquanda ridge, a morphologic structure present along the Rapolano Fault, on its East side. In the study are, its top is 100 m upper than the western flat sedimentation area. Slope deposits (bna) cover a wide zone between the fault and the ridge.

Nearby the fault, 12 single station ambient vibration recordings have been carried out, among which 6 fulfil class A reliability criteria and 6 others the class B criteria. Also an array measurement (A4) was realized on the Yellow sands and sandstones formation (PLIs), on the West side of the fault (Figure 37).

Single station measurements and HVSR curves

Along the fault, the HVSR curves show a clear peak in the 2 -15 Hz frequency band (Figure 54). The frequencies are the highest ones of the whole study, ranging from 2.5 to 7.8 (Hz). As in the previously studied zones, the frequencies increase eastwards, nevertheless, alongside the fault this rise is more intense. As well, the H/V measurements show the bigger amplitudes of the study with values comprised between 3.8 and 3.8. These wide peaks testify the presence of a progressive impedance contrast, probably thinning eastwards.

Curves computed from M1 and M2 recordings show another high amplitude peak (H/V=7) at 29 Hz and 50 Hz respectively. These peaks are related to thin sediment covers: terraced alluvial sediments (bnb) lying on travertines for M1 point, and slope deposits for M2 measuring point.

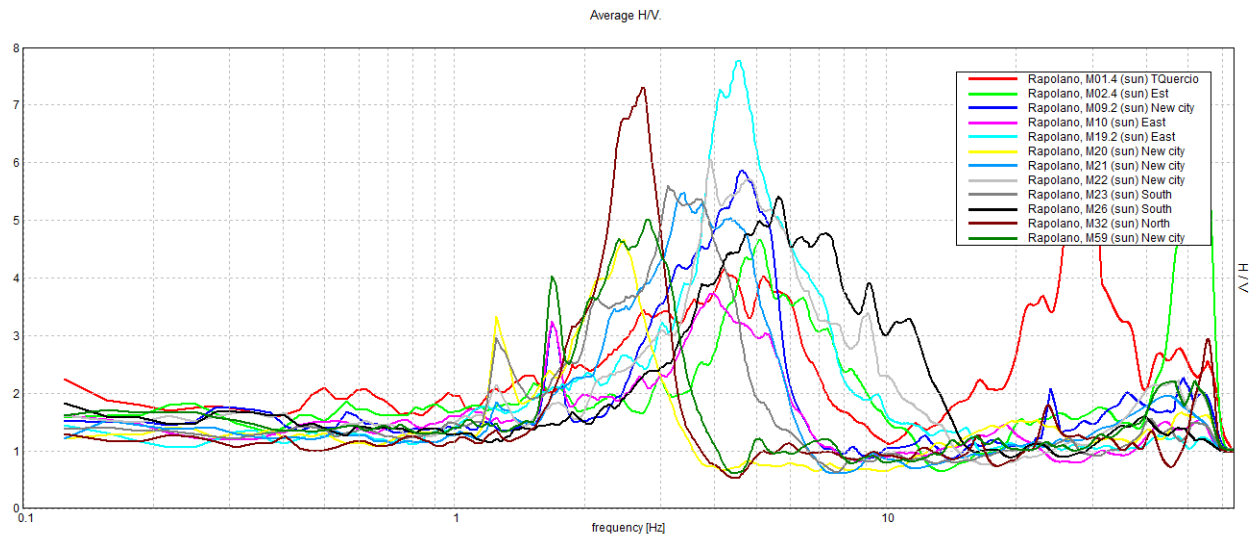

Figure 54. HVSR curves from Rapolano Fault area measuring points: M01, M02, M09.2, M10, M19, M20, M21, M22, M23, M26, M32, M59.

Array measurement A4 and dispersion curves

The multi-station measurement A4 was deployed in the North part of this zone, at 125 m of the Rapolano Fault. The first axis of the cross configuration is 90 m long and oriented toward North, whereas the second one is 70 m long and oriented westwards. The shortest inter-geophone distance is 2 m and the longest one is 107 m (Figure 55).

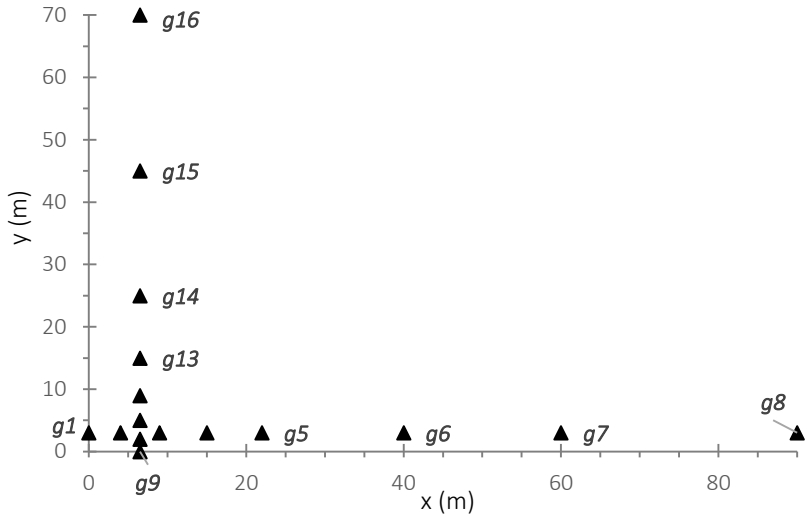

Figure 55. Array A4 configuration (the triangles represent the 16 geophones distribution).

The ESAC and f-k procedures used for the dispersion curves computation show a very similar trend from 4 to 13 Hz, the surface wave velocity (V_R) decreases regularly from 600m/s at 4 Hz to almost 300 m/s at 13 Hz (Figure 56). Not to take into account the small peak present on the f-k curve at 15.5 Hz, the joint inversion was performed with the curved computed with the ESAC procedure.

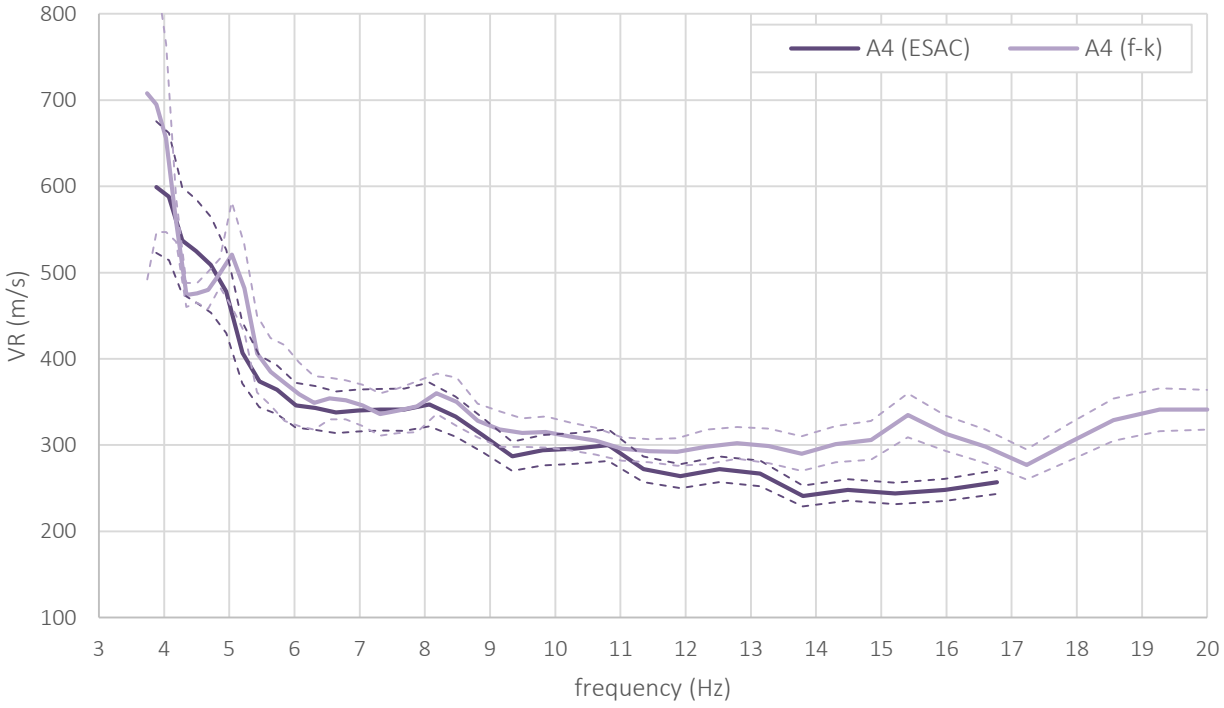

Figure 56. Array A4 dispersion curves (and 95% confidence intervals) computed with ESAC and f-k procedures.

Joint inversion A4

The S-wave velocity profile was obtained with a joint inversion combining the HVSR curve from measurement M59 and the dispersion curve computed with the ESAC procedure (Figure 57). The modelled dispersion curve takes into account the high velocities given by the f-k dispersion curve, at low frequencies, and the lower velocities given by the ESAC procedure at high frequencies.

The computed S-wave velocity – depth profile (Figure 58) shows a sharp velocity contrast at 31 m deep in which V_S increases from 345 m/s on the surface materials to 870 m/s on deeper materials.

This may be associated to an abrupt change from soft to stiffer geologic materials, probably the contact of the Neogene sediments and the pre-Neogene rocks, hypothesized on the other measurement sites. At 61 m deep the S-wave velocity increases up to 981 m/s.

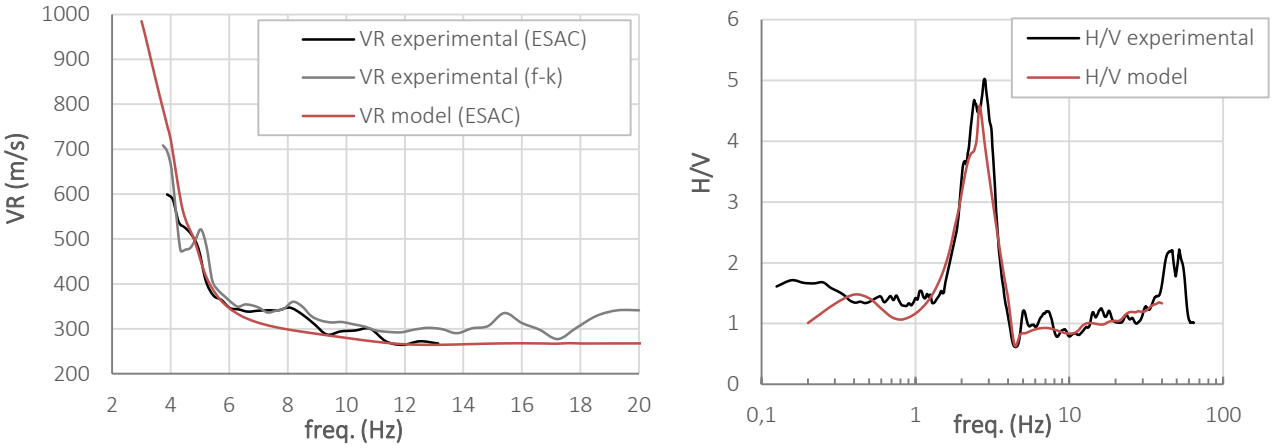

Figure 57. Figure 57. Inversion A4 experimental and model curves: dispersion curves (left) and HVSR curves (right).

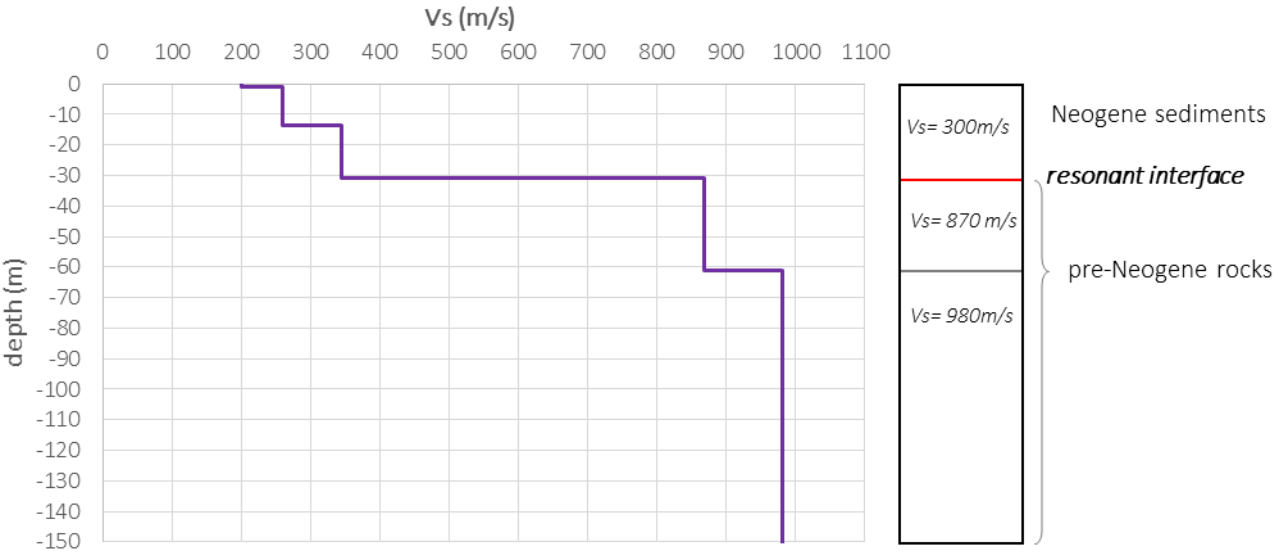

Figure 58. Inversion A4 S-wave velocity profile (left) and geological interpretation (right).

6. East Rapolano area

Along to the Rapolano Fault, on its East side, there is the Rapolano-Trequanda ridge. This is formed by pre-Neogene rocks of the non-metamorphic Tuscan successions. The formations present at the study are, from top to bottom (Figure 37): Scaglia Toscana (STO1 and STO4), Maiolica (MAI), Calcari ad aptici (APT), Diaspri (DSD) and Marne a Posidonomya (POD) formations. This last one is lying on (LIM) that doesn't outcrop at the study area. The non-metamorphic succession has suffered an anticlinal fold, parallel to the ridge, open and symmetrical.

Single station measurements and HVSR curves

In this area, 12 single station ambient vibrations recordings have been carried out. The computed HVSR curves fulfill class B reliability criteria.

First, 4 measuring points (M33, M34, M44.2 and M45) have been carried out on the Maiolica formation (MAI) and Scaglia Toscana formation (STO). The HVSR curves (Figure 59) are flat, namely there is no peak. This appearance reveals that there is no amplification phenomena. For this reason, these materials can be considered as a seismic bedrock.

HVSR computed from measurements realized at point M63 on Calcari ad aptici formation (APT), and M64 on Diaspri formation (DSD), show a low amplitude peak (H/V < 3) at 3Hz (M64) and 8Hz (M63). It may be due to the weathering of the superficial materials, so the top soften layers act as soft sediments. The fact that the peak is not well defined, namely it covers a large frequency band, indicates that the contact between the weathered rock and the mother rock is gradual.

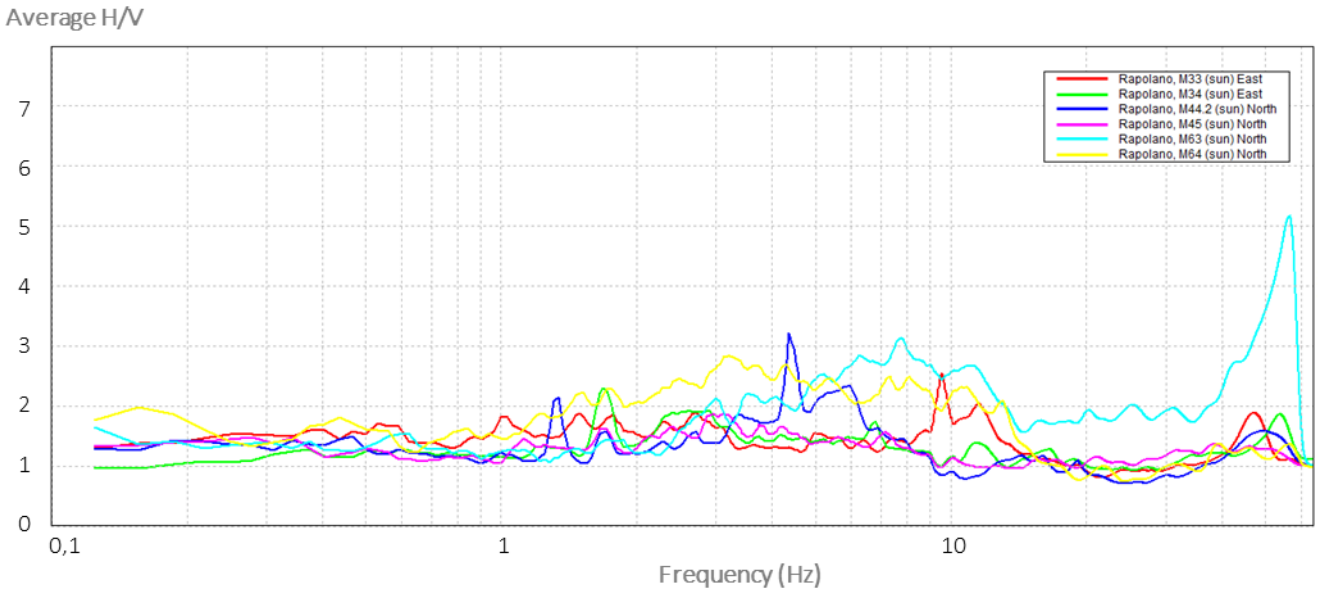

Figure 59. Flat HVSR curves from East Rapolano area measuring points: M33, M34, M44.2, M45, M63 and M64.

The HVSR curves obtained from measuring points located on the slope between the ridge and the urban area (M17, M35, M66, M67, M70 and M71) present a peak with amplitudes ranging from 3.2 to 6.4, between 2.3 Hz and 3.2 Hz (Figure 60). These ones cover a frequency-band comprise between 0.6Hz and 6Hz. It is also noticeable that four close measurements present the same anthropic disturbance at 0.6 Hz (M17. M35, M66 and M67). At first glance, seismic amplification phenomenon are not expected on these rocks as they represent the stratigraphic bedrock. Nevertheless the peaks' presence indicates the contrary. As the measures were made on a rather sloppy area this peaks may be explained because of topographic effects (cf. Figure 6, p.7). As well, weathering can be responsible of the superficial materials softening.

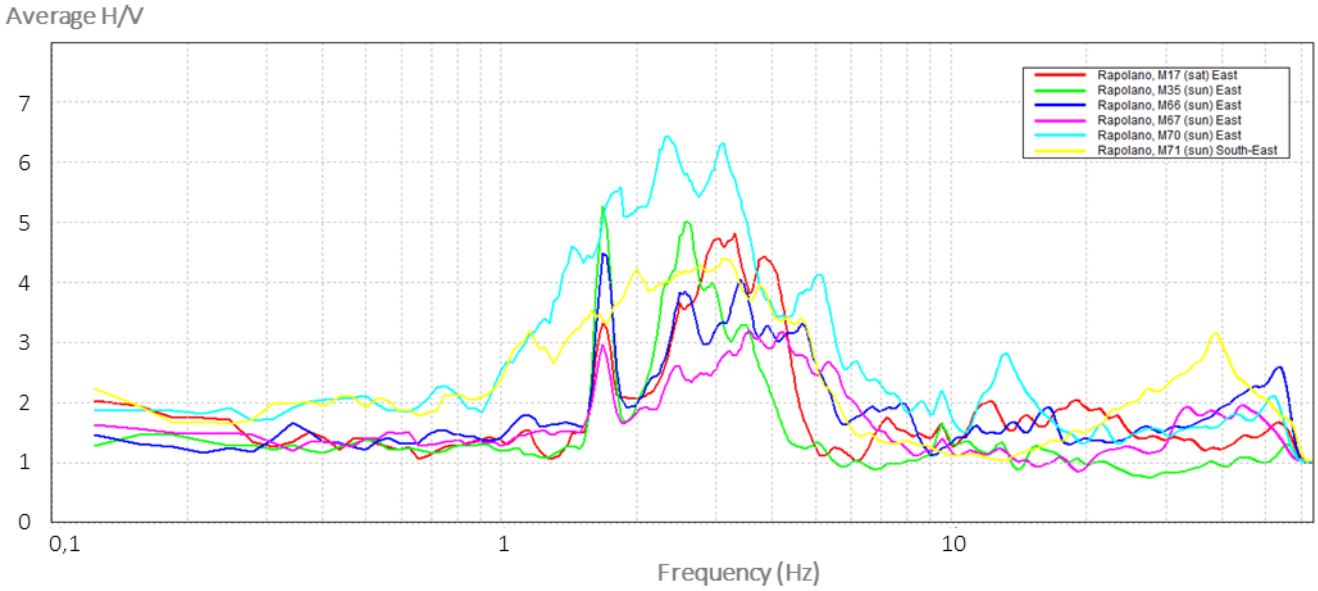

Figure 60. Non-flat HVSR curves from East Rapolano area measuring points: M17, M35, M66, M67, M70 and M71.

Nevertheless, the morphologic and stratigraphic characteristics support the hypothesis that the rocks of the Tuscan non-metamorphic succession represent the stratigraphic bedrock. This idea is confirmed by the flat HVSR curves, which indicate the presence of the seismic bedrock.

7. General interpretation

From the Rapolano Fault to West, the frequency and the amplitude of HVSR peaks decrease progressively. The peaks presence indicate the existence an impedance contrast. The frequencies' trend indicates that the sedimentary cover, above this contrast, gets thicker westwards. The S-wave velocity - depth profiles validate this hypothesis and give the depth of the impedance contrast. This seismic contact is in concordance with the stratigraphic contact that separates Neogene sedimentary cover and the the bedrock, made of pre-Neogene rock of the non-metamorphic Tuscan succession. This is confirmed by the seismic profile carried out perpendicularly to Rapolano Fault and its interpretation (Figure 27, p.30).

The information obtained from the geological map, from the shear wave – depth profiles obtained from array measurements and from other geological surveys carried out in the study area have been summed up in three cross sections directed perpendicularly to the Raplano Fault (Figures 61 and 62). It has been possible to draw the contact between the Neogene sediments and the pre-Neogene basement rocks.

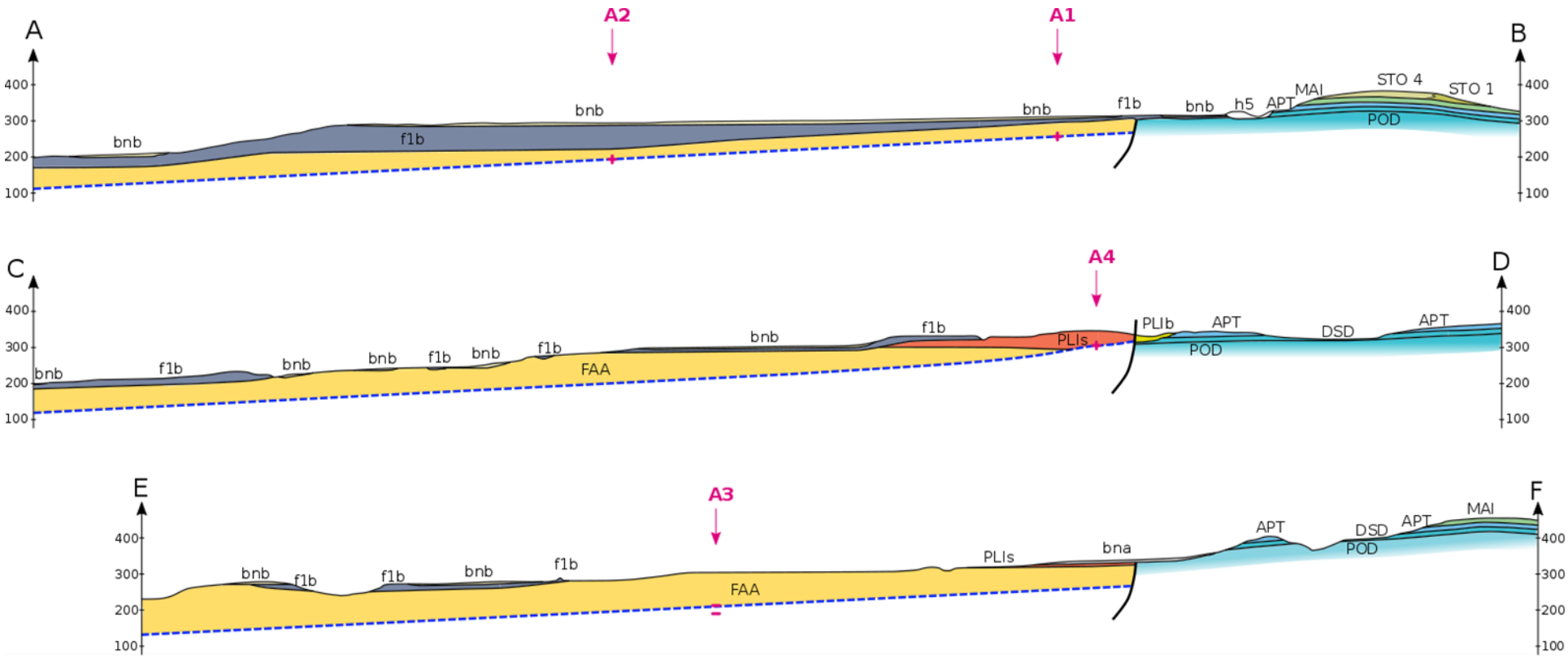

A3 Array measurement (impedance contrast)

Impedance contrast

QUATERNARY DEPOSITS

HOLOCENE DEPOSITS: Anthropic deposits: backfills (**h5**), Slope deposits (**bna**).

MIDDLE-LATE PLEISTOCENE DEPOSITS: Alluvial terrace deposits (**bnb**), travertines and continental limestones (**f1b**).

MARINE PLIOCENE DEPOSITS

Yellow sands and sandstones (**PLIs**); Azure clays (**FAA**); Marine polymictic conglomerates (**PLIb**)

PRE-NEOGEN ROCKS OF –THE NON-METAMORPHIC TUSCAN SUCCESION

Macignio (**MAC**); Scaglia Toscana (**STO**); Maiolica (**MAI**); Calcari ad aptici (**APT**); Diaspri (**DSD**); Marne a Posidonomya (**POD**).

Figure 61. Cross sections (the location is presented in Figure 62).

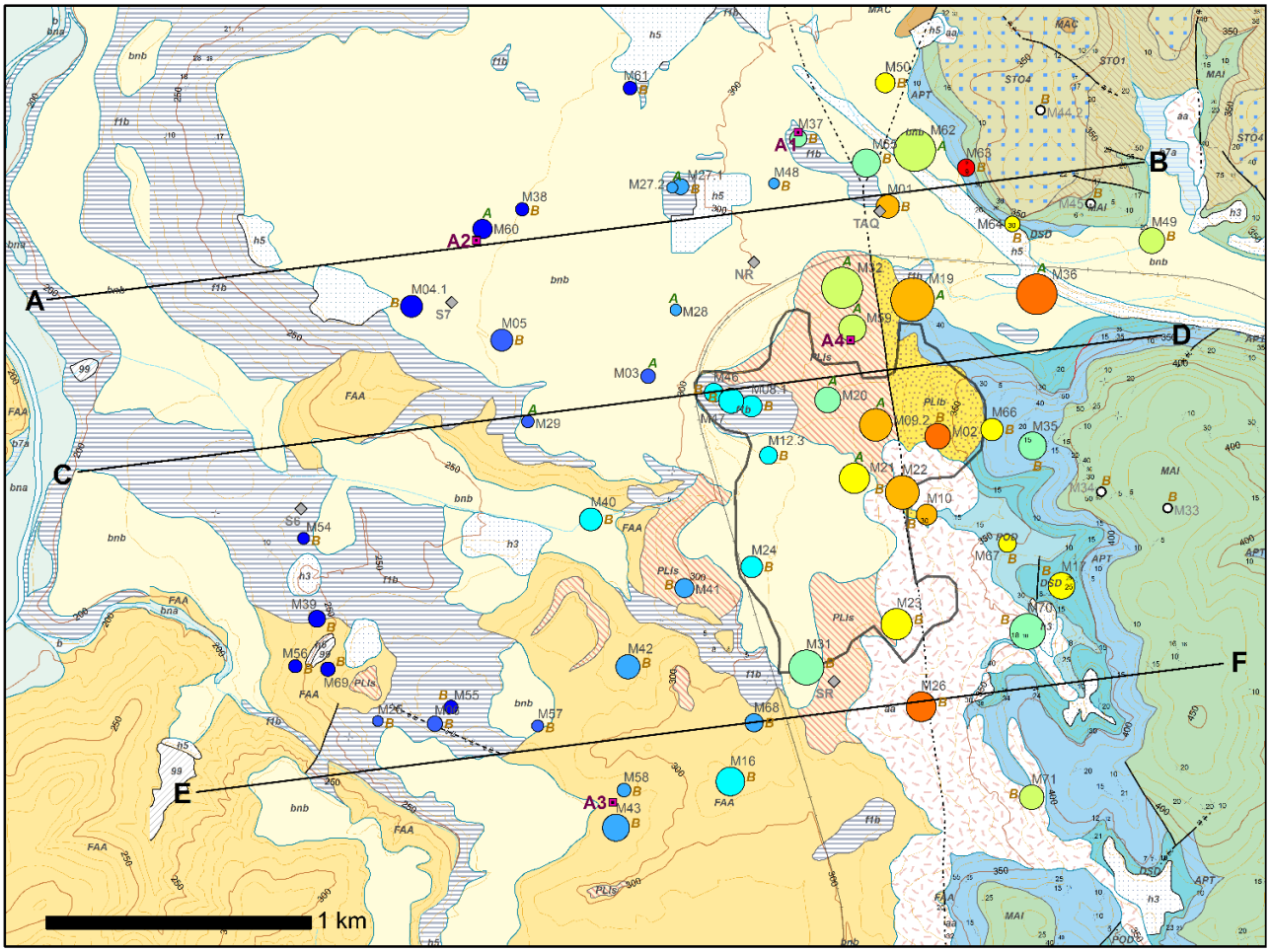

Figure 62. Location of the cross sections.

CONCLUSION

Since the last decades, passive seismic methods are popular for subsoil mechanical characterization in geotechnical earthquake engineering. These techniques have demonstrated the capability to yield information on the low frequency range and consequently at larger depths, for a relatively cheap exploration cost.

A large density single station measurements over Rapolano Terme area, computed with the HVSR technique, allowed to determine areas subjected to resonance phenomena, and to characterize it giving the amplification frequency as well as qualitative information about its intensity. Few multi-station ambient vibrations recordings have been analysed with the frequency-wavenumber (f-k) and the spatial extended autocorrelation methods (ESAC) in order to retrieve phase velocity dispersion curves. The combination of HVSR curves and dispersion curves on a joint inversion procedure has been used to retrieve reliable shear wave velocity – depth profiles. To mitigate problems associated with the non-uniqueness of the inverse problem, a genetic algorithm has been used. To validate these results and to reduce uncertainties, the outcomes have been compared with geologic surveys, boreholes and other seismic data.

Thus, seismic passive techniques consent to obtain a better knowledge of the local geological setting. The trend of HVSR peaks' frequencies and the S-wave profiles support the presence of a resonant interface at more than 100m deep, gently dipping westward. This discontinuity may represent the contact between the pre-Neogene bedrock and the Neogene sediments of the Siena Bassin. As well, the survey validates the existence of the Rapolano Fault. Therefore, this work corroborates the usefulness of passive seismic techniques.

REFERENCES

Aki, K., 1957. Space and time spectra of stationary stochastic waves, with special reference to microtremors.

Albarello, D., 2014. Sismica passiva a stazione singola (metodo HVSR) - Lecture notes.

Albarello, D., Cesi, C., Eulilli, V., Guerrini, F., Lunedei, E., Paolucci, E., Pileggi, D., Puzzilli, L.M., 2011. The contribution of the ambient vibration prospecting in seismic microzoning: an example from the area damaged by the April 6, 2009 L'Aquila (Italy) earthquake. Boll. Geofis. Teor. Ed Appl. 52, 513–538.

Asten, M.W., Henstridge, J.D., 1984. Array estimators and the use of microseisms for reconnaissance of sedimentary basins. Geophysics 49, 1828–1837.

Baldi, A.M., Marzocchi, A., Menegoli, M., 1992. Nuove individuazioni di giacimenti di anidride carbonica in Toscana. Boll Assoc Min. Subalp. 29, 335–345.

Belvaux, M., Roullé, A., Auclair, S., Vanoudheusden, E., Barras, A.-V., 2012. Limites des methodes de caracterisation des effets de site dans les microzonages sismiques. Journ. Natl. Géotechnique Géologie L'Ingénieur JNGG2012.

Bernoulli, D., Kälin, O., Patacca, E., 1979. A sunken continental margin of the Mesozoic Tethys: The Northern and Central Apennines: Symposium" Sédimentation jurassique W Européen."

Bertini, G., Cameli, G.M., Costantini, A., Decandia, F.A., Di Filippo, M., Dini, I., Elter, F.M., Lazzarotto, A., Liotta, D., Pandeli, E., 1991. Struttura geologica fra i monti di Campiglia e Rapolano Terme (Toscana meridionale): stato attuale delle conoscenze e problematiche. Studi Geol Camerti 1, 155–178.

Bonini, M., Sani, F., 2002. Extension and compression in the Northern Apennines (Italy) hinterland: Evidence from the late Miocene-Pliocene Siena-Radicofani Basin and relations with basement structures. Tectonics 21, 1–1–1–32.

Bonnefoy-Claudet, S., 2004. Nature du bruit de fond sismique: implications pour les études des effets de site (PhD thesis). Université Joseph-Fourier - Grenoble I.

Bonnefoy-Claudet, S., Cotton, F., Bard, P.-Y., 2006. The nature of noise wavefield and its applications for site effects studies: a literature review. Earth-Sci. Rev. 79, 205–227.

Bossio, A., Costantini, A., Lazzarotto, A., Liotta, D., Mazzanti, R., Mazzei, R., Salvatorini, G., Sandrelli, F., 1993. Rassegna delle conoscenze sulla stratigrafia del neoautoctono toscano. Mem Soc Geol It 49, 17–98.

Brogi, A., 2008. Fault zone architecture and permeability features in siliceous sedimentary rocks: insights from the Rapolano geothermal area (Northern Apennines, Italy). J. Struct. Geol. 30, 237–256.

Brogi, A., 2007. Fault zone architecture and permeability features in siliceous sedimentary rocks: insights from the Rapolano geothermal area (Northern Apennines, Italy). J. Struct. Geol. 30, 237–256.

Brogi, A., 2004. Faults linkage, damage rocks and hydrothermal fluid circulation: tectonic interpretation of the Rapolano Terme travertines (southern Tuscany, Italy) in the context of Northern Apennines Neogene-Quaternary extension. Eclogae Geol. Helvetiae 97, 307–320.

Brogi, A., 2002. Relazione tra strutture distensive neogenico-quaternarie ed i depositi di travertino nell'area di Rapolano Terme (Appennino Settentrionale). Atti Ticinensi Sci. Della Terra 43, 41–54.

Brogi, A., Capezzuoli, E., 2009. Travertine deposition and faulting: the fault-related travertine fissure-ridge at Terme S. Giovanni, Rapolano Terme (Italy). Int. J. Earth Sci. 98, 931–947.

Brogi, A., Capezzuoli, E., Aqué, R., Branca, M., Voltaggio, M., 2009. Studying travertines for neotectonics investigations: Middle–Late Pleistocene syn-tectonic travertine deposition at Serre di Rapolano (Northern Apennines, Italy). Int. J. Earth Sci. 99, 1383–1398.

Brogi, A., Capezzuoli, E., Gandin, A., 2007. I travertini delle Terme di S. Giovanni (Rapolano Terme, Appennino Settentrionale) e loro implicazione neotettonica. Il Quat. 20, 107–124.

Brogi, A., Lazzarotto, A., Liotta, D., 2005. Structural features of southern Tuscany and geological interpretation of the CROP 18 Seismic Reflection Survey (Italy). Boll. Della Soc. Geol. Ital. Vol. Spec. 213–236.

Capon, J., 1969. High-resolution frequency-wavenumber spectrum analysis. Proc. IEEE 57, 1408–1418.

Carmignani, L., Decandia, F.A., Fantozzi, P.L., Lazzarotto, A., Liotta, D., Meccheri, M., 1994. Tertiary extensional tectonics in Tuscany (northern Apennines, Italy). Tectonophysics 238, 295–315.

Castellaro, S., Albarello, D., 2011. Tecniche sismiche passive: indagini a stazione singola. Ing. Sismica 2.

Castellaro, S., Mulargia, F., 2009. The effect of velocity inversions on H/V. Pure Appl. Geophys. 166, 567–592.

Costantini, A., Lazzarotto, A., Sandrelli, F., 1982. Conoscenze geologico strutturali. Il Graben Siena CNR-PFE-RF 9, 11–33.

D'Amico, V., Picozzi, M., Albarello, D., Naso, G., Tropenscovino, S., 2004. Quick estimates of soft sediment thicknesses from ambient noise horizontal to vertical spectral ratios: a case study in southern Italy. J. Earthq. Eng. 8, 895–908.

Decandia, F.A., Lazzarotto, A., 1972. Ritrovamento di macroforaminiferi oligocenici nella parte inferiore del Macigno del Chianti in localita'Farnetella (Siena). Boll. Della Soc. Geol. Ital. 91, 511–521.

Fäh, D., Kind, F., Giardini, D., 2001. A theoretical investigation of average H/V ratios. Geophys. J. Int. 145, 535–549.

Gandin, A., 1982. Considerazioni stratigrafico-paleogeografiche. Il Graben Siena 9, 34–36.

Gandin, A., Sandrelli, F., 1992. Caratteristiche sedimentologiche dei corpi sabbiosi intercalate nelle argille plioceniche del Bacino di Siena. G. Geol. 54.

Goldberg, D.E., 1989. Sizing populations for serial and parallel genetic algorithms, in: Proceedings of the 3rd International Conference on Genetic Algorithms. Morgan Kaufmann Publishers Inc., pp. 70–79.

Guillier, B., Cornou, C., Kristek, J., Moczo, P., Bonnefoy-Claudet, S., Bard, P.Y., Fäh, D., 2006. Simulation of seismic ambient vibrations: does the H/V provide quantitative information in 2D-3D structures, in: Third International Symposium on the Effects of Surface Geology on Seismic Motion Grenoble, France.

Guo, L., Andrews, J., Riding, R., Dennis, P., Dresser, Q., 1996. Possible microbial effects on stable carbon isotopes in hot-spring travertines. J. Sediment. Res. 66.

Guo, L., Riding, R., 1999. Rapid facies changes in Holocene fissure ridge hot spring travertines, Rapolano Terme, Italy. Sedimentology 46, 1145–1158.

Guo, L., Riding, R., 1998. Hot-spring travertine facies and sequences, Late Pleistocene, Rapolano Terme, Italy. Sedimentology 45, 163–180.

Guo, L., Riding, R., 1994. Origin and diagenesis of Quaternary travertine shrub fabrics, Rapolano Terme, central Italy. Sedimentology 41, 499–520.

Guo, L., Riding, R., 1992. Aragonite laminae in hot water travertine crusts, Rapolano Terme, Italy. Sedimentology 39, 1067–1079.

Gutenberg, B., 1958. Microseisms. Adv. Geophys. 5, 53–92.

Ibs-von Seht, M., Wohlenberg, J., 1999. Microtremor measurements used to map thickness of soft sediments. Bull. Seismol. Soc. Am. 89, 250–259.

Kalin, O., Patacca, E., Renz, O., 1979. Jurassic pelagic deposits from Southeastern Tuscany; aspects of sedimentation and new biostratigraphic data. Eclogae Geol. Helvetiae 72, 715–762.

Lacoss, R.T., Kelly, E.J., Toksöz, M.N., 1969. Estimation of seismic noise structure using arrays. Geophysics 34, 21–38.

Lazzarotto, A., 1973. Caratteri strutturali dei nuclei mesozoici di Montalceto, Trequanda e Piazza di Siena (Prov. di Siena).

Lazzarotto, A., Constantini, A., Brogi, A., Carmignani, L., Grazziosi, B., Gianetti, L., 2008. Carta geologica regionale - sezione 297120 (Rapolano Terme).

Lazzarotto, A., Sandrelli, F., 1977. Stratigrafia e assetto tettonico delle formazioni neogeniche nel bacino del Casino (Siena). Boll. Della Soc. Geol. Ital. 96, 747–762.

Liotta, D., 1996. Analisi del settore centro-meridionale del bacino pliocenico di Radicofani (Toscana meridionale). Boll. Della Soc. Geol. Ital. 115, 115–143.

Liotta, D., 1994. Structural features of the Radicofani basin along the Piancastagnaio (Mt. Amiata)–S. Casciano dei Bagni (Mt. Cetona) cross section. Mem Soc Geol It 48, 401–408.

Liotta, D., Salvatorini, G., 1994. Evoluzione sedimentaria e tettonica della parte centro-meridionale del bacino pliocenico di Radicofani. Studi Geol. Camerti Vol Spec 1, 65–77.

Losacco, U., 1952. La struttura del territorio di Rapolano e Lucignano (Siena e Arezzo). Boll Soc Geol Ital 70, 402–434.

Losacco, U., Del Giudice, D., 1958. Stratigrafia e tettonica degli affioramenti mesozoici posti fra le colline di Rapolano ed il Monte Cetona (Siena). Boll Soc Geol Ital 77, 1–32.

Lunedei, E., Albarello, D., 2010. Theoretical HVSR curves from full wavefield modelling of ambient vibrations in a weakly dissipative layered Earth. Geophys. J. Int. 181, 1093–1108.

Lunedei, E., Albarello, D., 2009. On the seismic noise wavefield in a weakly dissipative layered Earth. Geophys. J. Int. 177, 1001–1014. doi:10.1111/j.1365-246X.2008.04062.x

Martini, I.P., Sagri, M., 1993. Tectono-sedimentary characteristics of Late Miocene-Quaternary extensional basins of the Northern Apennines, Italy. Earth-Sci. Rev. 34, 197–233.

Milani, I., 2013. Indagini geofisiche a supporto della Microzonazione Sismica di I^{o} Livello dell'area pedemontana del Comune di Massa (master thesis). Università di Siena.

Minissale, A., Kerrick, D.M., Magro, G., Murrell, M.T., Paladini, M., Rihs, S., Sturchio, N.C., Tassi, F., Vaselli, O., 2002. Geochemistry of Quaternary travertines in the region north of Rome (Italy): structural, hydrologic and paleoclimatic implications. Earth Planet. Sci. Lett. 203, 709–728.

Mucciarelli, M., Gallipoli, M.R., 2001. A critical review of 10 years of microtremor HVSR technique. Boll Geof Teor Appl 42, 255–266.

Nakamura, Y., 1989. A method for dynamic characteristics estimation of subsurface using microtremor on the ground surface. Railw. Tech. Res. Inst. Q. Rep. 30.

Nogoshi, M., Igarashi, T., 1971. On the amplitude characteristics of microtremor (part 2). Jour Seism Soc Jpn. 24, 26–40.

Ohori, M., Nobata, A., Wakamatsu, K., 2002. A comparison of ESAC and FK methods of estimating phase velocity using arbitrarily shaped microtremor arrays. Bull. Seismol. Soc. Am. 92, 2323–2332.

Ohrnberger, M., Schissele, E., Cornou, C., Bonnefoy-Claudet, S., Wathelet, M., Savvaidis, A., Scherbaum, F., Jongmans, D., 2004. Frequency wavenumber and spatial autocorrelation methods for dispersion curve determination from ambient vibration recordings, in: Proc. of 13th World Conf. on Earthquake Engineering, Vancouver, BC, Canada. pp. 1–6.

Okada, H., 2003. The microtremor survey method. Society of Exploration Geophysicists with the cooperation of Society of Exploration Geophysicists of Japan [and] Australian Society of Exploration Geophysicists.

Pagliaccia, S., 2013. Metodi di sismica passiva applicati alla Microzonazione Sismica di I^{o} livello della pianura del Comune di Massa (master thesis). Università di Siena.

Paolucci, E., 2010. Il contributo della sismica passiva alla microzonazione delle aree colpite dal sims del 6 Aprile 2009 (master thesis). Università di Siena.

Parolai, S., Picozzi, M., Richwalski, S.M., Milkereit, C., 2005. Joint inversion of phase velocity dispersion and H/V ratio curves from seismic noise recordings using a genetic algorithm, considering higher modes. Geophys. Res. Lett. 32.

Passerini, P., 1965. Il Monte Cetona (Provincia di Siena). Pacini Mariotti.

Picozzi, M., 2005. Joint inversion of phase velocity dispersion and H/V ratio curves from seismic noise recordings (PhD thesis). Università di Siena.

Picozzi, M., Parolai, S., Richwalski, S.M., 2005. Joint inversion of H/V ratios and dispersion curves from seismic noise: Estimating the S-wave velocity of bedrock. Geophys. Res. Lett. 32.

Pileggi, D., 2013. Intensive and extensive application of ambient vibration recording: critical issues in different geological settings (Phd thesis). Università di Siena.

Scherbaum, F., Hinzen, K.-G., Ohrnberger, M., 2003. Determination of shallow shear wave velocity profiles in the Cologne, Germany area using ambient vibrations. Geophys. J. Int. 152, 597–612.

Schmidt, R.O., 1981. A signal subspace approach to multiple emitter location spectral estimation. Ph Thesis Stanf. Univ.

Seo, K., 1997. Comparison of measured microtremors with damage distribution. JICA Res. Dev. Proj. Earthq. Disaster Prev. 306–320.

SESAME, W., 2004. Guidelines for the implementation of the H/V spectral ratio technique on ambient vibrations-Measurements, processing and interpretation. SESAME European research project, Deliverable D23. 12., Project No. EVG1-CT-2000-00026 SESAME, 62 pp.

Sibson, R.H., 1992. Fault-valve behavior and the hydrostatic-lithostatic fluid pressure interface. Earth-Sci. Rev. 32, 141–144.